NASA Contractor Report 174896

Development of a Temperature Measurement System With Application to a Jet in a Cross Flow Experiment

Candace Wark and John F. Foss

Michigan State University
East Lansing, Michigan

April 1985

Prepared for
Lewis Research Center
Under Grant NAG 3-245

NASA
National Aeronautics and
Space Administration

FORWARD

The following manuscript is presented in two parts. Part I is the discussion of a temperature measurement system which was used in the experimental program discussed in Part II. The two discussions are presented separately since the temperature measurement system is not solely intended for the present experimental program; i.e., it is a system that will be quite useful in many other experimental programs. Those details which are specific to the present experimental program will be found in Part II.

This document is, with one important exception, taken from the M.S. thesis of the senior author (C.E. Wark). At the time of the thesis preparation, it was not recognized that an experimental procedure error (a constant volume flow rate and not a constant mass flow rate was used from the metering nozzle to the jet exit plane) had introduced an error into the computation of J for the heated flow condition. The J values, of the thesis, were thought to be constant (16,64) whereas their true values are shown in this report.

TABLE OF CONTENTS

TABLE OF CONTENTS (Continued)

LIST OF SYMBOLS

A_1	area of isotherm I
A_s	surface area of thermocouple bead
A_x	cross sectional area of thermocouple wire
C_d	discharge coefficient
c_p	specific heat at constant pressure
c	specific heat (see equation I.1)
d	diameter of jet orifice (10mm)
d.c.f.	disturbed cross flow
d_w	diameter of thermocouple wire (from Petit et al. (1982))
E_i	input voltage
E_o	output voltage
E_{off}	offset voltage
$E_{t.c.}$	voltage associated with temperature at thermocouple
E_{ref}	voltage associated with temperature at reference junction
E_f	energy at frequency f
g	acceleration due to gravity
G	gain
h	convective heat transfer coefficient
J	momentum flux ratio ($\rho_j V_j^2/\rho_\infty U_\infty^2$)
k	conductivity
k_g	thermal conductivity of gas (Petit et al. (1982))
k_w	thermal conductivity of wire (Petit et al. (1982))
l	distance between thermocouple prongs
L_1	(see Figure 20)
L_2	(see Figure 20)

$\dot{W}_s$	work rate
x	streamwise coordinate (see Figure 4)
y	transverse coordinate (see Figure 4)
X	streamwise lab coordinate (see Figure 11)
Y	transverse lab coordinate (see Figure 11)
Z	lab coordinate (see Figure 11)
ρ	density
λ	time constant
ν	kinematic viscosity
η	jet coordinate (parallel to Y) (see Figure 11)
ξ	jet coordinate (tangent to jet trajectory) (see Figure 11)
ζ	jet coordinate (perpendicular to ξ and η) (see Figure 11)
Θ	non-dimensional temperature (Kamotani and Greber (1971))
$\bar{}$	mean value

PART I
TEMPERATURE MEASUREMENT SYSTEM

CHAPTER 1

INTRODUCTION

1.1 Temperature Measurements

Accurate temperature measurements have become increasingly important in many areas of combustion, heat transfer, and fluid mechanics research. The relevance of such measurements to combustion and heat transfer research is quite obvious whereas, in fluid mechanics research, one often desires to obtain information regarding a fluid flow problem by using heat as a passive contaminant to thermally mark the region of interest in the flow.

Several methods for measuring temperature exist. Bimetallic and liquid-in-glass thermometers utilize the familiar process of thermal expansion. Optical techniques include Raman Scattering and Rayleigh Scattering; both of which require sophisticated equipment (Peterson 1979). Another method uses thermistors which are in the class of sensors whose resistance changes with temperature. A thermoelectric sensor, (thermocouple) is composed of two dissimilar materials which form a closed ciruit. If the two junctions sense different temperatures, an electromotive force (emf) will be established. This effect,

which was discovered in 1821 by T.J. Seebeck, is the basis for thermoelectric temperature measurement. In 1834, J.C.A. Peltier discovered that when current flows across the junction of two metals heat is either released or absorbed at that junction. This can, therefore, cause a junction to be at a temperature different from that of its surroundings. In 1851 W. Thomson found that an additional emf is produced when there is a temperature gradient along a homogeneous wire. The total emf generated in a thermocouple is due to both the Peltier emf which is proportional to the difference in junction temperatures and the Thomson emf which is proportional to the difference between the squares of the junction temperatures. These proportionality constants depend on the two dissimilar materials used, and can in principal be found from a calibration of the thermocouple with a known temperature. In actual practice however, the total voltage is of interest and therefore the emf's generated by the Peltier and Thomson effects are not determined separately. It should be noted that irreversible Joule heating effects (I^2R) are present and will raise the temperature of the circuit above the local surroundings, however if the current in the circuit is that due to the thermoelectric effect only, Joule heating can be neglected (Doebelin 1966).

Errors involved in using thermocouples may result from radiation, conduction, or time constant effects. These effects cause the measured temperature of the probe to be different from that of the surrounding medium. The radiation error is a result of the difference in temperature caused by radiation from the wire or prongs to the surrounding walls. Conduction of heat, between the thermocouple wires

and the prongs, will introduce error into the temperature measurement This error being known as the conduction correction. The response time of the thermocouple can also result in temperature measurement errors and, of the above three effects, has received the most attention in the available literature.

Radiation from the probe is proportional to the fourth power of the temperature, and thus will have a correction which increases sharply with temperature. As pointed out by Bradley and Matthews (1968), the magnitude of the correction decreases as wire diameter decreases. Moffat (1958) performed a series of tests to determine the effect that various levels of radiation loss had on the response time of a 16 gage round-wire loop junction thermocouple. For gas temperatures up to 1600°F it was found that radiation had a small effect on the response of the probe.

The distance (l) from the temperature sensing junction to the support prongs is a critical factor if conduction effects are to be negligible. Petit et al.(1982) use the ratio $l/l_c = (2l/d_w)((k_g/k_w)Nu)^{1/2}$ to determine the relative importance of conduction effects; specifically, if $l/l_c > 10$ then conduction effects are assumed to be negligible. Bradley and Matthews (1968) use the ratio l/d_w to characterize conduction effects. The authors do not give a value for this ratio but cite some specific examples.

The response time of a thermocouple, also known as its time constant (λ), is a function of both the heat transfer coefficient (h),

and the surface area of the thermocouple bead (A_s). The heat transfer coefficient is in turn a function of velocity and temperature. The most widely used methods for the determination of the time constant are the internal heating techniques. Such techniques as proposed by Shepard and Warshawsky (1952) and Kunugi and Jinno (1959) have been employed by Petit et al. (1982), Lockwood and Moneib (1979) and Ballantyne and Moss (1977). These techniques determine the time constant based on the transient behavior of the thermocouple when the wire is run with a periodic current or after the removal of a DC current.

Petit et al.(1982) made comparisons between the internal heating technique of Shepard and Warshawsky (1952) and an external heating technique described in Petit et al. (1979). A 3.5μm dia. Pt-Rh 10% wire is subjected to a sinusoidal or square current and is located just upstream, in a known flow field, from the given thermocouple. Their results showed significant differences in the measured time constants between the internal and external heating techniques, which the authors attributed to both Joule and Peltier effects.

Compensation for the time response of the thermocouple probe can be performed using either analog or digital techniques. The basis for which electrical circuits compensate in part for the time response of the probe was formulated by Shepard and Warshawsky (1952). The electrical circuit requires a prescribed time constant for use in a differentiating circuit. Ballantyne and Moss (1977) studied the signal distortion resulting from the use of an average time constant value in the electrical circuit. The authors found that where there

were large local variations in the time constant values, significant distortion of the compensated temperature statistics resulted. In regions of moderate heat transfer fluctuations however, the analog technique would seem to work well if one could obtain a correct average value for the time constant. Lockwood and Moneib (1979), in measuring temperature fluctuations in a heated round free jet, obtained good results using this method. Digital compensation requires fast sampling rates and a moderate amount of processing time. The main advantage of using digital compensation is that an average value for the time constant need not be used, instead variations of λ, if known, could be implemented into the processing software.

Of the two junctions in a thermoelectric circuit, one is commonly referred to as a reference junction. The reference junction must be kept at a known temperature if one is to determine the temperature at the desired location. An ice bath is very common and its temperature is reproducible to about .001°C (Doebelin 1966). Another method is to allow the reference junction to sense ambient temperature; the net emf thus generated would then correspond to a temperature difference with respect to the ambient.

When using a single thermocouple, one can obtain statistical quantities of temperature at discrete locations in space or a temperature time series at a given point in space. An array of several thermocouples will provide for the above mentioned quantities and, if all thermocouples are sampled simultaneously, will also provide for instantaneous isothermal maps of the given flow field. The present

temperature measurement system is a multi-point, fast response, simultaneously sampled array of 66 thermocouples, which can be used to both evaluate the temporal evolution of the instantaneous temperature field and obtain temperature statistics at discrete values in the flow field.

1.2 The role of the Time Constant in a Temperature Measurement System

1.2.1 The First Order Response Equation

The time constant (λ) is the parameter in the first order response equation which describes the relationship between the true temperature value at the thermocouple location (T_c) as a function of the measured temperature value (T_m). This equation can be derived from a thermal energy balance for the thermocouple bead; namely

$$-\rho c \forall \, \partial T_m/\partial t = hA_s(T_m-T_c) + k_1 A_x \, \partial T/\partial x\Big]_{x_1} - k_2 A_x \, \partial T/\partial x\Big]_{x_2} \quad \text{(eq I.1)}$$

Where $\forall$ and A_s are, respectively, the volume and surface area of the bead, k_1 and k_2 are the thermal conductivities of the wires connected to the bead at x_1 and x_2, A_x is the cross sectional area of the wires and h is the convective heat transfer coefficient.

If the wire is sufficiently long with respect to the diameter of the wire (Petit et al 1982 and Bradley and Mathews 1968), then conduction is negligible. Equation I.1 then reduces to

$$-\rho c \forall (dT_m/dt) = hA_s(T_m-T_c) \quad \text{(eq. I.2)}$$

which can be written in the form

$$\lambda(dT_m/dt) + T_m = T_c \qquad \text{(eq. I.3)}$$

where $\lambda = \rho c \Psi / h A_s$. For a given wire material, i.e. for given values of ρ and c, it is seen that λ depends upon the ratio of the bead's volume to surface area (Ψ/A_s), and upon the reciprocal of the convection coefficient, h^{-1}. From convective heat transfer considerations, h is a function of the velocity and the thermal properties of the fluid. The latter may be expressed as a function of temperature for the given test section pressure, which is essentially constant for the small overheat values of the present study. Considering the former, h may be approximated as being proportional to $u^{1/2}$ for a laminar boundary layer; hence, the time constant λ would be expected to be proportional to $u^{-1/2}$.

1.2.2 The Role of λ in the Data Acquisition Process

The true temperature (T_t) may be determined from the measured temperature (T_m) if the latter measurement is supplemented with a simultaneous evaluation of λ and dT_m/dt. Specifically, consider that a high-rate time series of $T_m(t)$ values is available and that the time derivative (dT_m/dt) is evaluated from these data. T_c can then be calculated from (I.3). The data samples, so provided, could be used to form a sample population of the temperature values that exist in the flow field. The statistical values of interest can then be determined from this sample population.

The general data acquisition procedure, that is considered herein, is for three samples to be acquired in rapid sequence: $T_m)_{k-1}$, $T_m)_k$, $T_m)_{k+1}$, which allows dT_m/dt to be defined from a central difference scheme and the corresponding value of $T_c)_k$ to be computed. The $T_c)_k$ values are retained as the primitive data for further evaluation.

It is noteworthy that the mean value, of the T_c values so defined, would be independent from λ under a relatively non-restrictive assumption. Specifically, consider that the velocity magnitude (u) is simultaneously measured with the T_m value. The corrected temperature (T_c) is then given by I.3 where $\lambda=\lambda(u)$ is used for the time constant. Using an over-bar to denote the mean of the sample population and a prime to denote the deviation (i.e., difference between a given realization and its mean value), the equation for the mean value of the corrected temperature of the sample population is:

$$\overline{T}_c = \overline{T}_m + \overline{\lambda}\overline{(dT_m/dt)} + \overline{\lambda'(dT_m/dt)'} \qquad \text{(eq. I.4)}$$

For a stochastic process, $\overline{(dT_m/dt)}=0$ and $\overline{T}_c=\overline{T}_m$ if there is no correlation between the λ and (dT_m/dt) deviations.

The variance of the sample population is, however, clearly affected by the time constant value. This can be shown as follows. Subtracting I.4 from I.3 yields

$$T_c')_k = T_c)_k - \overline{T}_c = T_m)_k - \overline{T}_m + \lambda_k(dT_m/dt)_k - \overline{\lambda'(dT_m/dt)'} \qquad \text{(eq I.5)}$$

It will be assumed that the correlation: $\overline{\lambda(dT_m/dt)}$ is zero for this analysis. Given this assumption, the variance of the sample population is

$$\overline{T_c'^2} = \overline{T_m'^2} + 2\overline{T_m')_k\lambda_k(dT_m/dt_k)} + \overline{\lambda_k^2(dT_m/dt)^2} \qquad \text{(eq I.6)}$$

The second term, r.h.s. of (I.6) is not expected to have a significant value; the third term is, however, always positive and hence the sample variance for the corrected temperature will exceed that of the measured temperature if $\lambda > 0$.

The following chapters of Part I identify the physical temperature measurement system and the data acquisition scheme. Chapter 2 provides results for, and a description of the method used to determine, the time constant values for all thermocouples. A brief discussion of the velocity dependence of the time response is also included. The measured temperature value is digitally corrected for the time constant of the thermocouple; this correction scheme is explained in Chapter 3.

CHAPTER 2

TEMPERATURE MEASUREMENT SYSTEM

2.1 THE PHYSICAL SYSTEM

2.1.1 Thermocouples and Support Array

A schematic representation of the present thermocouple probe is shown in Figure 1a. The diameter of the probe body is 1.58mm and the overall length of the probe is 153mm. The micro-fine wire thermocouples (7.62 μm dia.) are supported by .235mm dia. prongs separated by 1.59mm (see Figure 1b). The thermocouples used in this study were type E which is made up of a positive conductor of nickel-chromium (chromel) and a negative conductor of copper-nickel (constantan), the sensitivity of the type E thermocouple is 42.5 μ volts/°F (Doebelin 1966).

The 72 thermocouples are supported in the array shown in Figures 2 and 3. The frame is 146mm square. There are 18 modular elements with four thermocouples supported in each modular element as shown in Figure 3. The 18 modular elements are connected by "forks" with two

of the corner elements secured to the frame. The area blockage at the measurement point is 1.5%, and at a downstream distance of 102mm, the area blockage is 42%. Figure 2.14 in Schlicting (1968) shows that the affect on the velocity field at the measurement point would be negligible even if the forks and modular elements created a 100% blockage.

2.1.2 Reference Junctions and Assembly

The 72 reference junctions for the thermocouples are located in the boundary layer bleed passage of the Free Shear Flow Laboratory (FSFL) flow facility (Figure 4). The reference junctions sense T_∞ and they have a relatively large time constant since the wire diameter is large (.8mm). The thermocouples and reference junctions are connected via 72 twisted pair shielded cables. The cables are 35 feet in length. Extra lengths of chromel and constantan were welded on to the leads of the thermocouple probes, as shown in Figure 2 , to ensure that no second thermocouple effect would be present in the measurements; i.e., if the chromel/copper or constantan/copper junctions were subjected to a temperature above the ambient value, T_∞, an additional emf would be induced.

2.1.3 Electronic Processing Units

A schematic reprsentation of one of the four electronic processing boards is shown in Figure 5. Each processing board has 20 sample and hold units (detail shown in Figure 6), one multiplexer with 32

channels and 20 amplifiers. The resistors used to amplify the thermocouple signal were metal film with a 1% tolerance; their values were selected to give a nominal gain of 500. The reference junctions were mounted on the back of the processing boards thereby reducing 60 Hz noise pickup by the leads connecting the reference junctions and processing boards. Placement of the processing boards in the FSFL flow facility can be seen in Figure 4.

The processing boards were designed and built by Sigmon Electronics.

2.1.4 Data Acquisition System

The input to the processing boards is a voltage corresponding to the temperature difference between the thermocouple probe and the associated reference junction, $T_m - T_\infty$. The signal is amplified, sampled and held, multiplexed and presented by the processing boards to a four channel TSI 1075X analog to digital converter. The multiplexers on the processing boards are controlled by a DEC DRV11 interface board which allows the user to pick the starting channel and the number of channels on each board to be read. The 12 bit analog to digital converter (A/D) has a 0-+5 volt range; therefore, the resolution of the A/D is 1.2 millivolts. By connecting all channels of the A/D to a common signal, it was found that the accuracy of the A/D was ±2.4 millivolts. The four channels have matched 50kHz input filters and are sampled simultaneously. The A/D is controlled by a direct memory

access interface board (DRV11B) which is installed in a Charles River Data Systems PDP1123 microcomputer.

2.2 System Performance Evaluation

2.2.1 Evaluation of the processing boards

Several pertinent characteristics of the processing boards were evaluated prior to the connection of the thermocouples. The characteristics checked were i) the gain for each channel, ii) simultaneous sampling of all channels and iii) the sampling rate threshold of the multiplexers. Since all 80 pairs of resistors are not identical, the amplification of the thermocouple voltages will not be identical for all channels. The evaluation of the gain (G) for each channel was performed as follows. Known d.c. voltages (E_i) were applied to the inputs (points 2,3 of Figure 6) for all channels and the previously discussed data acquisition system was used to sample the output (E_o) of each channel. For the transfer function:

$$E_o = G(E_i - E_{off}) \qquad \text{(eq. I.7)}$$

where E_{off} = offset voltage, the gain (G) was obtained by a linear regression fit to Equation I.7 for the data pairs: (E_i, E_o). The offset value, determined by a separate procedure as described in chapter 3, was performed by giving the channels a sequence of DC voltages and using the previously discussed data acquisition system to sample all channels. A linear relationship exists between the thermo-

couple reading and the input DC voltage; namely, the thermocouple reading is equal to the channel offset plus the DC voltage multiplied by the channel gain. By using a linear regression routine, the value for the gain for every channel was found.

To determine if all channels were sampled simultaneously, a common signal was input to each of the channels and the channel outputs were compared. Specifically, a nominally 200 Hz sine wave from a signal generator was applied to the channels and a visual comparison of the outputs, from various channels, showed that the sample and hold units were sampled simultaneously.

It was observed that the multiplexers would sometimes get "lost" at high sampling rates; i.e., it seemed that the multiplexers on the processing boards did not start on the user specified starting channel. This hardware problem was compensated for by the data acquisition software, as described in the following chapter.

2.2.2 Thermocouple Time Constant Evaluation

The experimental configuration, to determine the time constant values, consisted of placing a 5μm diameter tungsten hot-wire probe directly upstream of the subject thermocouple. The hot-wire probe was positioned easily and precisely by means of a traversing mechanism. This is shown schematically in Figure 7.

The data acquisition system discussed above was used to sample the subject thermocouple and the hot-wire output. During the time period that the A/D is sampling, the hot-wire anemometer is switched from operate to stand-by, thereby causing an impulsive decrease of the heating current to the hot-wire. The hot-wire has a sufficiently fast response that the thermocouple essentially senses a step change in temperature. Approximately five runs at a constant flow speed ($\simeq$ 7mps) were performed for each thermocouple.

A schematic representation of a thermocouple's response (with $\lambda \simeq$ 5msec) to the hot-wire can be seen in Figure 8. The initial flat portion of the thermocouples' response is attributed to the separation distance between the hot-wire and thermocouple, and the convection velocity. The asymptotic value of the thermocouples' response would be the laboratory temperature (T_∞) for this case.

The solution to equation 3 can be written as follows:

$$\ln\left[(T_m-T_\infty)/(T_i-T_\infty)\right] = -\lambda^{-1}t \qquad \text{(eq. I.8)}$$

The terms in equation 4 were evaluated from the time constant data as follows. T_i was the initial value of the thermocouple just before the hot-wire anemometer was switched from operate to standby, T_m was the measured value at the sequence of sample times t, and T_∞ was the steady state value reached by the thermocouple after the passage of the trailing edge of the hot-wires' thermal wake. A linear regression routine was then used to determine λ (= $-\text{slope}^{-1}$) when the data were

fit to equaton I.8.

An average value for λ was determined based on nominally five data runs per thermocouple. Consistent values of λ ,per thermocouple, were found when the hot-wire probe was placed directly upstream of the thermocouple probe. This proper placement resulted in a relatively large $T_o - T_\infty$ ($\approx$24 °F) and a low standard deviation of the data when fit to equation 4. Oscilloscope traces of the thermocouples response were also observed to be very smooth.

The procedure described above proved to be a good check on the integrity of the thermocouples. This check revealed 66 good thermocouples, for which the variability of λ at 7mps was found to be 2.0 msec to 4.7 msec. A nominal uncertainity of $\pm$0.20 msec is associated with the λ value for a given thermocouple.

2.2.3 Reynolds Number Dependence of Time constants

In addition to the data runs at 7mps, time constant values for four thermocouples were also found for the range of velocities: 2mps to 10mps. The λ(Re) results can be found in Figures 9 and 10. Figure 9 is a representation of λ vs. u and Figure 10 is a plot of λ vs $u^{-1/2}$ where u is proportional to Re for a given diameter and the nominally constant kinematic viscosity values (6% difference between v_{max} and v_{min}).

The $\lambda(u)$ results appear to approach an asymptotic value of λ for large u. The experimental results of Figure 10 support the observations made in 2.2.2; specifically that λ is proportional to $u^{-1/2}$.

CHAPTER 3

DATA ACQUISITION PROCEDURE

3.1 Offset Determination

The voltage, that is sampled by the A/D represents the net emf: $[E_{t.c.}(y,z)-E_{ref}]$, plus the offset associated with the electronic components for that channel. The offset for each channel must be subtracted from the voltages sampled by the A/D before any other processing steps can be performed; therefore, determination of the 66 offsets is an important part of the data acquisition procedure.

By placing the thermocouple array in the ambient temperature flow field of the FSFL flow facility, the temperature sensed by the thermocouples (T_m) and reference junctions (T_m) will be approximately equal. Discrepancies between the two temperatures will exist insofar as there are thermal variations within the room; these thermal variations will hereafter be referred to as "thermal noise". The voltages sampled by the A/D will then simply be the offset values for the 66 channels, note that $[E_{t.c.}(y,z,)- E_{ref}]\approx 0$ for offset determination. It is important to note that a stabilization period is required for the offsets. Apparently this stabilization period is needed to bring the

processing boards to a steady state temperature value once the boundary layer bleed suction is activated.

3.2 Sampling Rate Considerations

Referring back to equation 3 one can see that the quantity dT_m/dt is essential in determining the corrected temperature value (T_c). Evaluation of dT_m/dt is performed using a central difference technique, therefore a high sampling rate is required.

When choosing a sampling rate, the rate threshold of the multiplexers must be considered (refer to Part 1 Chapter 2). It was found that at the highest sampling rate possible for the A/D(3.125 kHz for 80 channels) the multiplexers would get "lost"; i.e. they would not start on the user prescribed starting channel and hence, the order in which the data was stored in memory would not be correct. At the next highest sampling rate (1.56 kHz) the multiplexers would start on the prescribed starting channel only a portion of the time. Therefore a check is performed in software to determine if the order that the data is stored in memory is correct. If correct, then the data run will be further processed (as will be explained in the following section) and if incorrect then the values are deleted and another data run is taken. The "lost" condition of the multiplexers improves as the sampling rate decreases and the user can choose one of six sampling rates between 20 Hz and 1.56 kHz.

3.3 Time Constant Correction and Data Storage

Two modes of data storage are available to the user of the present temperature measurement system. A time series of data is required for studying the instantaneous behavior (e.g. instantaneous isothermal maps) of the flow field in question, and a histogram, composed of statistically independent samples, is used to determine statistical quantities at the discrete locations in space occupied by the thermocouples.

The data which are sampled and stored as a time series, are taken at a high sampling rate (1.56kHz) so that the measured temperature value can be corrected as in equation I.3. This high sampling rate (.64msec) is appropriate when considering the time constants of the thermocouples ($\simeq$4.5msec at 2mps) The value for the time constant used in equation I.3 is based on a user defined velocity or it can be based on a user defined function of velocity with temperature. As explained in the previous chapter, λ values were found for all thermocouples at a convection velocity of 7mps. Using these results, and if one assumes a common slope of $\simeq 5(\text{msec})/(\text{mps})^{1/2}$ (Figure 10) for all thermocouples, the value of λ for any velocity in the range $2 \leq u \leq 10$mps can be found for each thermocouple.

As noted in the Introduction, the first order correction of the measured temperature values needs to be performed in order to obtain accurate values for statistical quantities of the data. The corrected temperature value T_c, is used to build a histogram for each thermocouple. The program is written such that the user defines the minimum, the maximum and the number of intervals for the T_c distribution. For

each data run a total of seven points per thermocouple are sorted into the correct interval of the appropriate histogram. Although there are approximately 96 kBytes of memory used for the measured temperature values per data run, only seven statistically independent samples are kept. This seemingly excess amount of raw data is required because of the high sampling rate (.64 msec) necessary for the central difference scheme. The user specifies the number of points desired to develop the histograms and the appropriate number of data runs will be taken under software control.

PART II
JET IN A CROSS FLOW EXPERIMENT

CHAPTER 1

INTRODUCTION

A jet exiting into a cross flow is an example of a complex three dimensional flow field. The interaction of the jet fluid with cross stream fluid results in two large counter rotating structures which are one of the dominant features of this flow field (Figure 12). These structures are responsible for the distribution of entrained cross stream fluid within the jet.

The interaction of the jet with cross stream fluid results in high pressures on the upstream surface of the jet column. The downstream face of the jet is characterized by low pressure values and strong entrainment of the ambient fluid. A qualitative discussion of the flow field, including surface topology effects, is presented by Foss(1980).

The deflection of the jet makes it useful to define a system of jet coordinates (ξ,η,ζ). ξ follows the jet trajectory, η is perpendicular to ξ and parallel to Y, and ζ is perpendicular to both ξ and η. Figure 12 shows this system of coordinates and the lab coordinates

X, Y, and Z.

The important parameter in this problem is the momentum flux ratio ($J=\rho_j V_j^2/\rho_\infty U_o^2$). When the cross stream and jet fluid have the same density, the velocity ratio ($R=V_j/U_o$) is often used to characterize the problem.

Some of the physical applications of a jet exiting into a cross flow are i) the discharge from a chimney stack, ii) waste discharge in rivers, and iii) the cooling of combustion gases. The latter is the motivating application for the present study.

The study of a jet exiting into a cross flow has been the subject of numerous investigations. Keffer and Baines (1962) present velocity measurements at a large number of points in the flow field, for the velocity ratio values V_j/U_o of 2,4,6,8, and 10. Isobars for the velocity ratio values of 2.2 to 10 can be found in Fearn and Weston (1975). Ramsey and Goldstein (1971) used a large diameter thermocouple (.13cm) and obtained temperature profiles of a heated jet exiting into a cross stream at low $\rho_j V_j/\rho_\infty U_\infty$ values (.1 to 2)

Kamotani and Greber (1971) provide a substantial foundation for the present work. Their study was also motivated by the combustor cooling problem and they provide velocity and mean temperature information in planes that are perpendicular to the jet axis. Extensive reference to the detailed considerations in their report are made herein. Andreopoulos (1983) in a recent publication, provides infor-

mation regarding the mean and fluctuating thermal field for J≤4.0.

These previous studies have been performed with a relatively low disturbance cross flow. The flow field in a combustor is, however disturbed and it is this cross stream disturbance effect on the dynamics of a jet in a cross flow which is the primary focus of the present study.

The present study uses thermal energy to mark the jet fluid. The temperature measurement system described in Part I is used to investigate the temperature field downstream of the jet exit. The cross stream disturbance effect is investigated by comparing the results obtained for a jet exiting into a disturbed cross flow with those for a jet exiting into an undisturbed cross flow for a given momentum flux ratio. Two groups of momentum flux ratios: J=17,19,21 and J=67,76, and 84 and three jet overheat values: (T_j-T_∞)=22.2,41.7, and 61.1 °C were used in the present experiment.

CHAPTER 2

EXPERIMENTAL EQUIPMENT AND PROCEDURE

2.1 Experimental Equipment

2.1.1 Facility for the Cross Flow

A schematic representation of the FSFL wind tunnel can be seen in Figure 12. This flow facility provides a large, planar shear layer for use in the disturbed cross flow case of the present study. Specifically the jet exhausts into the free shear layer at a location of $\bar{u}/U_{ref} = .25$ at the end of the three meter test section. The $\bar{u}/U_{ref}$ and turbulence intensity profiles based on both the free stream and local velocities can be seen in Figures 13,14 and 15. The $\bar{u}/U_{ref} = .25$ (y=80cm) location in the free shear layer was chosen based on the relatively small velocity gradient and the relatively high turbulence intensity values existing at that point (Figures 13 and 15). It is pertinent to note that, based on the energy spectrum results at y=80cm (Figure 16), the high turbulence intensity values are caused by very low frequency fluctuations. For the undisturbed cross flow case, a "false wall" added to the FSFL flow facility (shown as a dotted line

in Figure 4) resulted in a quiescent flow field at the jet exit location. The turbulent intensity at this location was ≃.6% and the energy spectrum results can be seen in Figure 17.

A boundary layer plate, the leading edge of which has a parabolic profile, was positioned 203.2mm below the top of the Test Section Extension (T.S.E.) (Figure 18). An adjustable diffuser flap, for the parallel alignment of the leading edge stream line, was attached to the downstream edge of the boundary layer plate, (Figure 19).

2.1.2 Jet Delivery System and Exit Conditions

A Spencer blower is used to provide the necessary flow rate for the jet. The exhaust from the blower is ducted into a 136cm by 101cm plenum. This is shown schematically in Figure 18. Flow enters the jet delivery tube through a 6.35mm dia. sharp edge orifice. At a downstream distance of 10mm from the entrance orifice, a static pressure tap is located in the wall of a 25mm I.D. copper pipe. The static pressure from this tap, minus that of the plenum, was used to measure the flow rate. After the right angle bend, a 50mm I.D. galvanized pipe is used to deliver the flow to the jet exit.

The jet exits through a 10[illegible] dia. sharp edge orifice (Figure 18). Care was taken to ensure that the exit plane of the jet was flush with the lower surface of the boundary layer plate. The center of the exit orifice was located 260mm downstream from the leading edge

of the boundary layer plate, as shown in Figure 19. Figures 20 and 21 are plots of the cross stream boundary layers, just upstream from the jet exit orifice, for the undisturbed and disturbed cross flow conditions respectively. Also shown in figures 19 and 20, are the reference curves for a turbulent boundary layer in a zero pressure gradient flow, viz., $\bar{u}/U_\infty = (y/\delta)^{1/7}$, and the Blasius solution for a laminar boundary layer.

2.1.3 Jet Heating Considerations

A Superior Electric powerstat was used to supply a controlled voltage level, to a flexible resistance strip heater. The strip heater was wrapped around the copper delivery pipe in the plenum above the T.S.E.. Fiberglass insulation, 220mm in dia., was placed around both the strip heater/copper pipe and the galvanized delivery pipe to protect from heat loss to the surrounding plenum and/or cross flow (Figure 18). A reference thermocouple (wire dia of .254mm) is located 10mm upstream from the jet exit and was used to monitor the jet temperature. The leads of the thermocouple extend through the sides of the pipe and are connected via one of the shielded cables, to a channel on the processing boards.

2.2 Experimental Procedure

2.2.1 Velocity and Jet Temperature Determination

The cross stream velocity, (U_o), was determined, for the undisturbed cross flow case, by using a pitot-static pressure probe placed in the free stream of the FSFL flow facility. For the disturbed cross flow study, the U_o value was 1/4 of the velocity calculated from the pressure probe reading.

The mass flow rate through the delivery tube was determined using the static pressure (downstream from the entrance orifice) and the plenum pressure. The discharge coefficient, (C_d), which is required to correct for the non-uniform velocity profile at the orifice, was known a-priori as a function of pressure drop across the orifice. A thermometer located in the plenum, provided for the density value used in the flow rate calculation. The average jet velocity (V_j) was determined from the calculated mass flow rate.

The output from the reference thermocouple, used to monitor the jet temperature, is sampled using the previously discussed data acquisition system. Knowing the sensitivity of the type E thermocouple, 76.5μmvolts/°C, an output voltage corresponding to the desired jet temperature can be calculated. The desired output from the reference thermocouple is obtained by adjusting the voltage level of the powerstat.

It was found that a period of approximately one hour was required for the jet temperature to stabilize, however a period of three hours was required for the jet mass flow rate to stabilize. The latter was a direct result of the initial transient period of the Spencer blower.

2.2.3 The Temperature Measurement System

The results of Kamotani and Greber (1971) were used to determine an appropriate position of the thermocouple array with respect to the jet exit location. Their results include the V_j/U_o values of interest (4 and 8) for the present study. The thermocouple array was positioned in X/d (±0.25) corresponding to the chosen ξ/d value. The Z/d position (±0.35) was chosen such that the maximum amount of temperature field information would be obtained. (The Y/d (±0.25) placement was to simply center the array with respect to the jet exit.) The array was mounted on a pair of dove tail traverses, allowing for X and Y positioning, which were mounted on an aluminum plate positioned in Z by a scissors jack (see Figure 19). The measurement plane of the present study was located at X/D = 3.9 for the lower momentum flux ratios: Jξ21 and then moved to X/D = 3.5 for the higher momentum flux ratios: J267 where the displacement: ΔX/D, was accurately controlled: ±0.05.

The data acquisition procedure, discussed in Part I Chapter 3, is used to acquire the data for the present study. The following features are specific to the present experiment. i) The offsets asso-

ciated with the channels of the processing boards require a stabilization period (as noted in Part 1 Chapter 3), which was found to be approximately 45 minutes for the present study. ii) The sampling rate of 1.56 kHz (.64msec) is appropriate when considering the central difference scheme used to evaluate the term dT_m/dt; that is, .128 jet diameters of fluid will be convected downstream every .64msec. This estimate of the convected distance is based on a convection velocity of 2mps which is the value of the free stream velocity for all cases.

CHAPTER 3

DISCUSSION OF EXPERIMENTAL RESULTS

3.1 Introduction to Discussion of Results

The primary motivation for this experimental program was to determine the effects of cross stream disturbance on the jet in a cross flow problem. A secondary body of results is also presented; the influence of the momentum flux ratio in the ranges: $17 \lesssim J \lesssim 21$ and $67 \lesssim J \lesssim 84$, on the location of the jet column. This secondary body of results will be discussed after the general features of the measurements are identified. The influence of the disturbed cross stream will then be considered.

The influence of assuming that time constant values for each thermocouple could be taken as $\lambda=\lambda(2mps)$, was evaluated by processing one (high-rate time series) data set with the λ values: $\lambda=\lambda(5mps)$ and $\lambda=0$. The former represents an upper bound for the expected velocities at the X/d plane of the measurements (Kamotani and Greber (1971)) and the latter represents the absence of a time constant correction. From the considerations in article I.1.2.2, it is expected that negligible differences in the mean values of the measured ($\lambda=0$) and the

corrected: λ(2mps) and λ(5mps) should be obtained. Also, it is expected that the rms temperature values should vary as T'^2 (λ=0) < T'^2 (λ(5mps)) < T'^2 (λ(2mps)).

Using one of the time series data sets for: J=84, $T_j - T_\infty = 61.1^\circ C$, and a disturbed cross flow, the results shown in the following table were obtained.

	$T_R(\lambda) - \bar{T}_R(\lambda(2mps))$			$T_R'^2 - T_R'^2(\lambda(2mps))$		
	min	median	max	min	median	max
λ=0	-0.63	0.05	0.73	1.65	6.0	17.86
λ=5	-0.15	0.03	0.19	0.84	2.0	7.0

TABLE II.1 Influence of λ on measured temperature values.

Note: The "min", "median", and "max" refer to a given thermocouple (1-of-64) in the array.

The relatively small differences between the 2 and 5 mps time constant conditions support the inferrence that the use of a constant λ value does not exert a significant influence on the present results.

The temperature field results are most easily interpreted if the conduction of energy through the nozzle plate, and the corresponding thermal contamination of the boundary layer fluid, can be neglected. The magnitude of this contamination can be conservatively estimated by assuming that a thermal boundary layer began at the juncture of the nozzle plate and the boundary layer plate (L_1). A measure of the contamination is provided by the assumed two-dimensional boundary layer at the location of the jet centerline. Using the apapropriate heat

transfer relationship for this laminar boundary layer (e.g., Gebhart (1971)):

$$q = .664\ k\ (T_w - T_\infty)\ (U_\infty/\nu)^{1/2}\ (L_2^{1/2} - L_1^{1/2}) \qquad \text{(eq. II.1)}$$

and equating this to the flux of thermal energy carried by the boundary layer:

$$q = \int \rho c_p\ (T - T_\infty)\ u\ dy \qquad \text{(eq II.2)}$$

one can solve for the "non-dimensional thermal contamination measure":

$$\int \left[\ (T-T_\infty)/(T_w-T_\infty)\ \right]\ (u/U_\infty)\ d(y/d) =$$

$$.664\ (k/\rho c_p)/(U_\infty d)(U_\infty/\nu)^{1/2}\ ((L_2)^{1/2}-(L_1)^{1/2}) =$$

$$1.4 \times 10^{-2} \qquad \text{(eq. II.3)}$$

for U_∞ = 2mps and L_2=260mm and L_1 = 213mm. Hence, it is inferred that the boundary layer heating effect is of negligible importance for this flow field.

3.2 Thermal Energy Considerations

Applying the energy equation to the control volume shown in figure 21 one obtains

$$\dot{Q}-\dot{W}_s=d/dt_{c.v.}\int(V_I^2/2+gz+\tilde{u})\rho dV+_{c.s.}\int(V_I^2/2+gz+\tilde{u}+p/\rho)\rho V\cdot ndA \quad (II.4)$$

Assuming i) steady state, ii) heat-transfer rate and work rate between system and surroundings = 0, and iii) that the kinetic energy term is small compared with the enthalpy term, $(h=p/\rho+\tilde{u})$, equation II.4 reduces to

$$\int_{c.s._1} \rho c_p T\ V\cdot n\ dA = \int_{c.s._2} \rho c_p T\ V\cdot n\ dA \qquad \text{(eq. II.5)}$$

The above integral quantities if evaluated, would provide a good check on the experimental data; however, velocity information is not available from the present study. The present results provide contours of constant temperature (isotherms) for both the mean flow field and the instantaneous flow field. These results show that, at the X-location of the thermocouple array, both the mean and instantaneous temperatures existing in this flow field are substantially lower than the initial jet temperature. Namely, the peak temperatures do not exceed the value; $0.25(T_j-T_\infty)$. Equivalently, this result shows that substantial diffusion (i.e. molecular transfer) of thermal energy has occured between the jet exit and the observation plane since this is the sole agent that can reduce the energy state of a given fluid element. From (II.5), and for jet velocities which are approximately

equal to the cross stream velocity, it is apparent that the contamination field at c.s. 2 must be much larger than the area of the jet orifice. This characteristic of the isotherms is quite apparent as noted below.

3.3 Jet temperature considerations

For the present experiment, it was desired to use thermal energy as a passive scalar contaminant with which to mark the jet fluid. The passive contaminant assumption is given strong support by the Kamotoni and Greber (1971) study wherein T_j-T_∞=41.7°C and 177.8°C overheat values resulted in a quite small (≃2 percent) change in the z position of the maximum temperature.

This small change was observed at the x/d location of the present study and the change was opposite to that expected if a buoyancy effect were responsible. The effect of buoyancy is expected to be negligible since the Richardson number ($R_i=g(T_j-T_\infty)d/U_o^2T_r$) for the present study is small (R_i=0.005), see Townsend (1976). Figures 22-33 represent the mean isotherms for the momentum flux ratios: (J) of $17\leq J\leq 21$ and $67\leq J\leq 84$, and for three different overheat conditions: T_j-T_∞=22.2,41.7,and 61.1 °C for both the undisturbed and disturbed cross flow cases. These contours were obtained using the Surface II contouring package on the Cyber 750 at Michigan State University. The + signs on the figures represent the positions occupied by the thermocouples. The coordinates of all contours are those of the thermocouple array (s and t). (It is pertinent to note that the posi-

tion of the thermocouple array was not changed as the jet temperature was changed for a given J value.) Listed in the caption of each figure are the transformation equations between the array coordinates and the jet exit coordinates. The numerical values of the isotherms represent $1000x(T_c-T_\infty)/(T_j-T_\infty) = T_R$.

Figure 34 is a plot of the s component of the centroid as a function of momentum flux ratio for the several cases investigated. The centroid represents an integral measure of the temperature field; in this sense it represents a smoothing of the discrete data samples. The centroid was calculated by the equation

$$s_{c.g.} = \sum s_I A_I \,/\, \sum A_I \,, \quad t_{c.g.} = \sum t_I A_I \,/\, \sum A_I \qquad \text{(eq. II.6)}$$

where s_I is the s component of the centroid for each isotherm and A_I represents the area of each isotherm and was calculated using the digitizer on the Prime computer at Michigan State University.

The results, shown in Figure 34 are quite instructive. Firstly, the local variation in J, created by varying T_j with a constant volume flow rate into the heater tube, shows that the resulting centroid-momentum flux relationship is consistent with the global variations created by the increase in the volume flow rate. Secondly, a consistent pattern, from the four (experimentally independent) sets of data, is revealed wherein the jet penetration for the disturbed cross stream is less than that for the undisturbed case at the same J value. (Incidentally, the consistency of this pattern suggests that the

uncertainty estimate (±0.7) for the s-z transformation is too conservative.) As noted on the figure, the X/d locations of the two groups of momentum flux values are slightly different; it is inferred that the trend of increasing centroid distance, with respect to the J value, would be even more steep if the correction for the 11% change in X/d could be accounted for in this graphical representation. The influence of the isotherms, selected for the centroid evaluation, is seen to be a second order factor in the above interpretations. (The lack of a complete set of isotherms, within the space of the thermocouple array, required the calculation of the two "centroid" values that are presented in Figure 34 for the large J values.)

An alternative method of calculating the centroid is to consider the measured temperature as a discrete "mass" point and to compute the centroid of the distributed field of such "mass" points. Specifically, the centroid was calculated using the equation

$$s_{c.g.} = \sum s_i T_R \,/\, \sum T_R \quad , \quad t_{c.g.} = \sum t_i T_R \,/\, \sum T_R \qquad \text{(eq. II.7)}$$

where s_i, t_i are the coordinates for a given thermocouple. The results of this technique are not considered to be as valid a measure of the thermal field; however, this calculation is dramatically easier to execute and it will be employed where the use of the digitized isotherm contours would be impractical; see Section 3.5. The centroid results, using this method, are not presented herein. However, it is pertinent to note that the centroids, inferred from the isotherms,

show a much larger variation, and a more regular dependence upon, the momentum flux values than the centroids calculated from the discrete mass points.

A noteworthy aspect of the mean isotherms is the trend: "the maximum mean temperature decreases with increasing overheat". This decrease in maximum mean temperature can be seen in the mean isotherms for both the disturbed and undisturbed cross flow conditions (Figures 22-33).

The momentum flux ratio influence can also be seen when looking at the histograms obtained for all thermocouples in the thermocouple array. A selected few of these histograms can be seen in figures 35-42. Figures 35,37,39,and 41 represent the histograms for a thermocouple located in approximately the center of the jet while figures 36,38,40,and 42 are the histograms for thermocouples located farther from the boundary layer plate.

3.4 Comparison of Present Results with Kamotani and Greber

Significant differences can be found when comparing the mean isotherms of Kamotani and Greber (1971) with those of the present study. The absence of kidney shaped isotherms is one factor albeit this may relate to the vertical vs. the jet-axis-normal plane of the data. Compounding this difference in observation planes is the effect of an increased jet penetration and therefore the steep intersection between the jet column and the X/D= constant mearsurement plane. The

"steep intersection" is described in the following.

In order to compare the present results with these of Kamotani and Greber, it is required to provide a common momentum flux ratio as well as the same X/D location. Their comprehensive data for $Z_m(x)$ (i.e., the Z location of the maximum temperature) readily allows the latter; more complicated steps are required to provide the "same" momentum flux ratio. The apparently linear variation of $Z_{c.g.}$ with respect to J (see Figure 34) allows an approximate interpolation between the measured conditions, of the present study, to obtain a $Z_{c.g.}$ value that would correspond to the $R=8=V_j/U_0$ value of the Kamotani and Greber investigation.

Their equivalent J value is inferred to be:

$$J = \rho_j V_j^2 / \rho_0 U_0^2$$
$$= (T_0/T_j)R^2$$
$$= (530/600)8^2 = 56.5$$

and the corresponding $Z_{c.g.}$ value (from Figure 34) of the present study is 12.5.

The minor effect of the different X/D values (3.9 cf 3.5), was neglected in arriving at this value. A ratio of 1.03 was noted for $(Z_m/Z_{c.g.})$ for the present data. Combining these observations allows an estimated Z_m value to be added to the Kamotani and Greber centerline distribution; see Figure 43a. It is noted that the present jet penetration is much greater than for their study. A similar procedure

could not be readily executed for the lower R value: 4, of their study since it would have required an extrapolation from R=19 to R=14.1 on Figure 34. However, the inverse process: adding their data to a modified Figure 34, could be executed and the results are presented in Figure 43b. For this calculation, the $Z_m/Z_{c.g.}$ ratio was 1.11. It is again noted that the $Z_{c.g.}$ values are substantially greater for the present investigation.

It is inferred that the boundary conditions are responsible for depths for the strong differences in the penetration depths for the two studies. Specifically, the increased penetration of the jet for the present study is attributed to the higher effective momentum flux ratio which results from using the average velocity exiting from the sharp edge orifice. The velocity profile at the exit of the nozzle used by Kamotani and Greber (1971) is inherently more uniform than that at the exit of a sharp edge orifice and the momentum flux ratio, based on an average velocity, will be less for their nozzle. Another important difference between the two experiments is the cross stream boundary layer thickness compared with the jet exit diameter; $\delta/d < .1$ for Kamotani and Greber, $\delta/d \simeq 1.3$ for the present experiment.

3.5 Comparison of undisturbed with disturbed cross flow conditions

Figures 28-33 are contours of mean isotherms for the case where the jet exits into a disturbed cross flow. The shapes of these contours are very similar to those for the undisturbed cross flow case, (Figures 22-27); however, the maximum mean values for the disturbed

cross flow case are significantly lower than those for the undisturbed cross flow case. Additional differences are reflected in the contours of constant temperature standard deviations (Figures 44-55) and the associated histograms (Figures 35-42).

The contours of constant standard deviation show dramatic differences between the disturbed and undisturbed cross flow conditions. The values of the standard deviations are larger for the disturbed cross flow condition and the temperature standard deviation field is larger than that for the undisturbed case.

The histograms reveal a great deal of information regarding the differences between the undisturbed and disturbed cross flow cases. For example, compare figures 35 and 39. These two figures represent the histograms for thermocouples located near the maximum contour level for the specified J value and for the undisturbed and disturbed cross flow conditions respectively. The bimodal characteristic for the disturbed cross flow case, shows that ambient (cross stream) temperature fluid occupied this point in space for a significant fraction of time. Similar histograms exist for the larger J values; see Figure 37 and 41. These suggest that the jet trajectory excursions are a significant fraction of the jet width for the disturbed cross flow cases.

Six instantaneous time series, each approximately .8 seconds in length, were taken and stored for the $T_j-T_\infty=61.1^\circ C$ overheat cases: J=21 and 84, disturbed and undisturbed cross flow conditions. These

	J	$\sigma_{s_{c.g.}}$	$\sigma_{t_{c.g.}}$	K_{st}
undisturbed c.f.	21	.341	.253	.067
undisturbed c.f.	84	.233	.233	-0.13
disturbed c.f.	21	1.84	1.45	-0.33
disturbed c.f.	84	1.16	1.12	-0.45

TABLE II.2 Cross stream disturbance effect on centroid of temperature field

time series were formed from periodic (Δt=0.64msec) and simultaneous samples of the 64 thermocouples. The centroid ($s_{c.g.}, t_{c.g.}$) of the instantaneous temperature field was determined using equation II.7 and representative time series for the four cases are shown in Figures 56-59. (Note that the two coordinates of the centroid: $s_{c.g.}$ and $t_{c.g.}$, are shown separately). The increased movement of the jet column for the disturbed cross flow case is clearly seen in these figures. The following table shows the results using all six of the time series for the disturbed cross flow case and three of the time series for the undisturbed cross flow case.

The correlation coefficient ($K_{st}=\overline{s't'}/(\sigma_s\sigma_t)$ results presented in the above table show that the Y and Z motions of the jet are significantly correlated for the disturbed cross flow case. This correlation is considered to be representative of the cross flow itself rather the dynamics of a jet in a disturbed cross flow. That is, the $\overline{v'w'}$ correlation, that is suggested by the K_{st} values, would be expected from the large-scale secondary motion, for the related problem of a bounded jet, as documented by Holdeman and Foss (19). The time series records, Figures 56-59, indicate a low frequency translation of the

centroid. This is qualitatively similar to the (hot-wire anemometer derived) energy spectrum results presented in Figure 16.

Instantaneous isotherms can also be generated from the time series taken at the high sampling rate. A selected few of these isotherms are shown in Figures 60-67. These isotherms were selected based on the centroid time series shown in Figures 56-59. Referring to figures 56 and 57 (J=21), one can see that at approximately .2 and .65 seconds there are peak excursions of the jet centerline for the disturbed cross flow case. The isotherms for both the disturbed and undisturbed cross flow case at these two instants in time are shown in Figures 60-63. At the discrete points in time of approximately .3 and .58 seconds, figures 58 and 59 (J=84) show peak excursions of the jet centerline. The corresponding contours can be seen in Figures 64-67.

The migrating jet column is clearly seen when comparing the disturbed cross flow isotherms. For the disturbed cross flow, J=84, contours shown in Figures 66 and 67, the excursion is so great that the resulting two temperature fields hardly overlap. This is also true for the J=21 contours seen in Figures 62 and 63. The migration of the jet column for the undisturbed cross flow case is not as severe as can be seen in Figures 60,61,64,and 65.

Comparing the instantaneous contours with the mean contours, one can see that the differences are greater for the disturbed cross flow case. The maximum values for the instantaneous contours of the disturbed cross flow case are much larger than those of the mean

contours. The maximum instantaneous values for the disturbed cross flow case do not differ significantly from those for the undisturbed cross flow case. The mean temperature values are much lower however, because of the jet centerline excursions.

CHAPTER 4

CONCLUSIONS

The following conclusions are based on the results of the present study.

i) Substantial diffusion of thermal energy has occurred between the exit plane and measurement location, since the maximum temperatures recorded were $<.25(T_{jet}-T_{\infty})$ for both the undisturbed and disturbed cross flow cases.

ii) The present data allow the sensitivity of the jet penetration, to the magnitude of the momentum flux, to be quantified. In general, the disturbed cross stream case is less sensitive to the momentum flux rationalbeit the differences, between these two conditions, are neither large nor simply expressed.

iii) The present results show that the centroid of a heated jet has much larger excursions, for the jet exiting into a highly disturbed cross flow than for a jet exiting into an undisturbed cross flow.

iv) For both the undisturbed and disturbed cross flow cases, an instantaneous isotherm pattern can be significantly different from the mean isotherm pattern and this difference is more dramatic for the disturbed cross flow case. Specifically, the instantaneous maximum temperatures for the disturbed flow are similar in magnitude to those of the undisturbed case whereas the maximum mean temperature is substantially less for the disturbed cross flow compared with the undisturbed cross flow case.

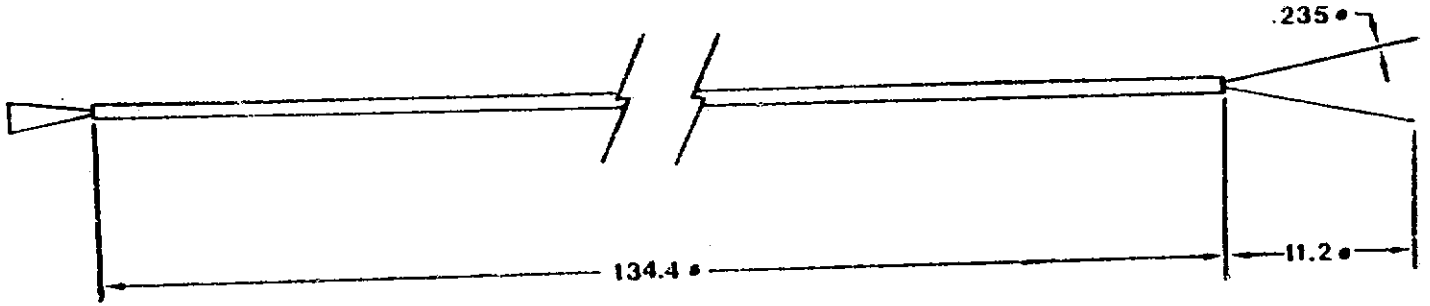

a) Dimensions of the Thermocouple Probe

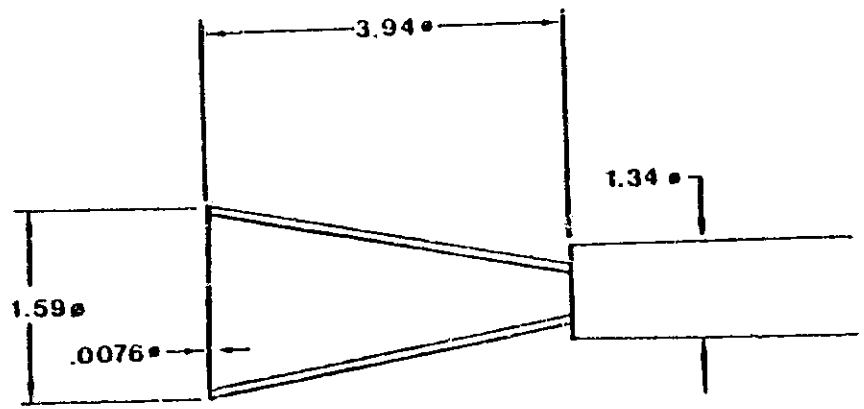

b) Detail of Temperature Sensing Junction

Figure 1. The Temperature Sensing Probe

Figure 2. Themocouple Array Assembly

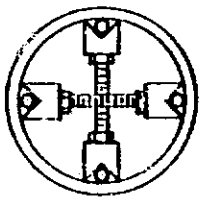

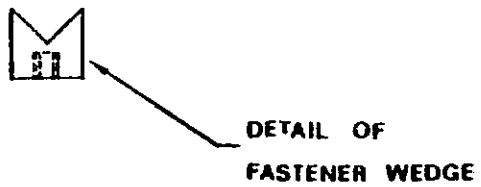

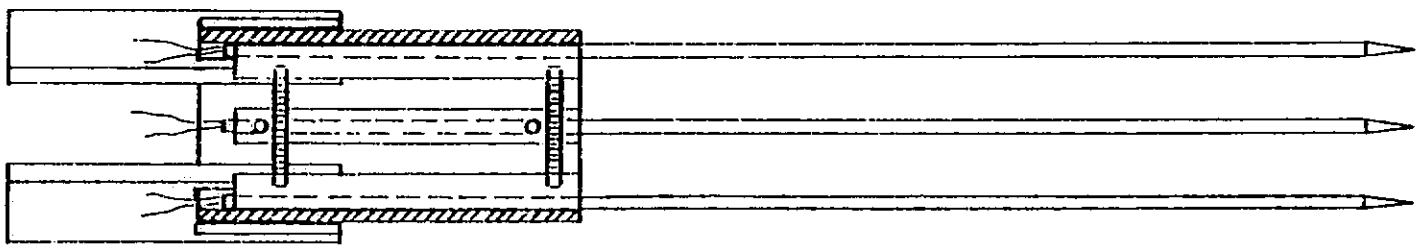

Figure 3. 1 of 18 Thermocouple Modular Elements

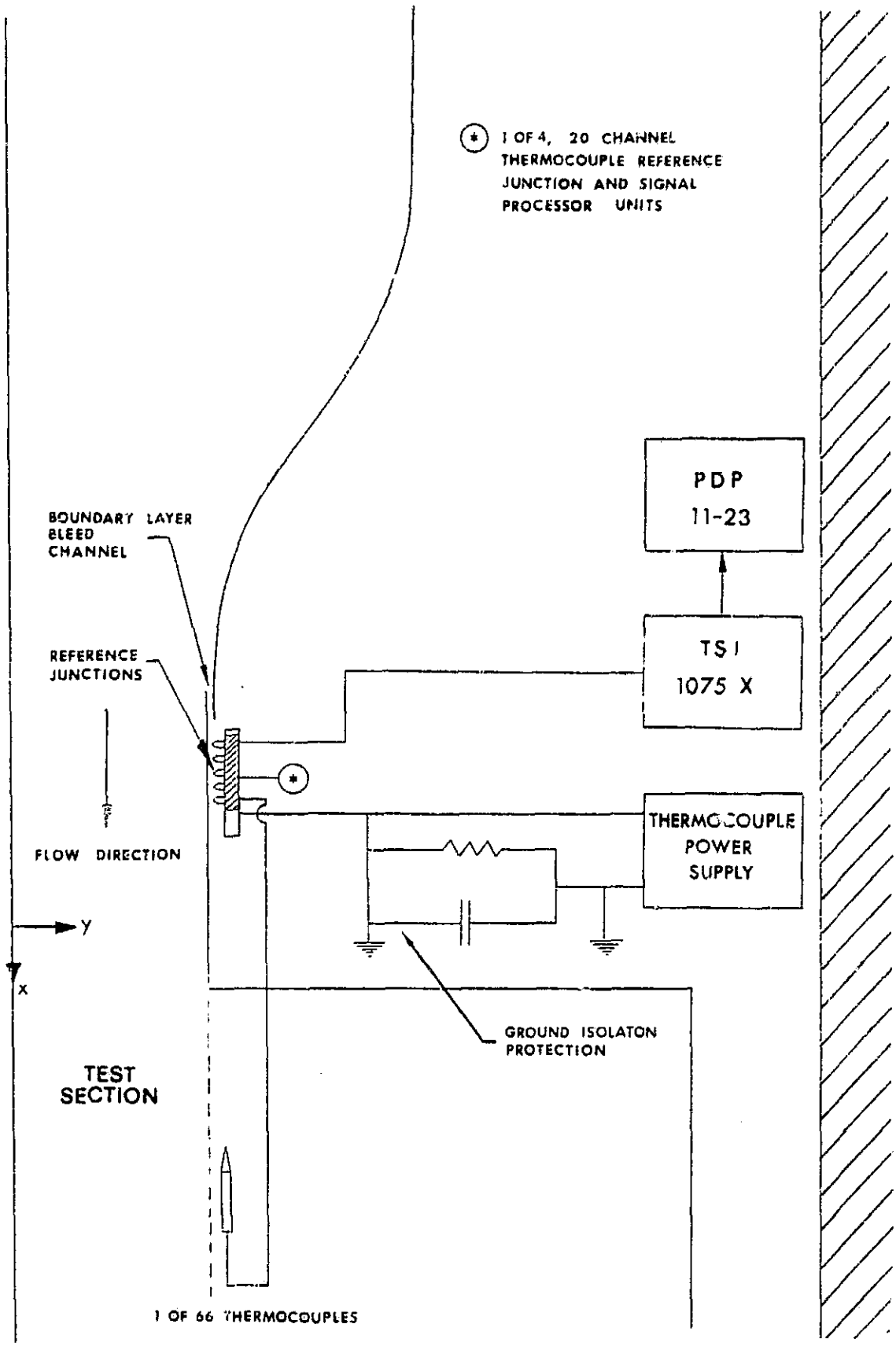

Figure 4. Schematic Representation of the Present Flow Facility

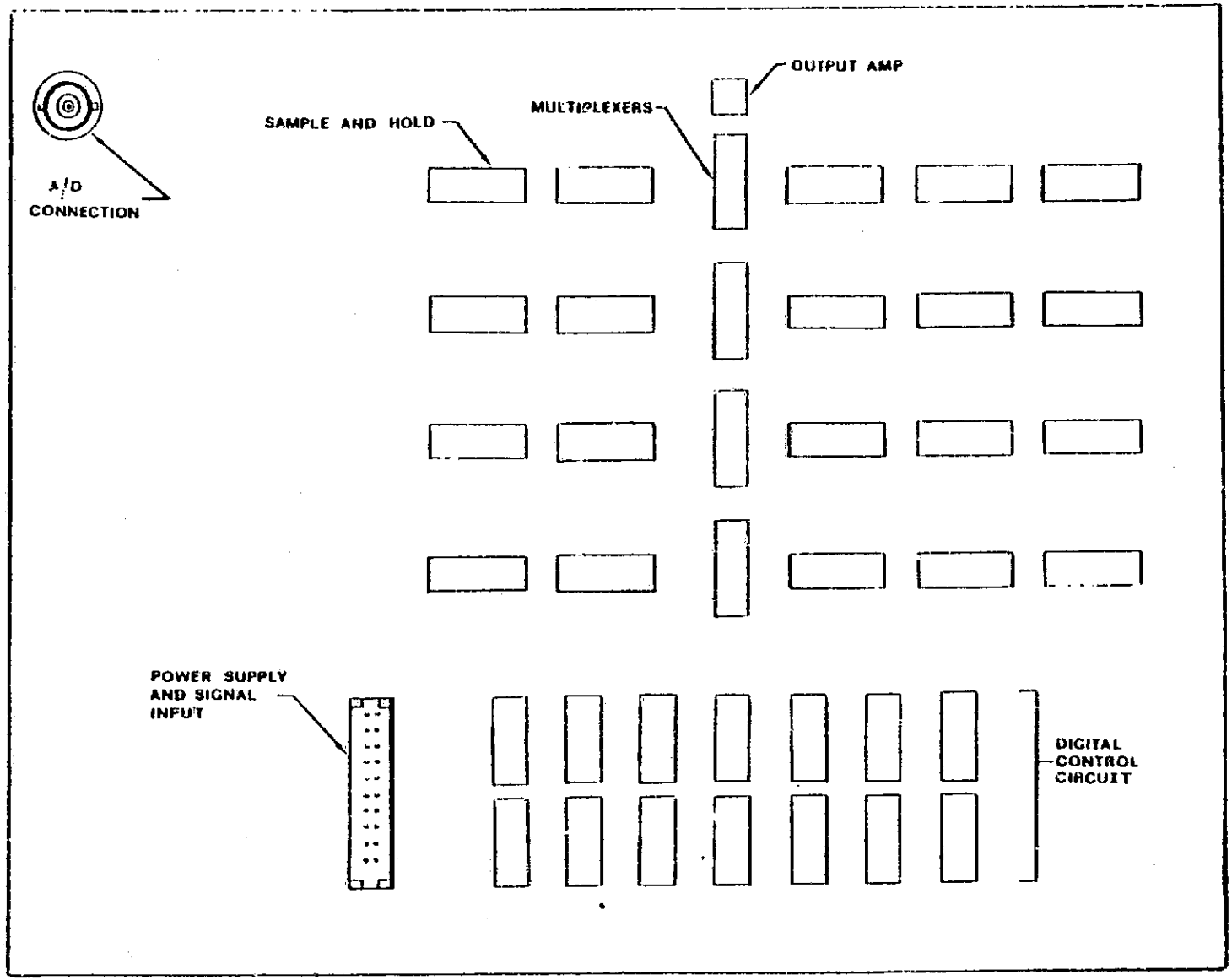

Figure 5. Schematic Representation of One of Four Electronic Processing Boards

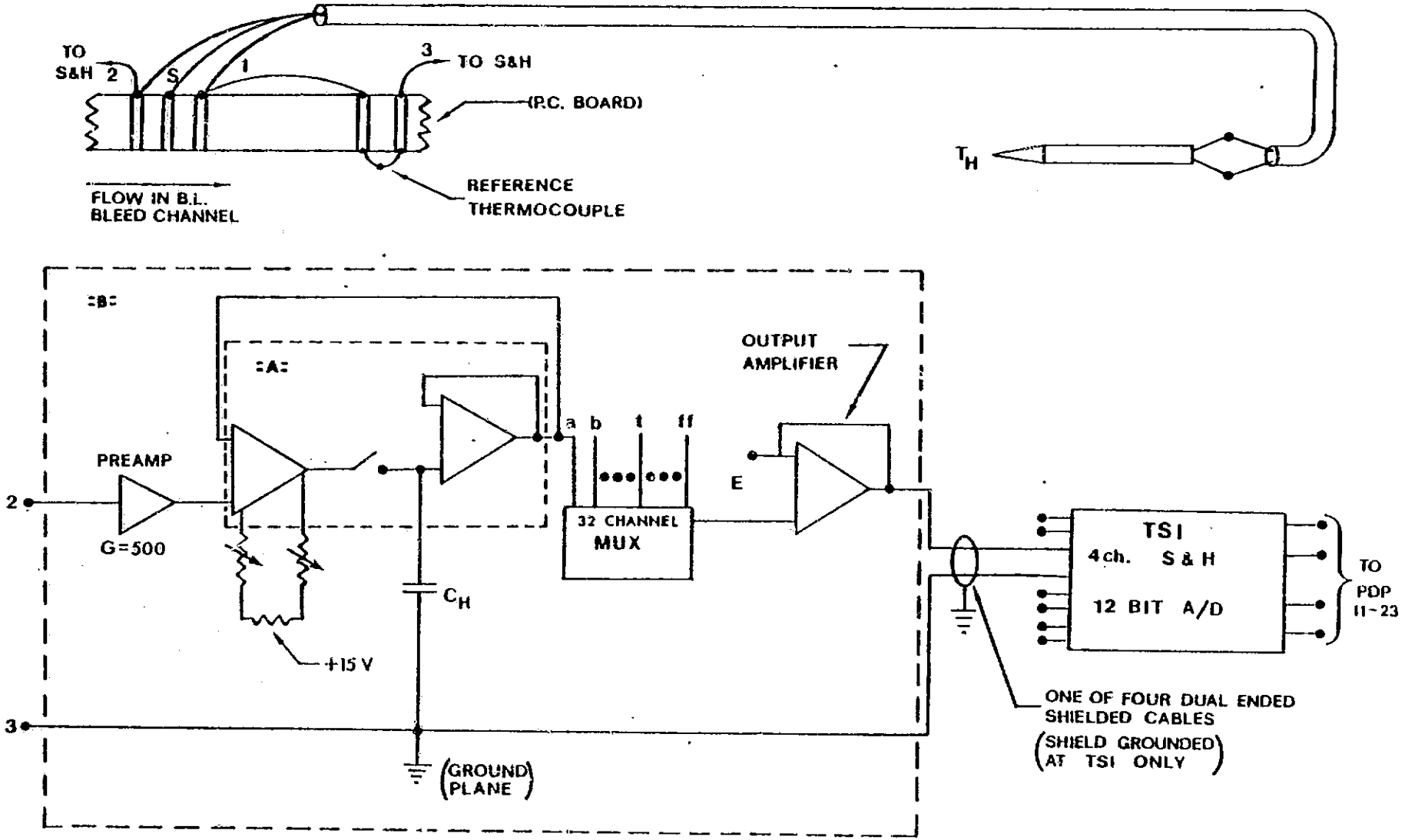

Figure 6. Detail of a Sample and Hold Circuit

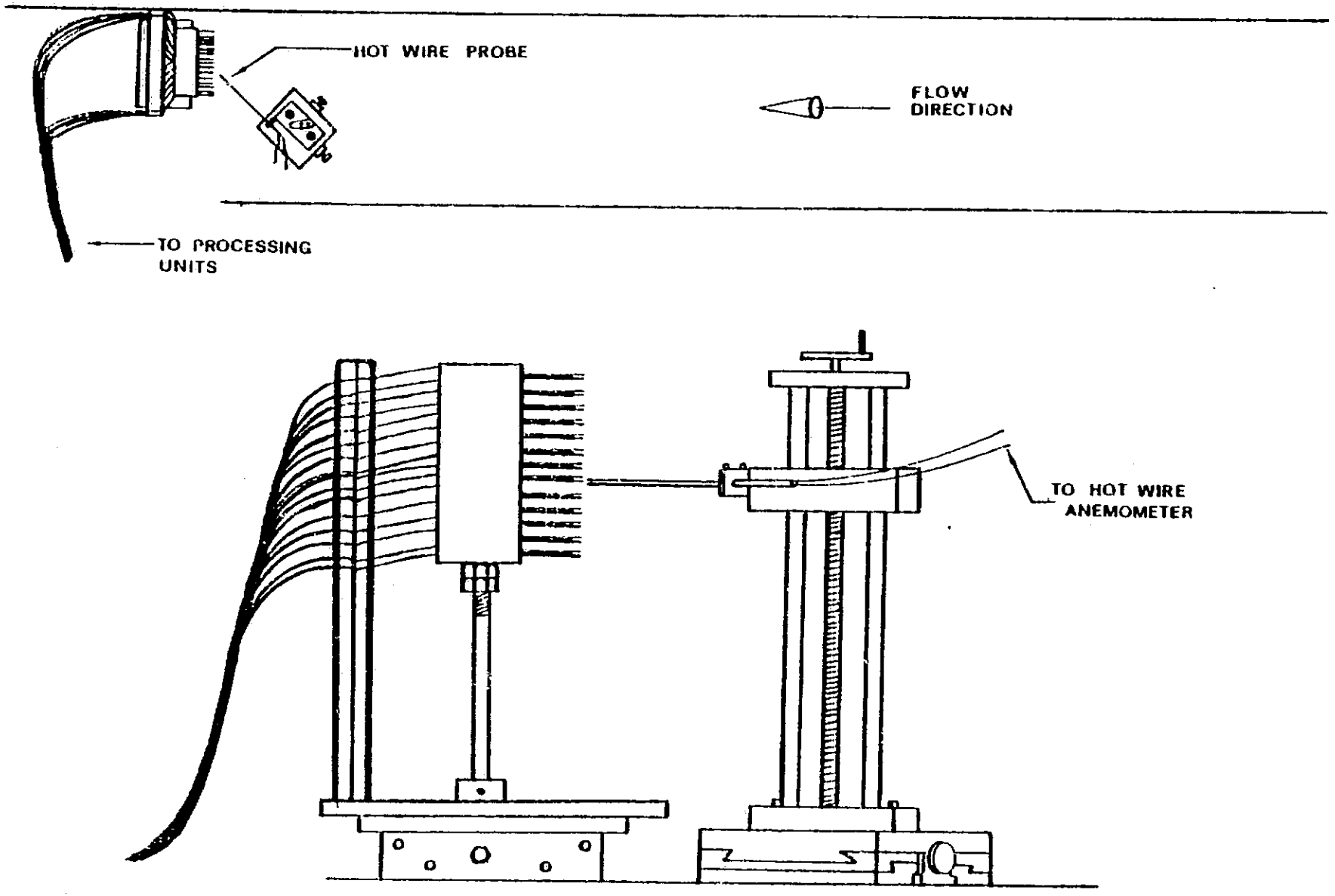

Figure 7. Experimental Configuration for the Time Constant Evaluation

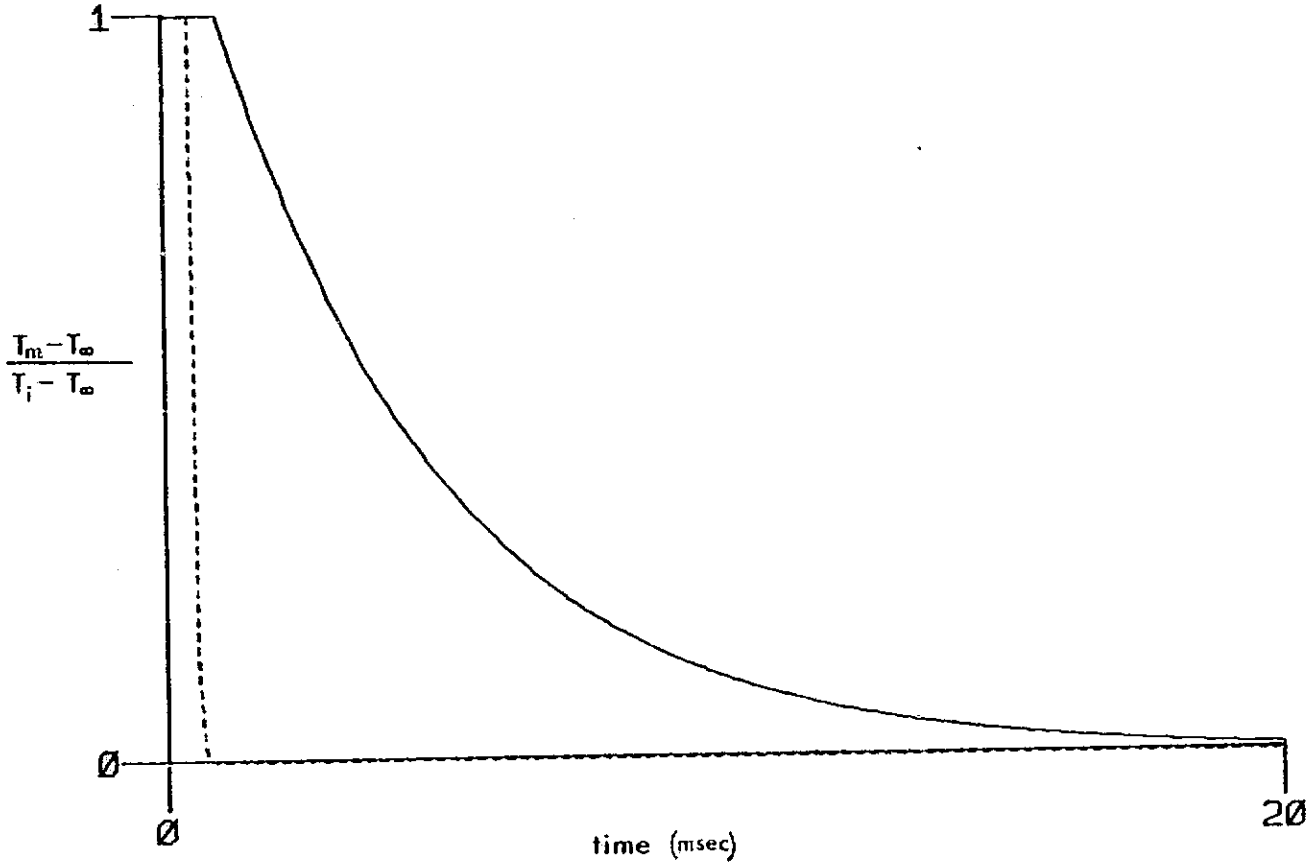

Figure 8. Schematic Representation of a Thermocouples Response to the Impulsive Removal of a Thermal Input

NOTE: A 5 msec time constant is used for this representation.

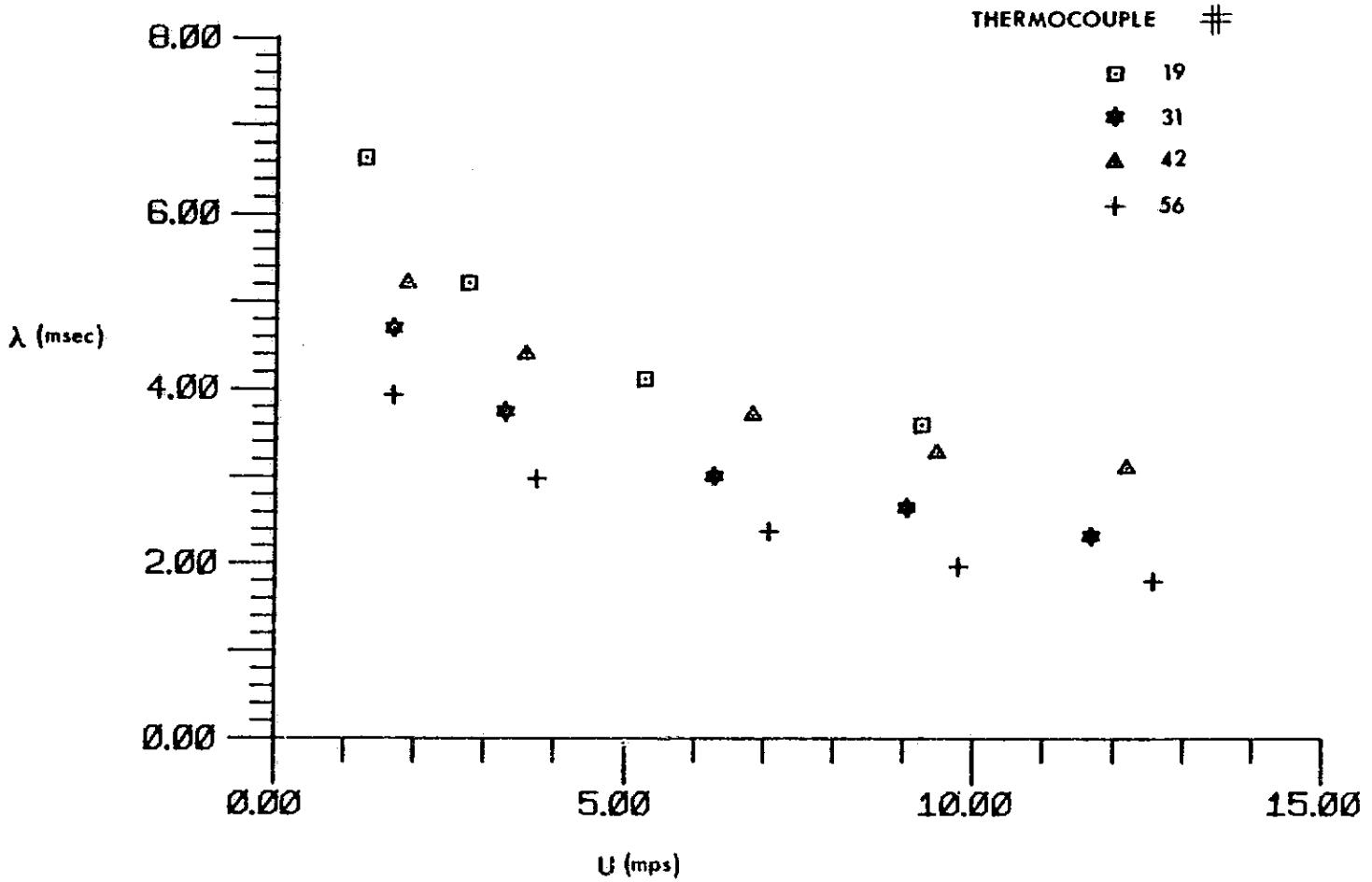

Figure 9. Plot of Time Constant (λ) as a Function of Velocity (u)

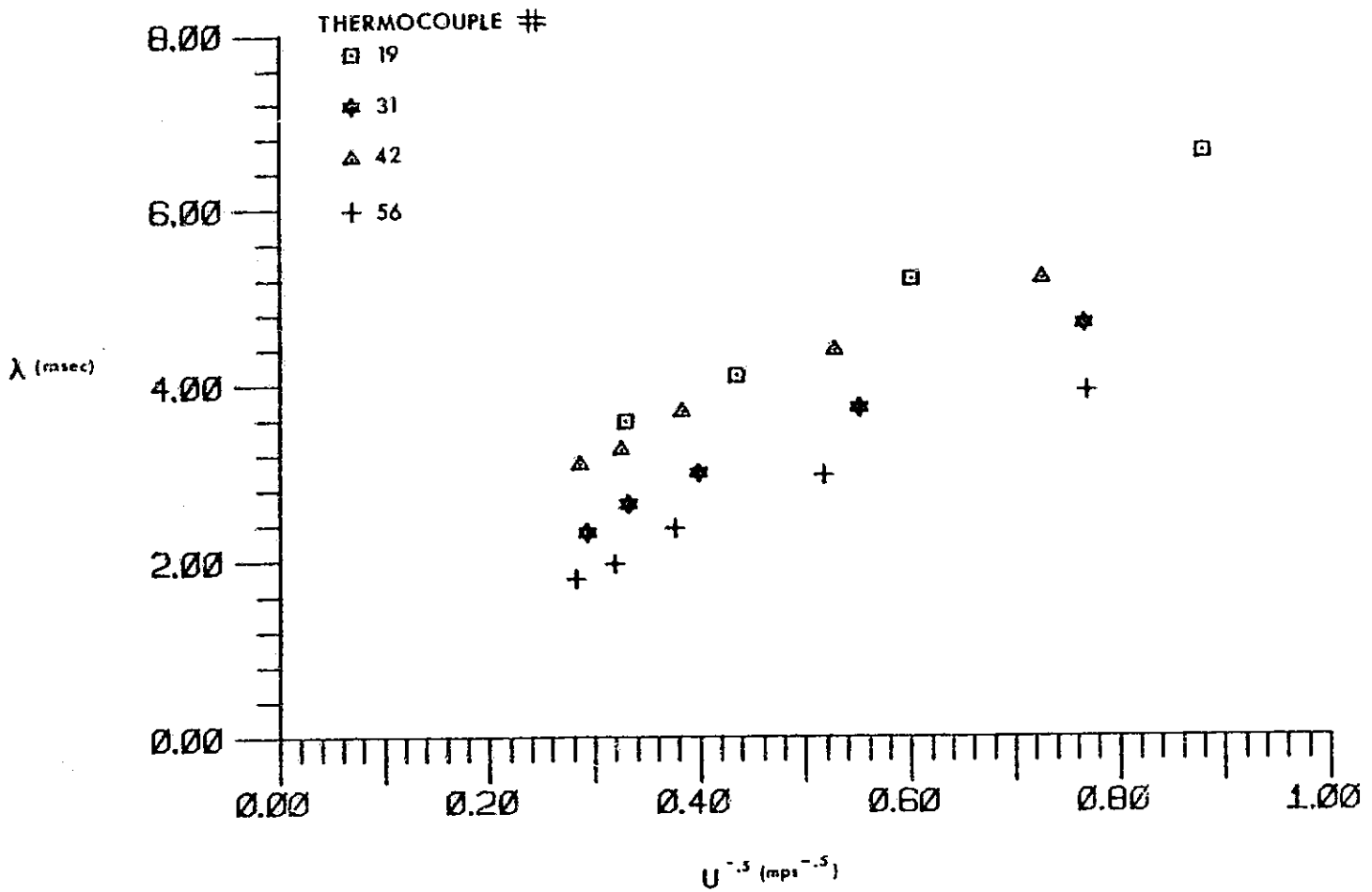

Figure 10. Reynolds Number Dependence of λ

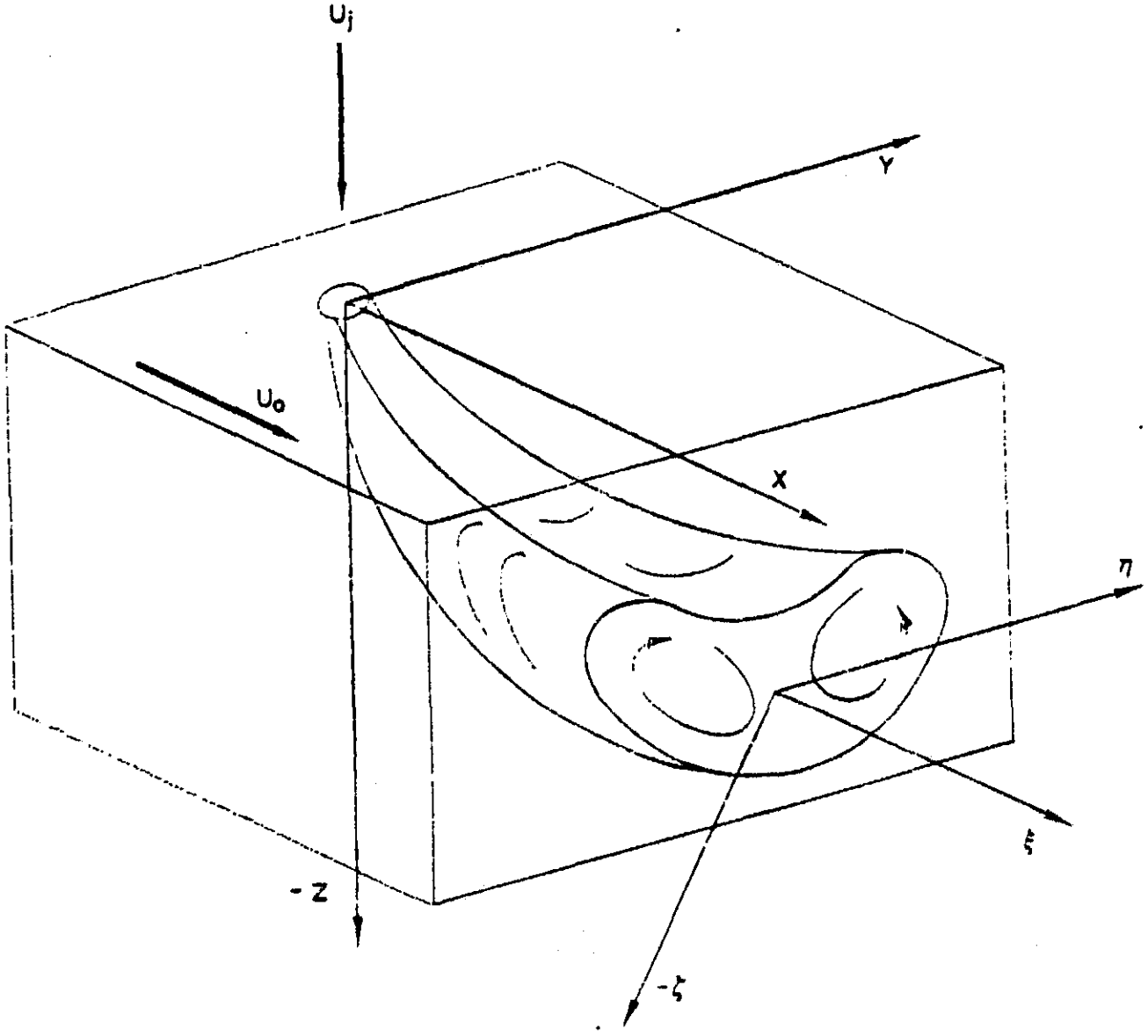

Figure 11. Schematic Representation of Jet Trajectory, Showing Lab Coordinates (x, y, z) and Jet Coordinates (ξ, η, ζ)

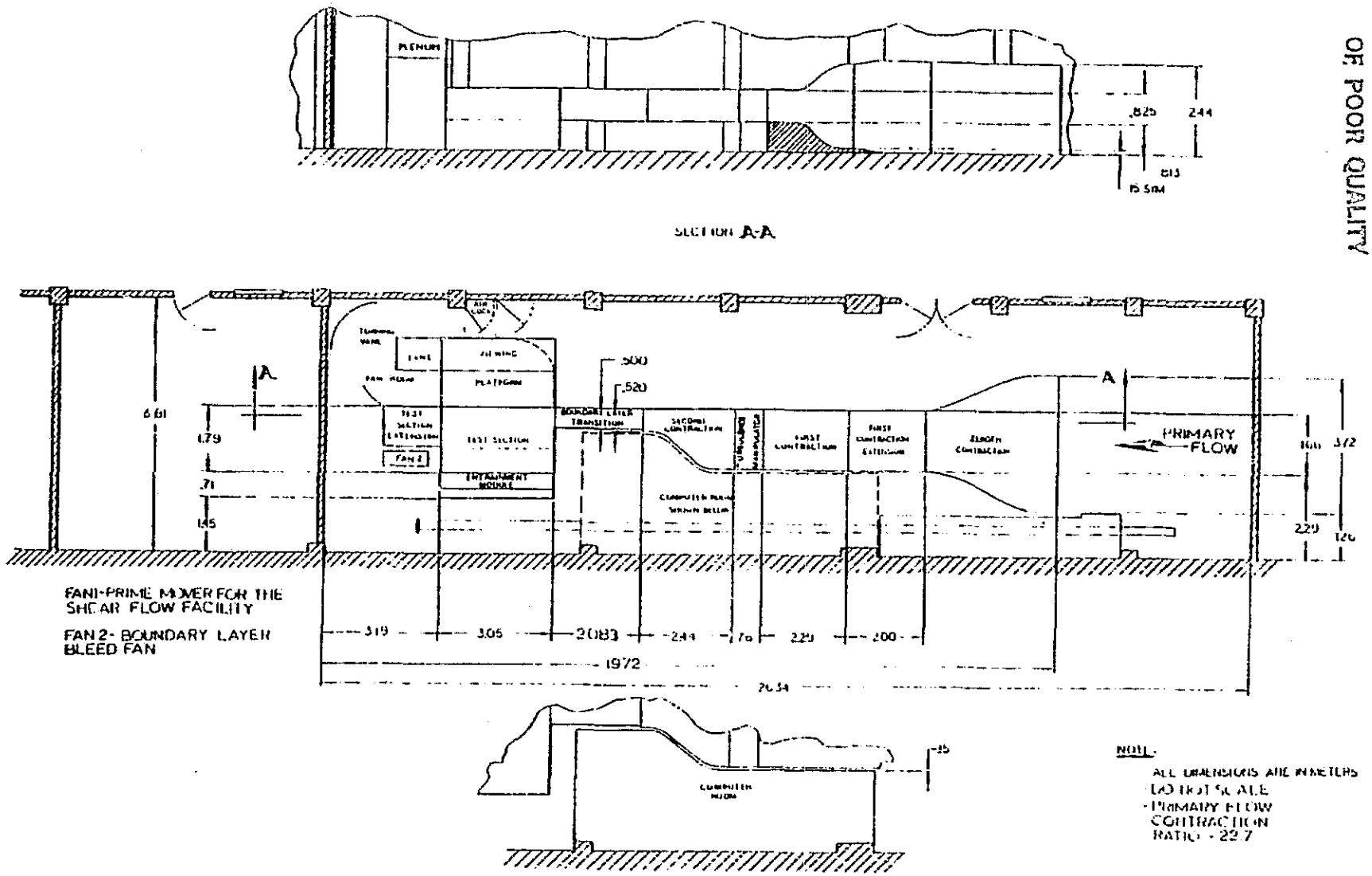

Figure 12. Schematic Representation of the FSFL Wind Tunnel

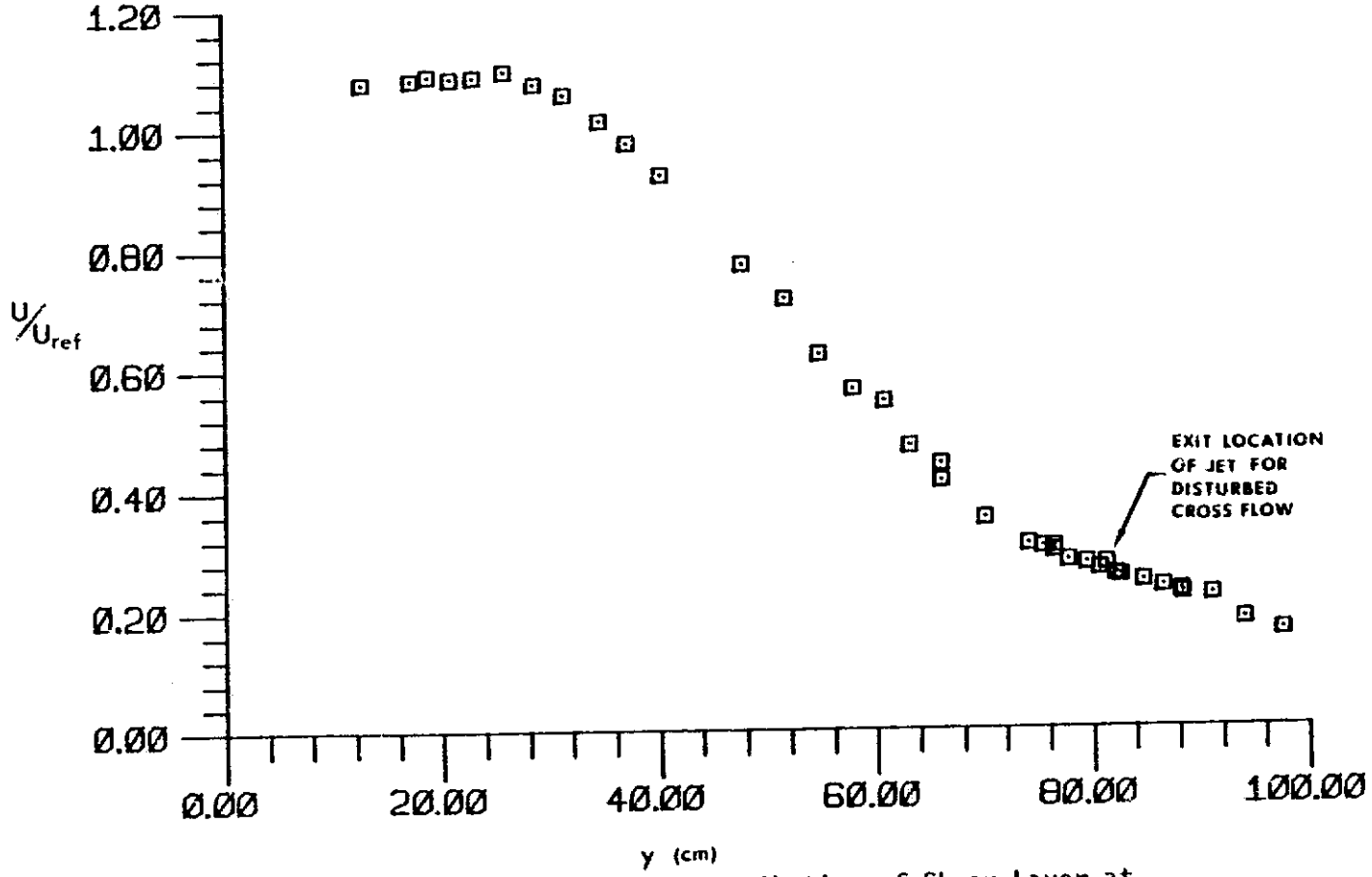

Figure 13. Normalized Velocity Distribution of Shear Layer at Jet Exit Location

NOTE: Traverse location is at z/d = -10 (below boundary layer plate).

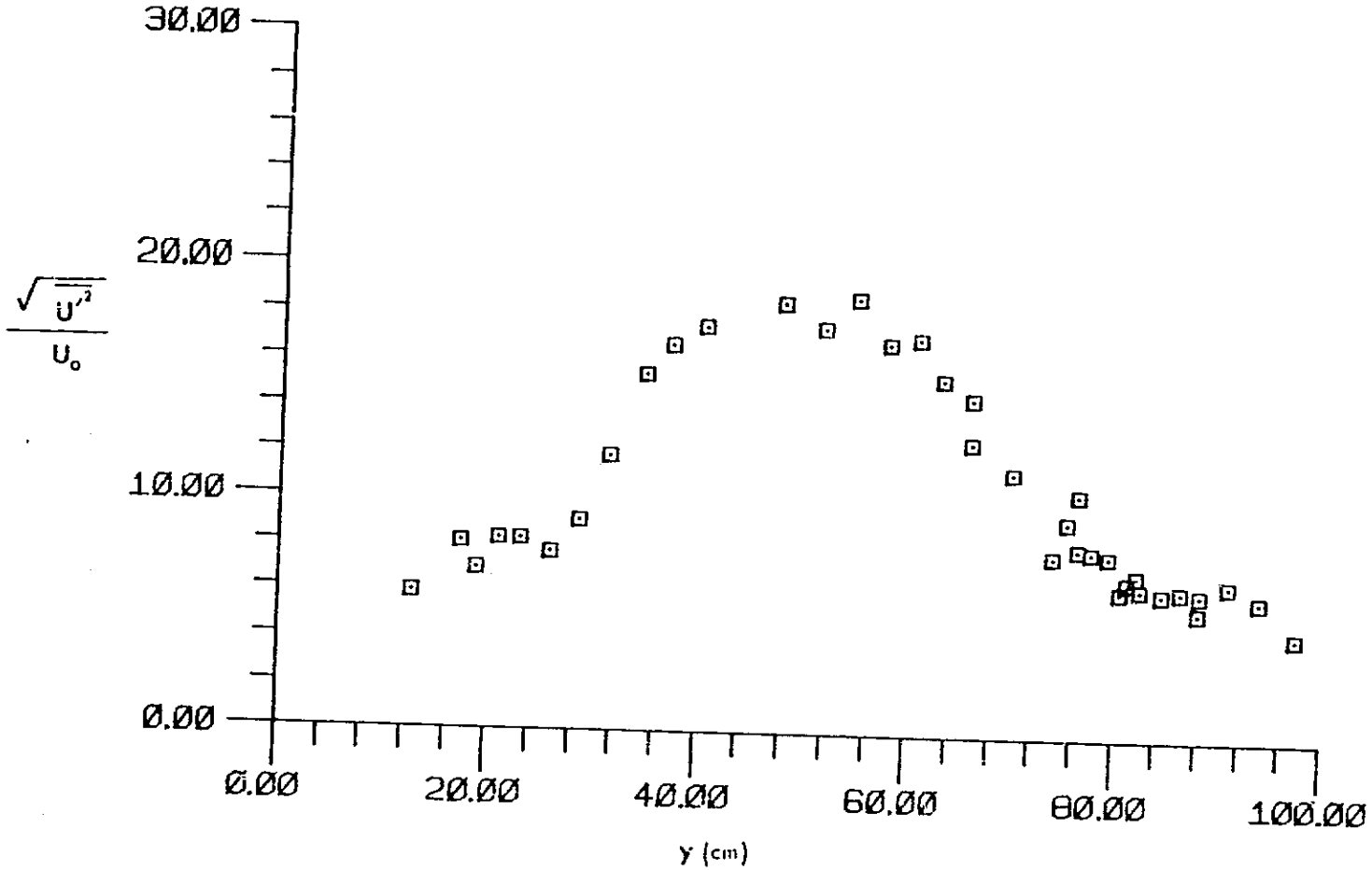

Figure 14. Turbulence Intensity Normalized on Free Stream Velocity

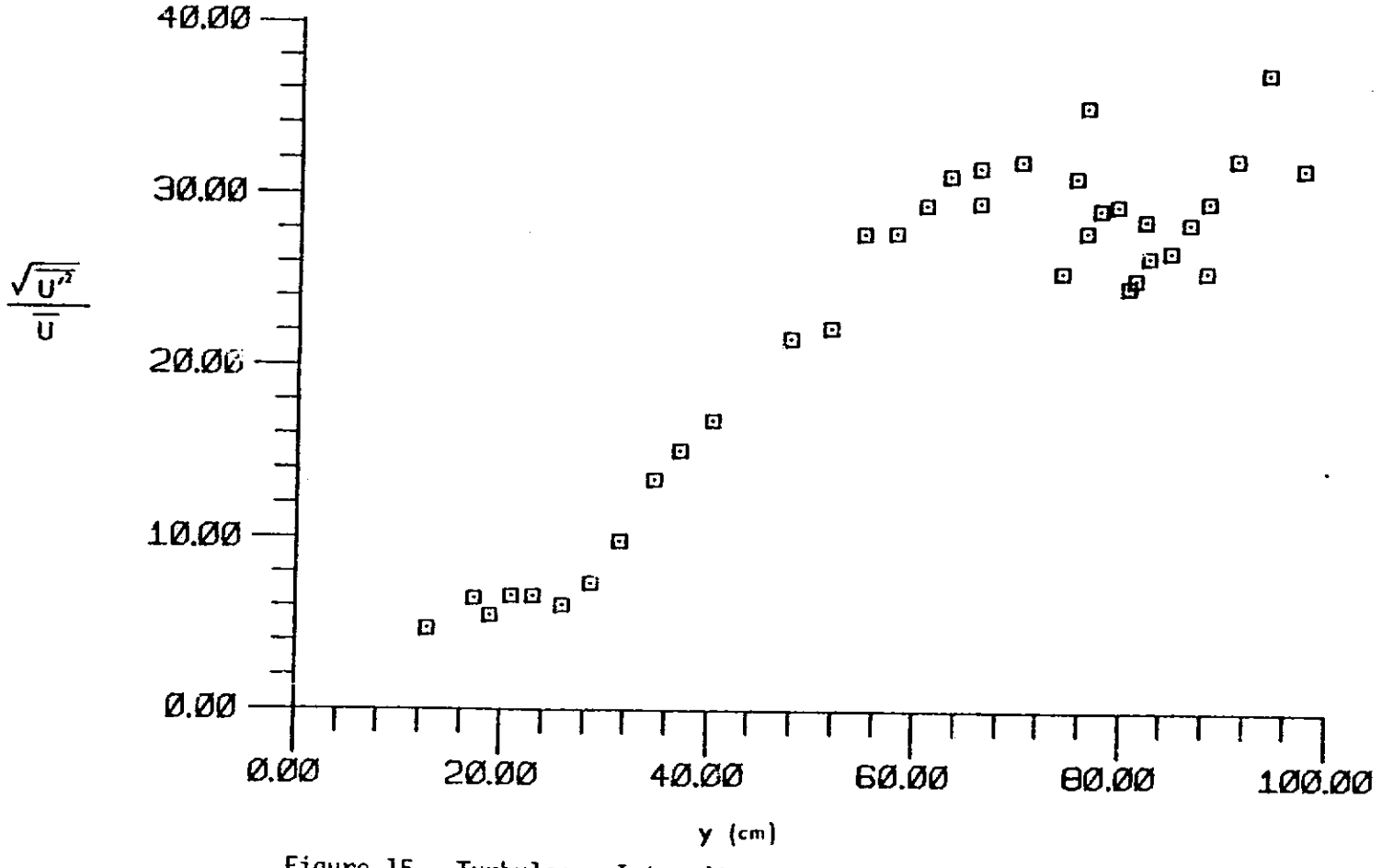

$\frac{\sqrt{\overline{U'^2}}}{\overline{U}}$

Figure 15. Turbulence Intensity normalized on Local Mean Velocity

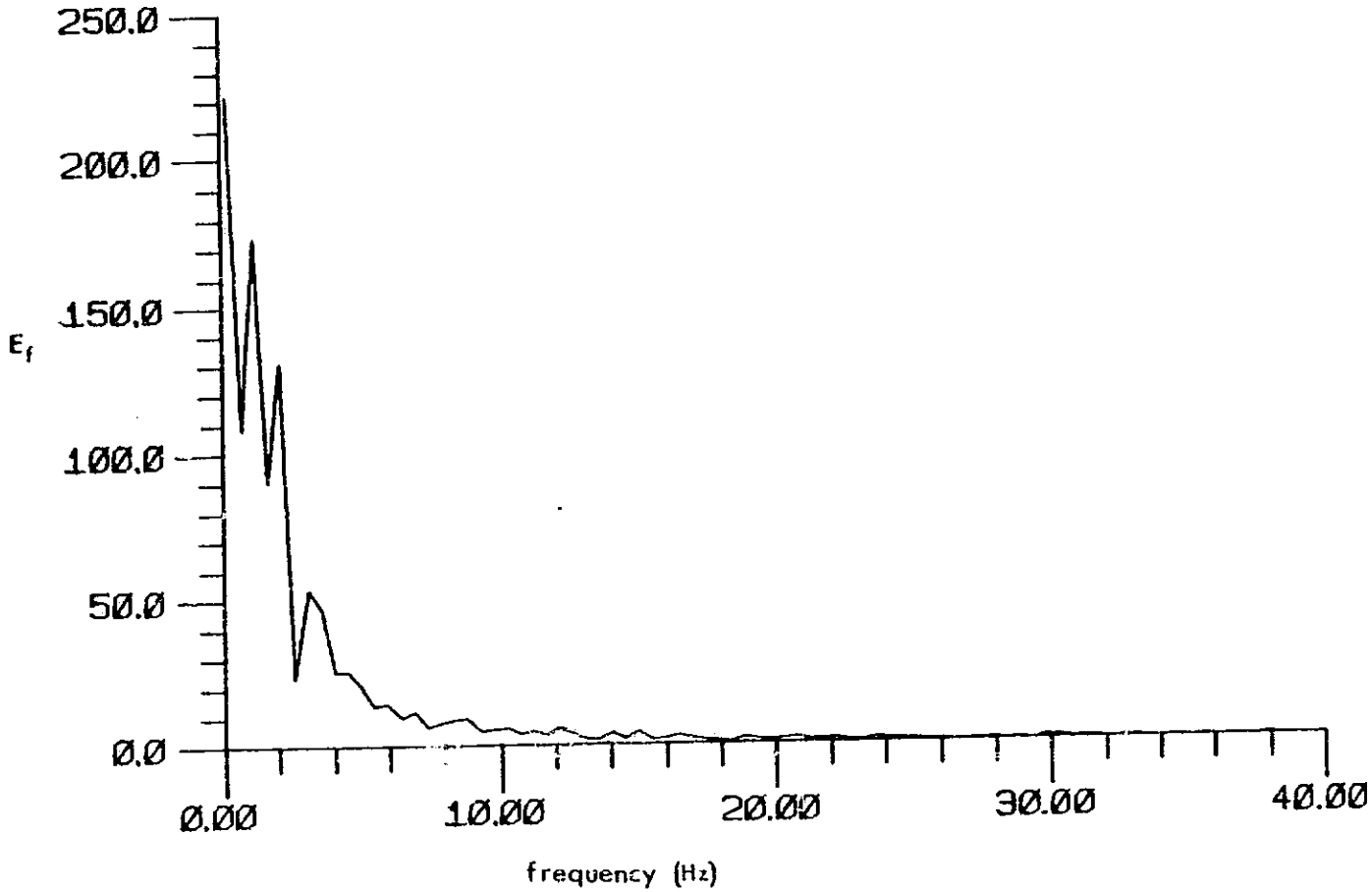

Figure 16. Energy Spectrum Results at Jet Exit Location for Disturbed Cross Flow Case

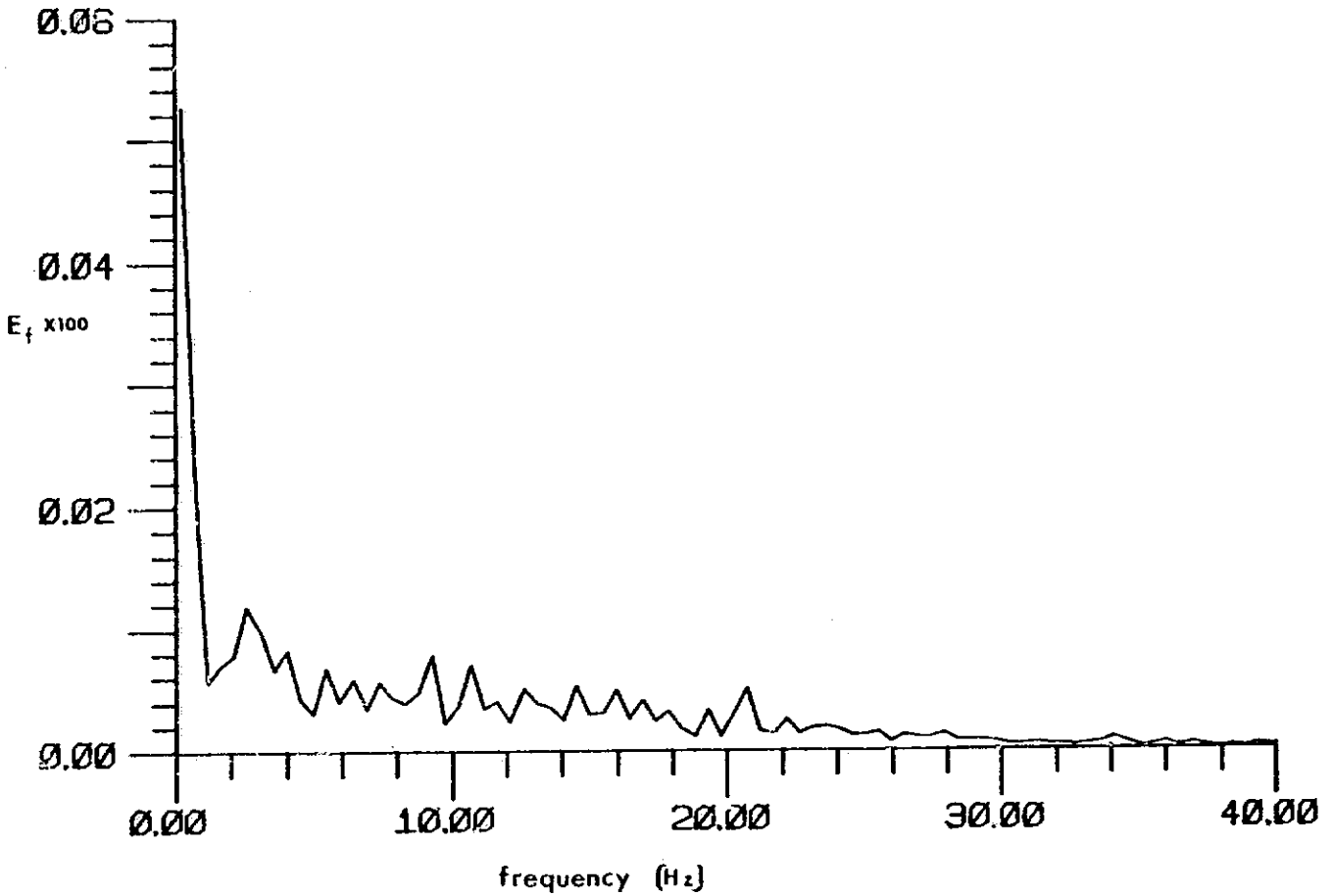

Figure 17. Energy Spectrum Results at Jet Exit Location for Undisturbed Cross Flow Case

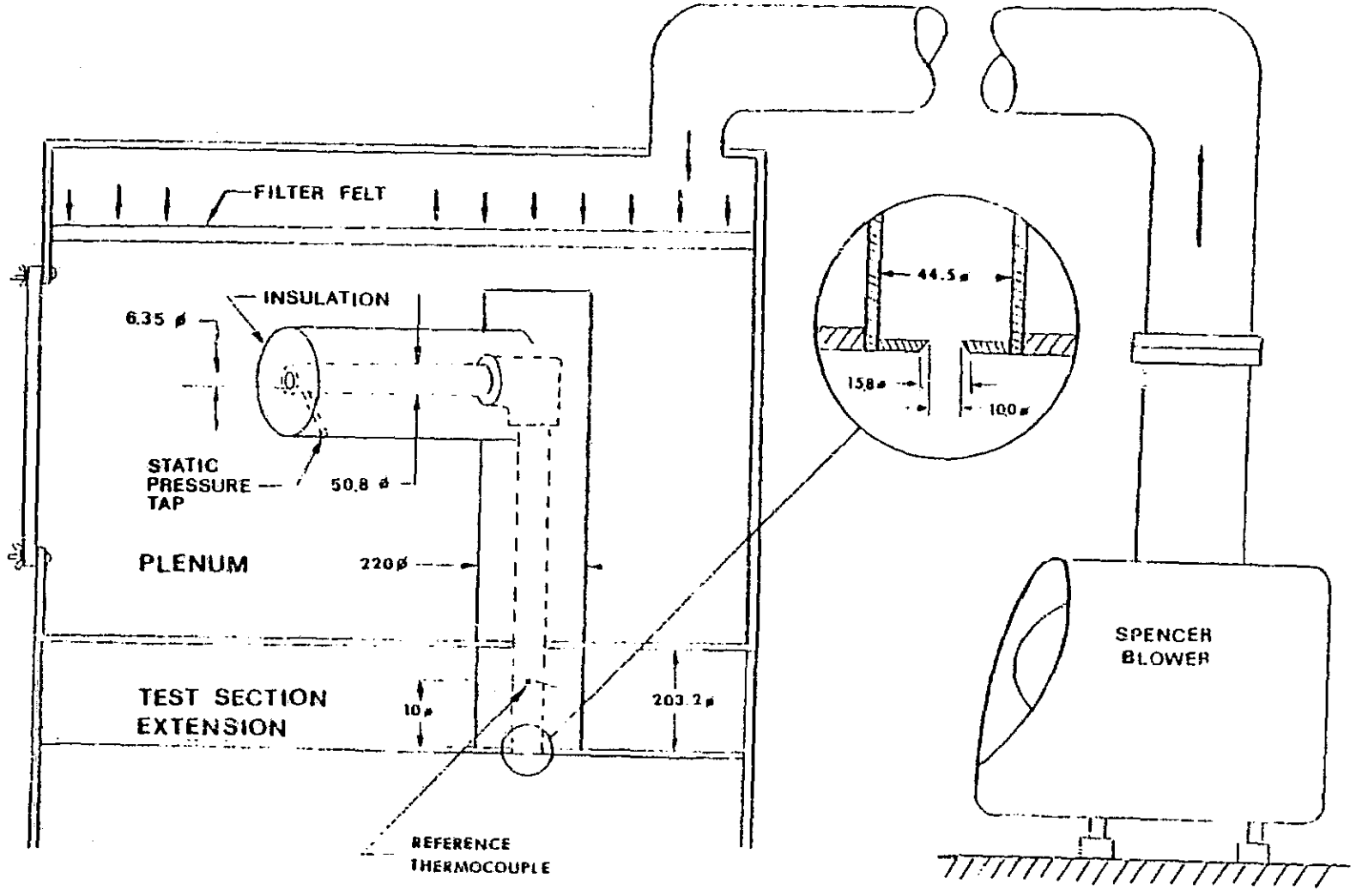

Figure 18. Schematic of Jet Supply and Exit Conditions

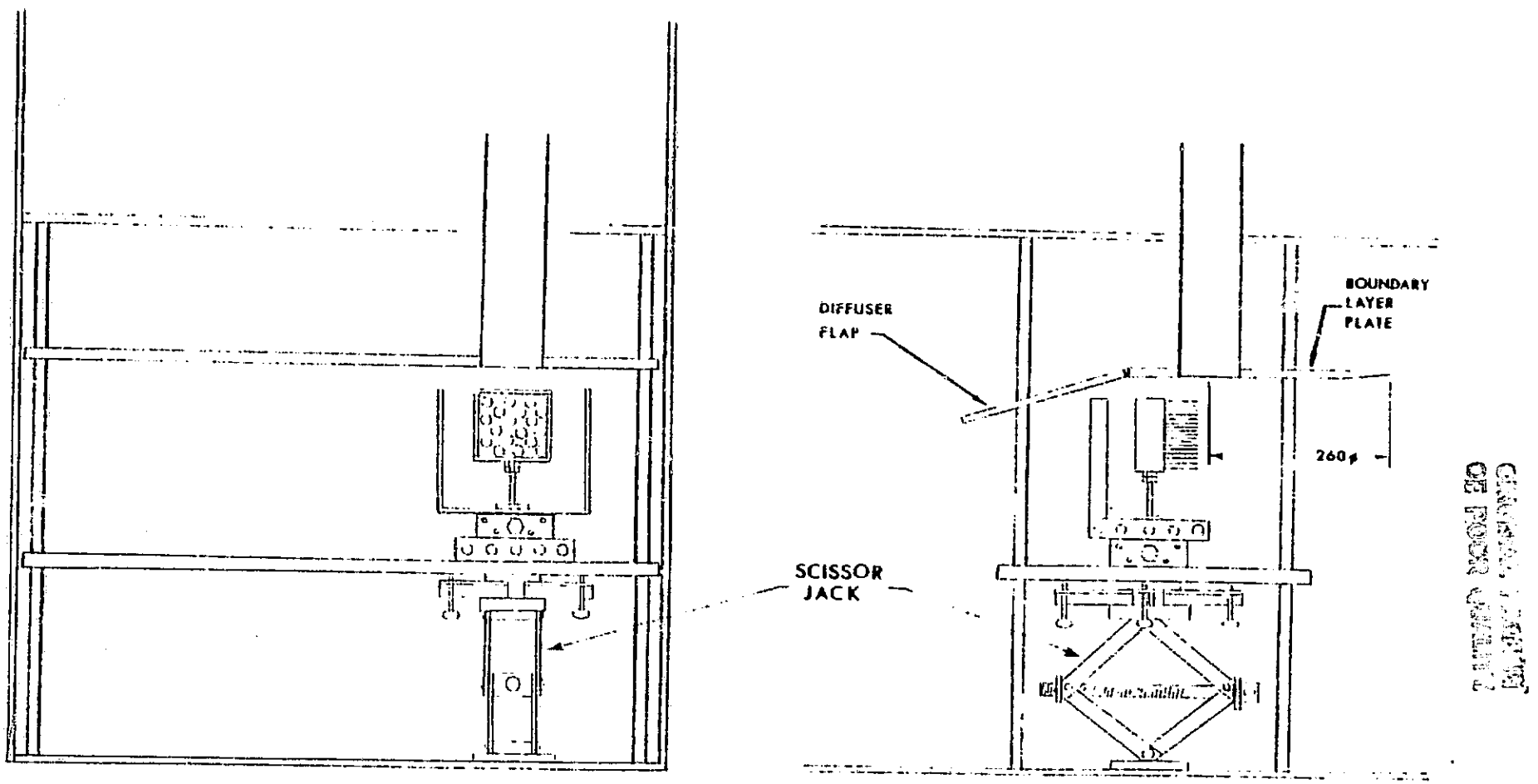

Figure 19. Placement of Thermocouple Array in Flow Facility

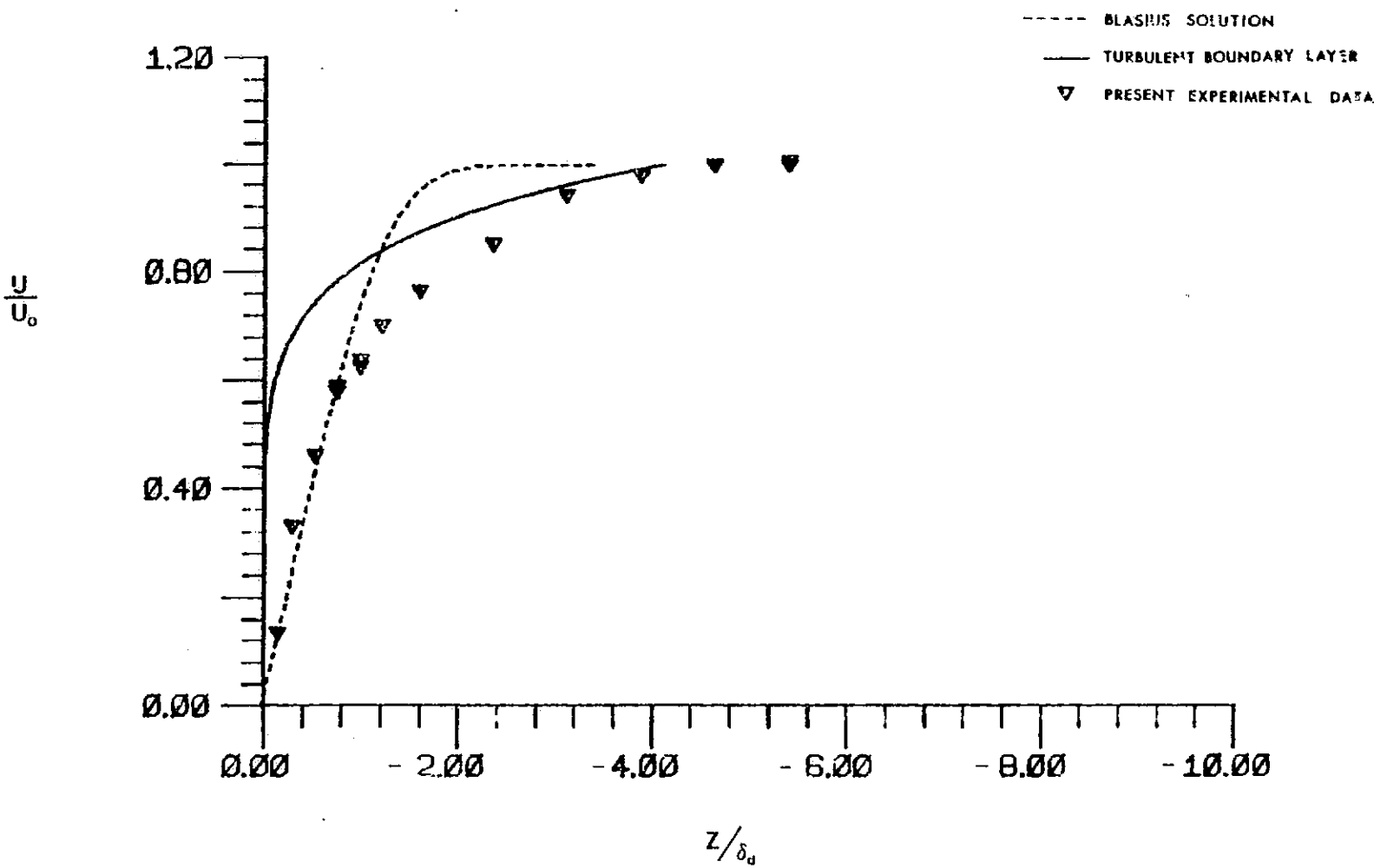

Figure 20. Cross Stream Boundary Layer for Undisturbed Cross Flow Case

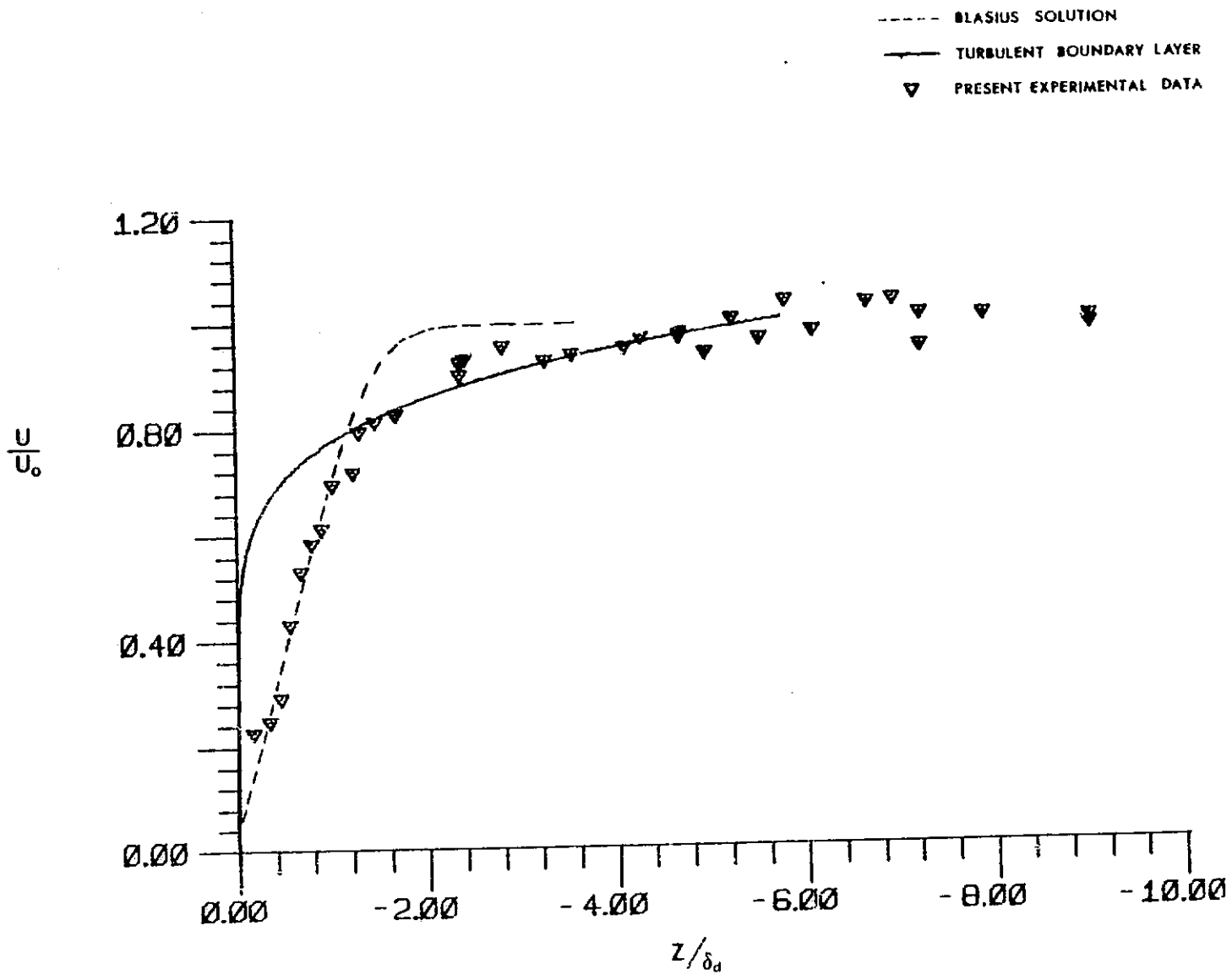

Figure 21. Cross Stream Boundary Layer for Disturbed Cross Flow Case

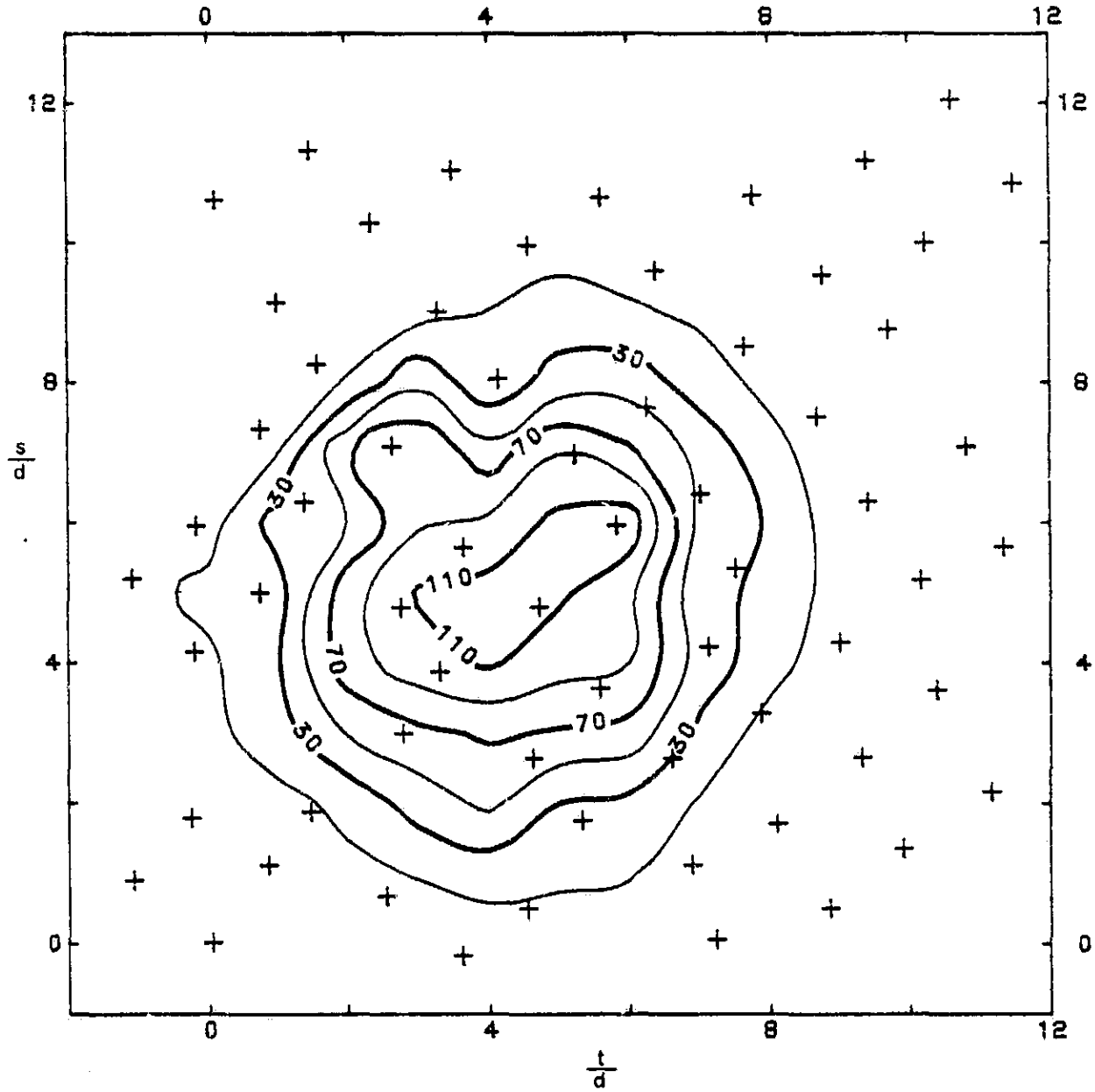

Figure 22. Undisturbed Cross Flow (u.c.f.) Mean Temperature Isotherms $J = 17$, $T_{jet} - T_{\infty} = 22.2°C$

NOTE: Contours shown are $\frac{T_c - T_{\infty}}{T_{jet} - T_{\infty}} \times 1000$ $s/d = 14.1\ (\pm .7) - z/d$,

$t/d = 4.3(\pm .5) - y/d$

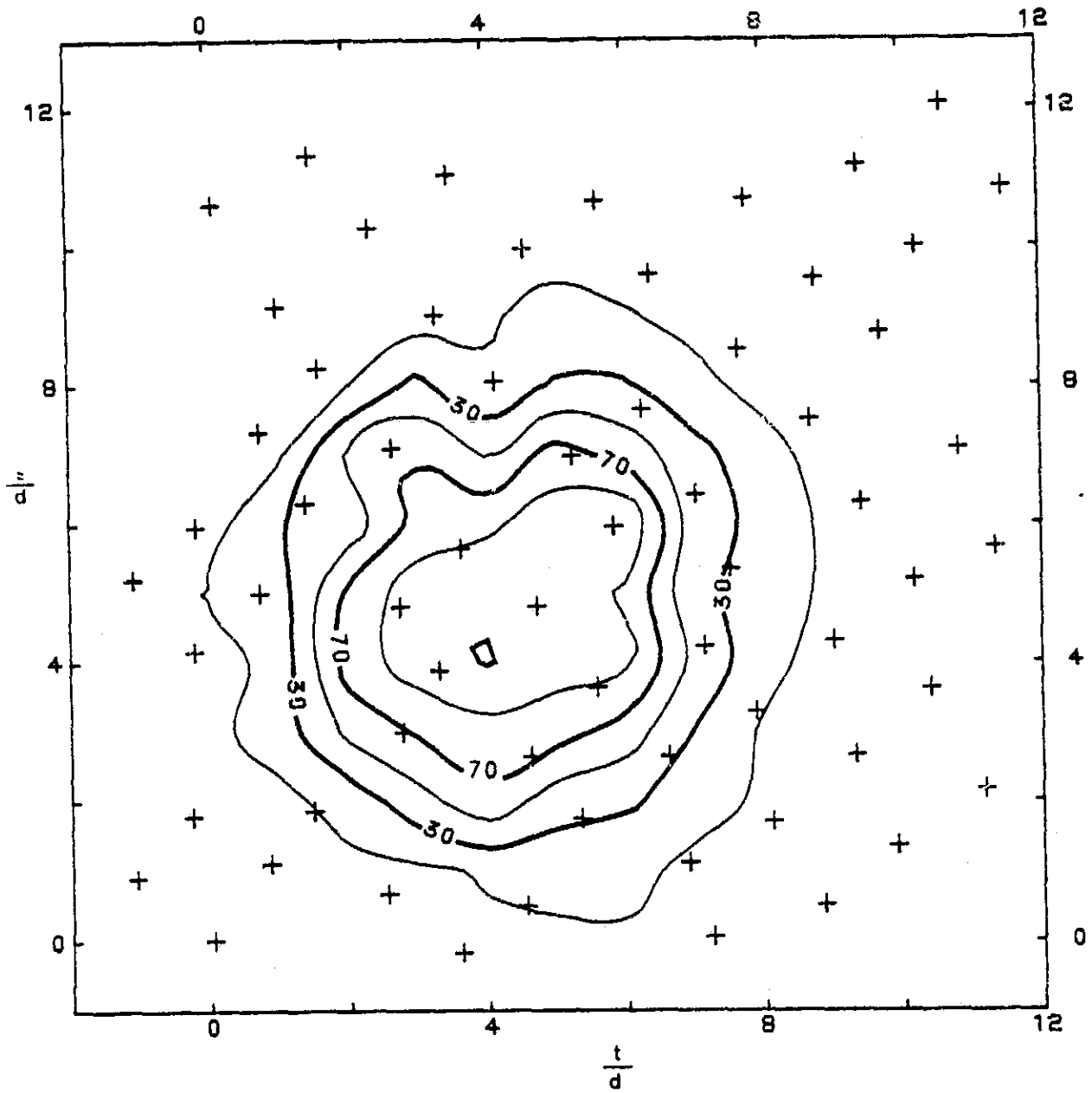

Figure 23. u.c.f. Mean Temperature Isotherms: J = 19, $T_{jet} - T_{\infty}$ = 41.7°C

NOTE: s/d = 14.1(± .7) - z/d, t/d = 4.3(± .5) - y/d

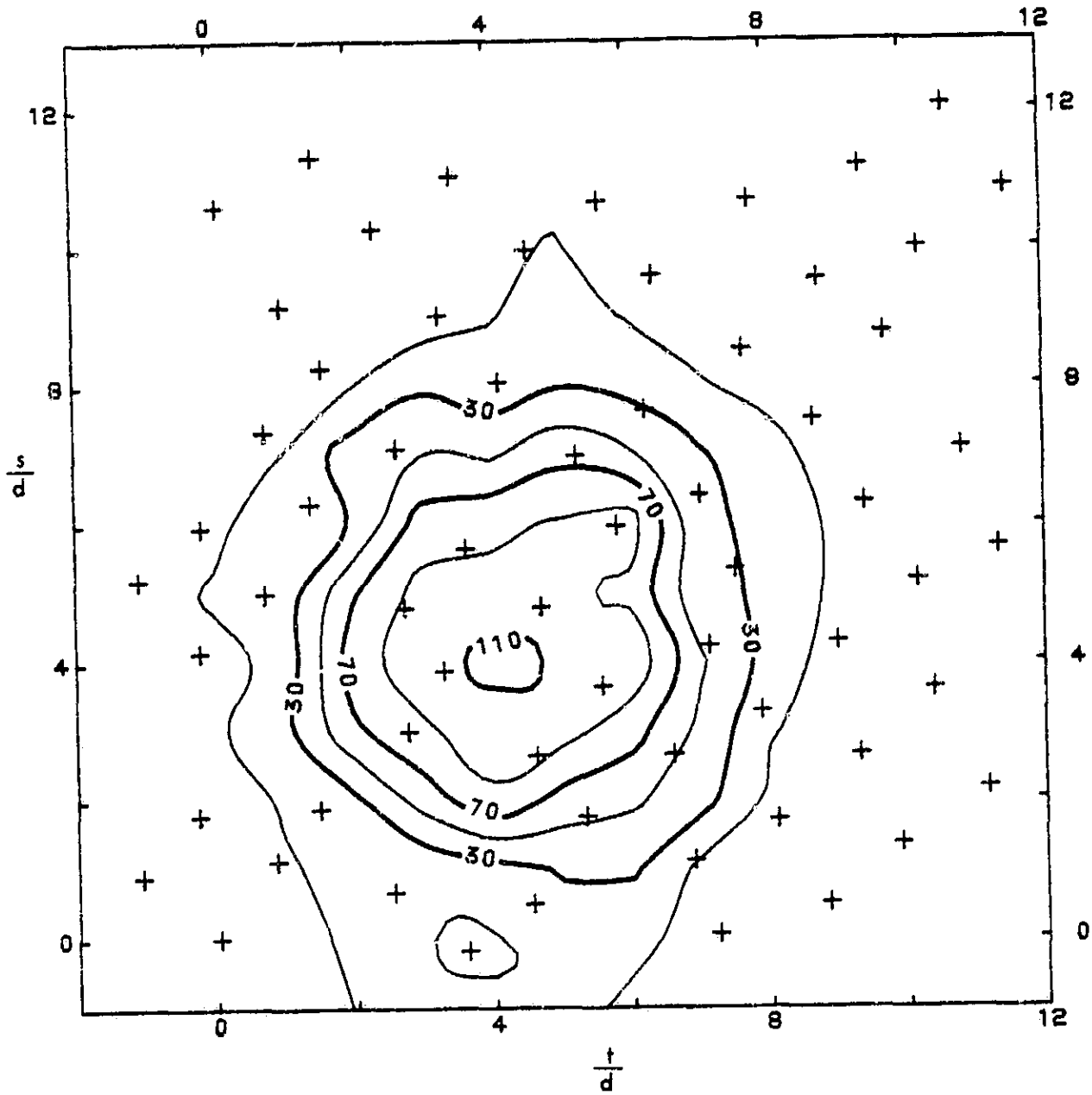

Figure 24. u.c.f. Mean Temperature Isotherms: $J = 21$, $T_{jet} - T_{\infty} = 61.1°C$

NOTE: $s/d = 14.1(\pm .7) - z/d$, $t/d = 4.3(\pm .5) - y/d$

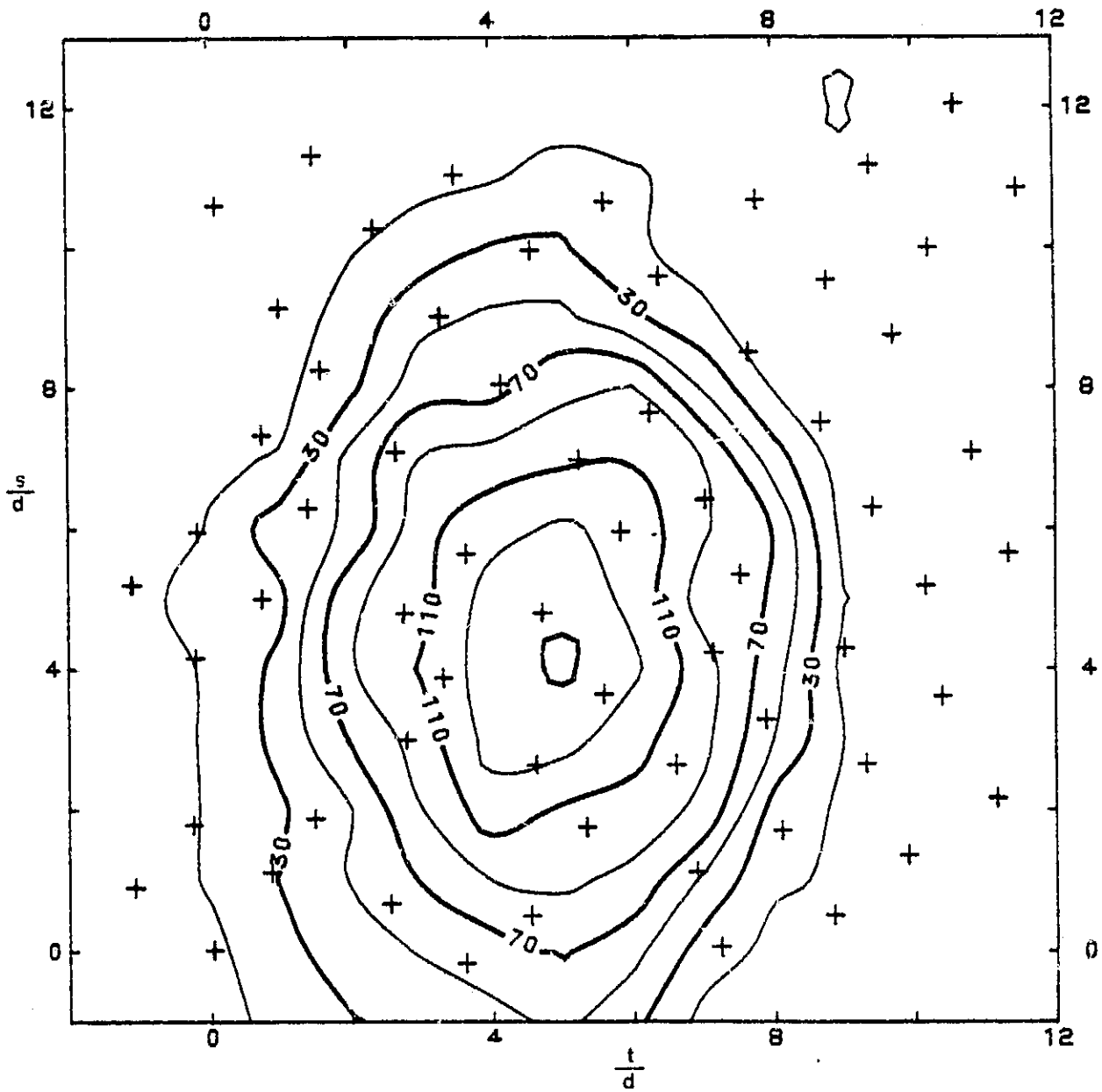

Figure 25. u.c.f. Mean Temperature Isotherms: J = 67, $T_{jet} - T_{\infty}$ = 22.6°C

NOTE: s/d = 17.9(± .7) - z/d, t/d = 4.3(± .5) - y/d

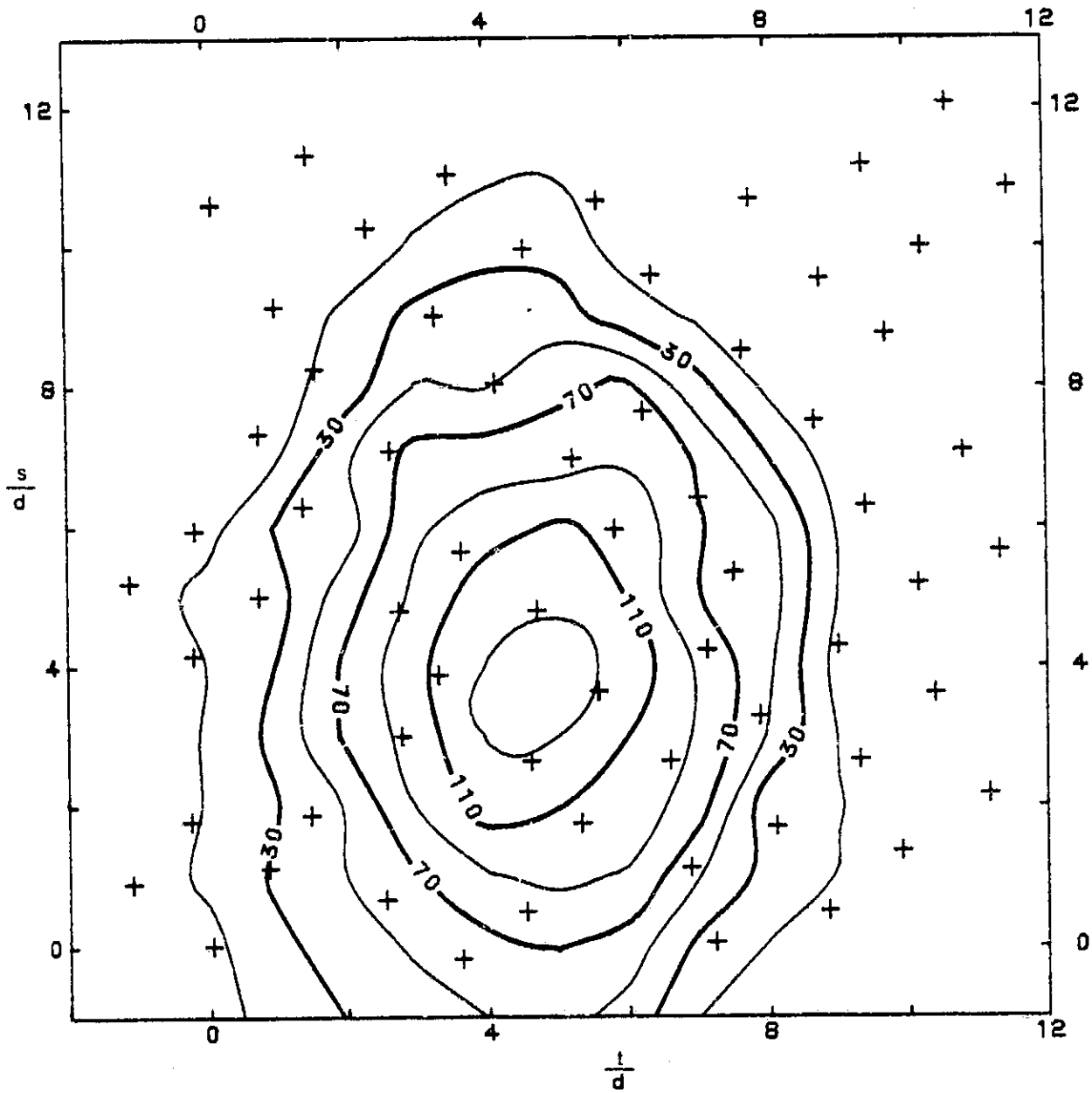

Figure 26. u.c.f. Mean Temperature Isotherms: J = 76, $T_{jet} - T_{\infty}$ = 41.7°C

NOTE: s/d = 17.9(± .7) - z/d, t/d = 4.3(± .5) - y/d

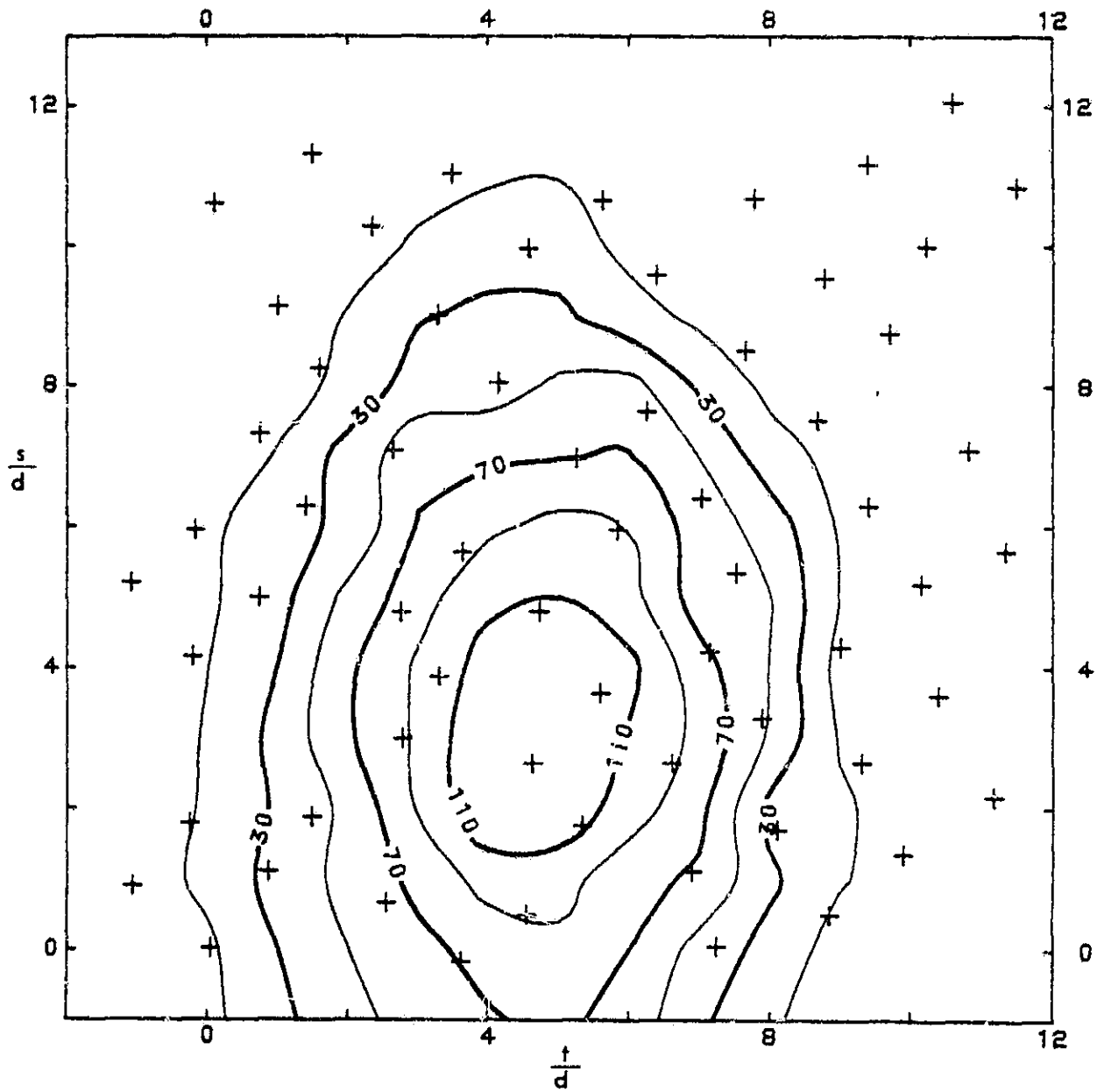

Figure 27. u.c.f. Mean Temperature Isotherms: J = 84, $T_{jet} - T_{\infty}$ = 61.1°C

NOTE: s/d = 17.9(± .7) - z/d, t/d = 4.3 (± .5) - y/d

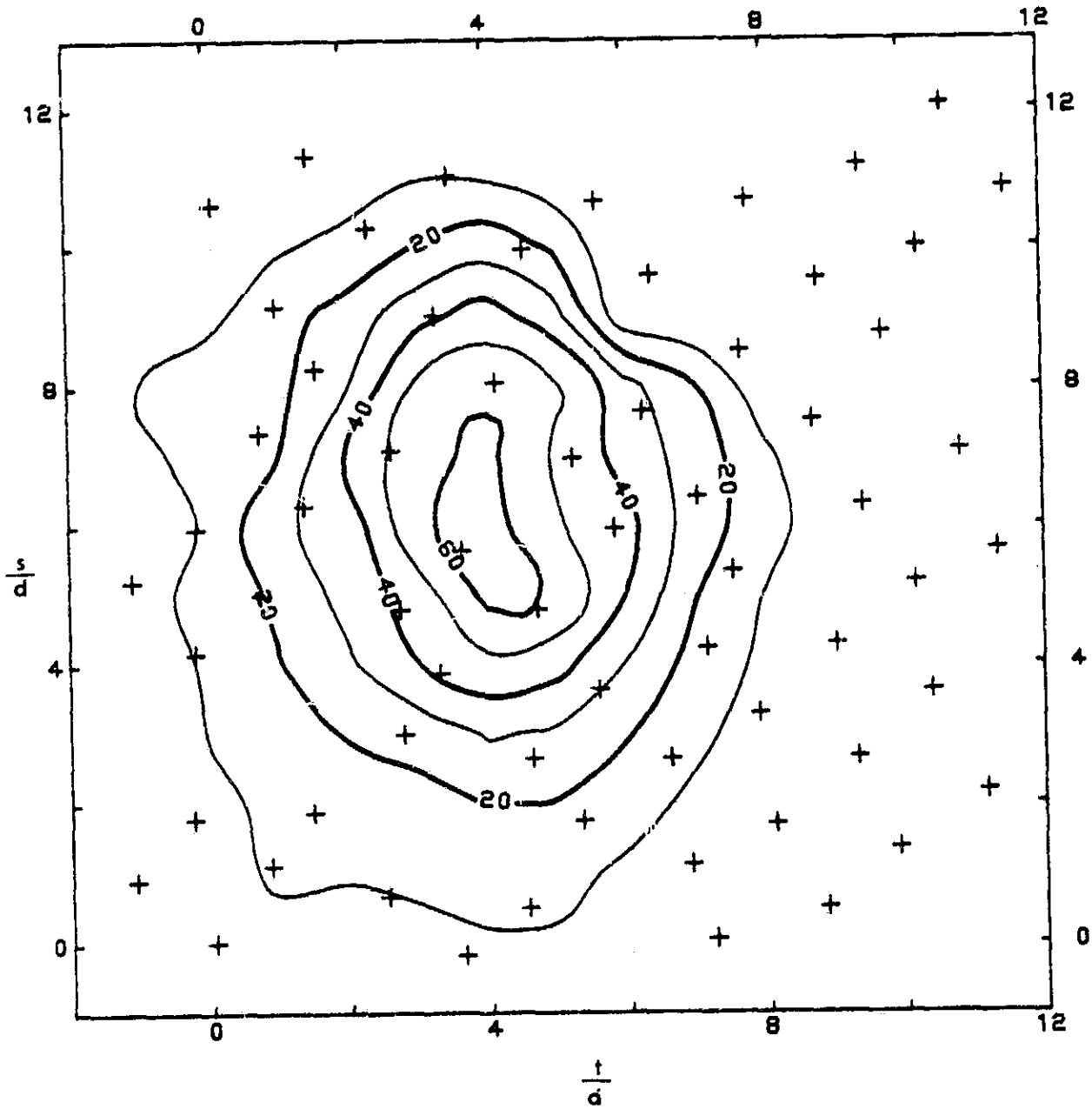

Figure 28. Disturbed Cross Flow (d.c.f.) Mean Temperature Isotherms: $J = 17$, $T_{jet} - T_{\infty} = 22.2°C$

NOTE: $s/d = 14.1(\pm .7) - z/d$, $t/d = 4.2(\pm .5) - y/d$

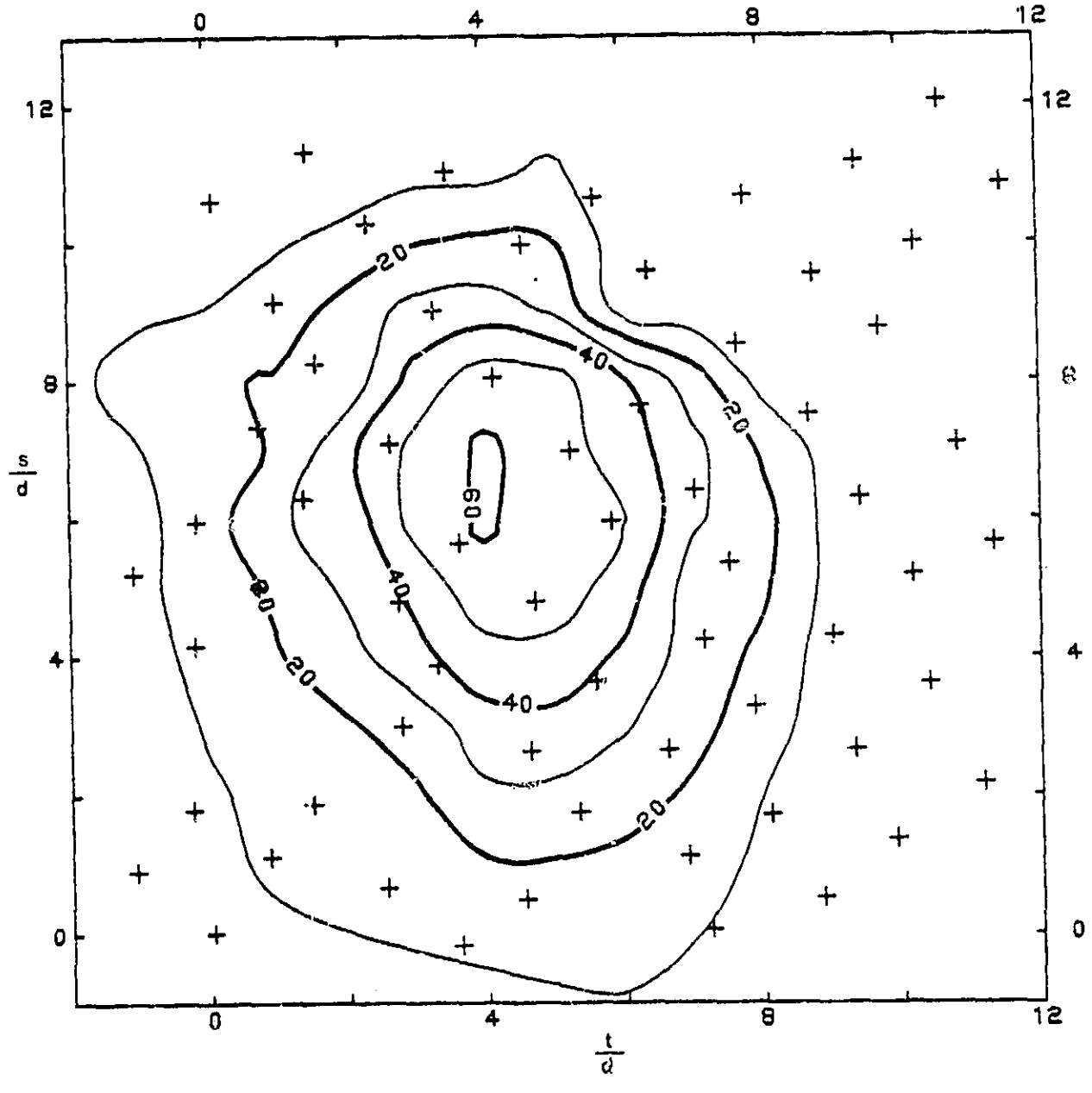

Figure 29. d.c.f. Mean Temperature Isotherms: J = 19, $T_{jet} - T_{\infty}$ = 41.7°C

NOTE: s/d = 14.1(± .7) - z/d, t/d = 4.2(± .5) - y/d

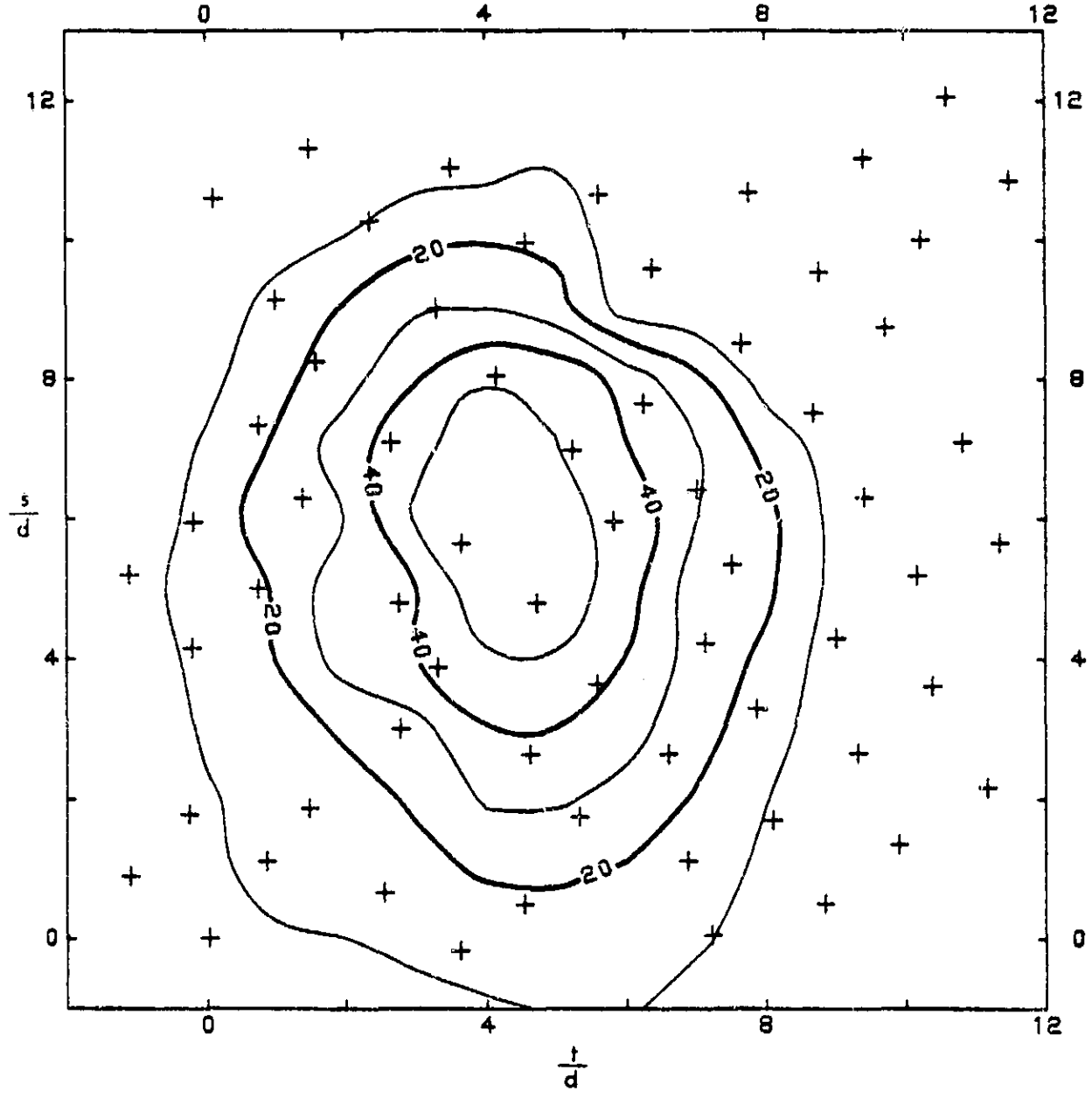

Figure 30. d.c.f. Mean Temperature Isotherms: J = 21, $T_{jet} - T_{\infty} = 61.1°C$

NOTE: s/d = 14.1(± .7) - z/d, t/d = 4.2(± .5) - y/d

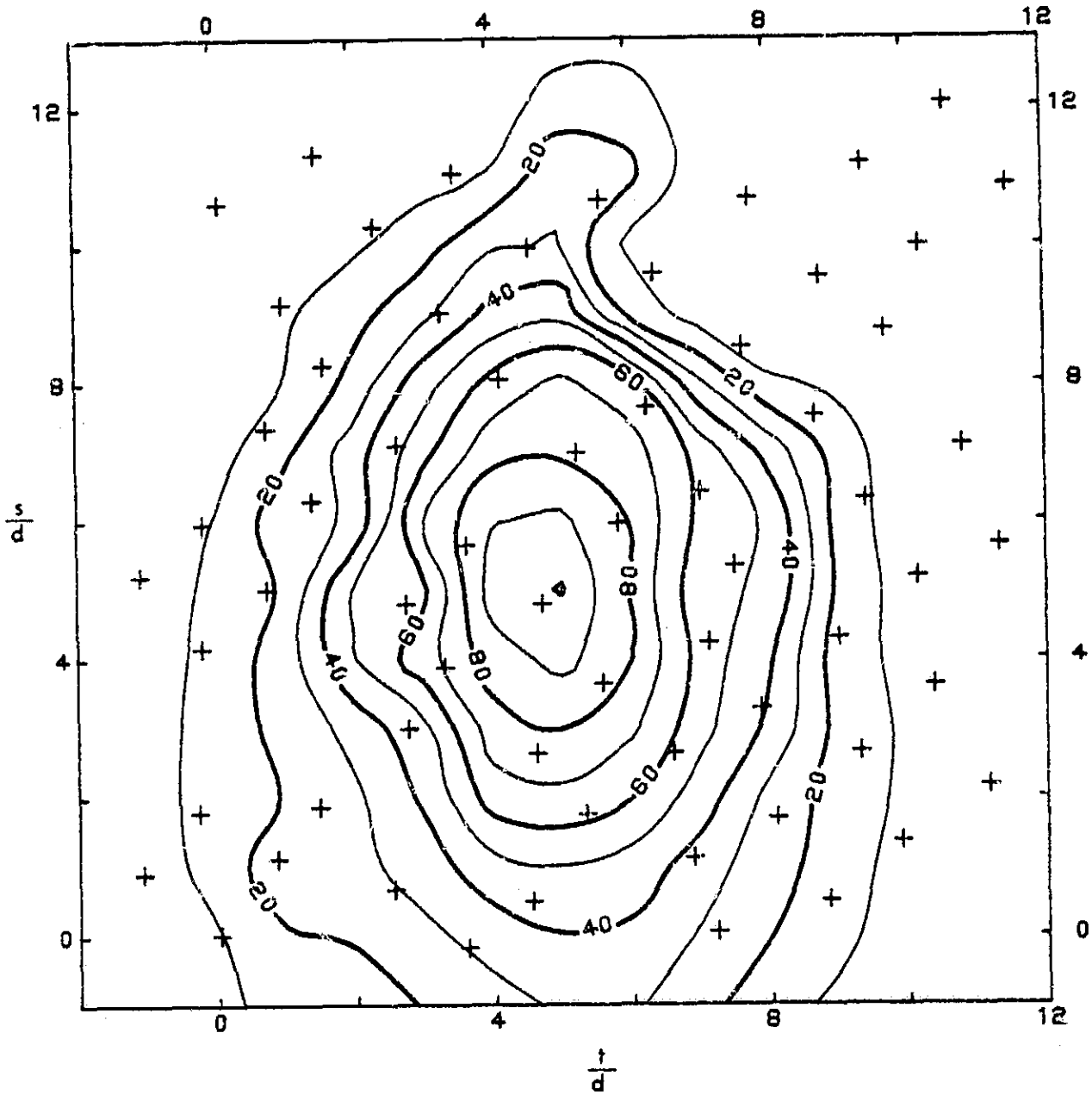

Figure 31. d.c.f. Mean Temperature Isotherms: J = 67, $T_{jet} - T_{\infty} = 22.2°C$

NOTE: s/d = 16.8(± .7) - z/d, t/d = 4.2(± .5) - y/d

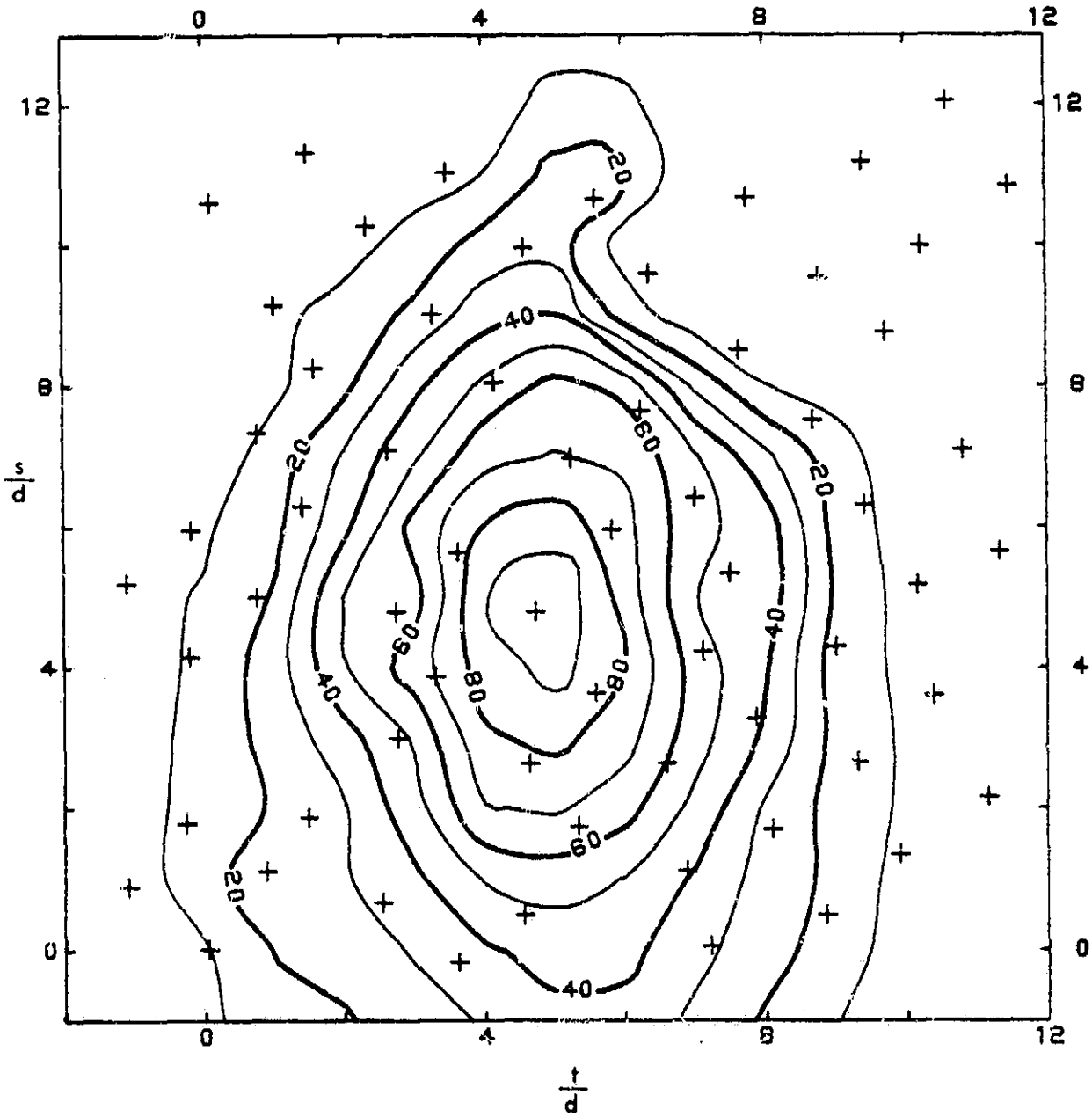

Figure 32. d.c.f. Mean Temperature Isotherms: J = 76, $T_{jet} - T_{\infty}$ = 41.7°C

NOTE: s/d = 16.8(± .7) - z/d, t/d = 4.2(± .5) - y/d

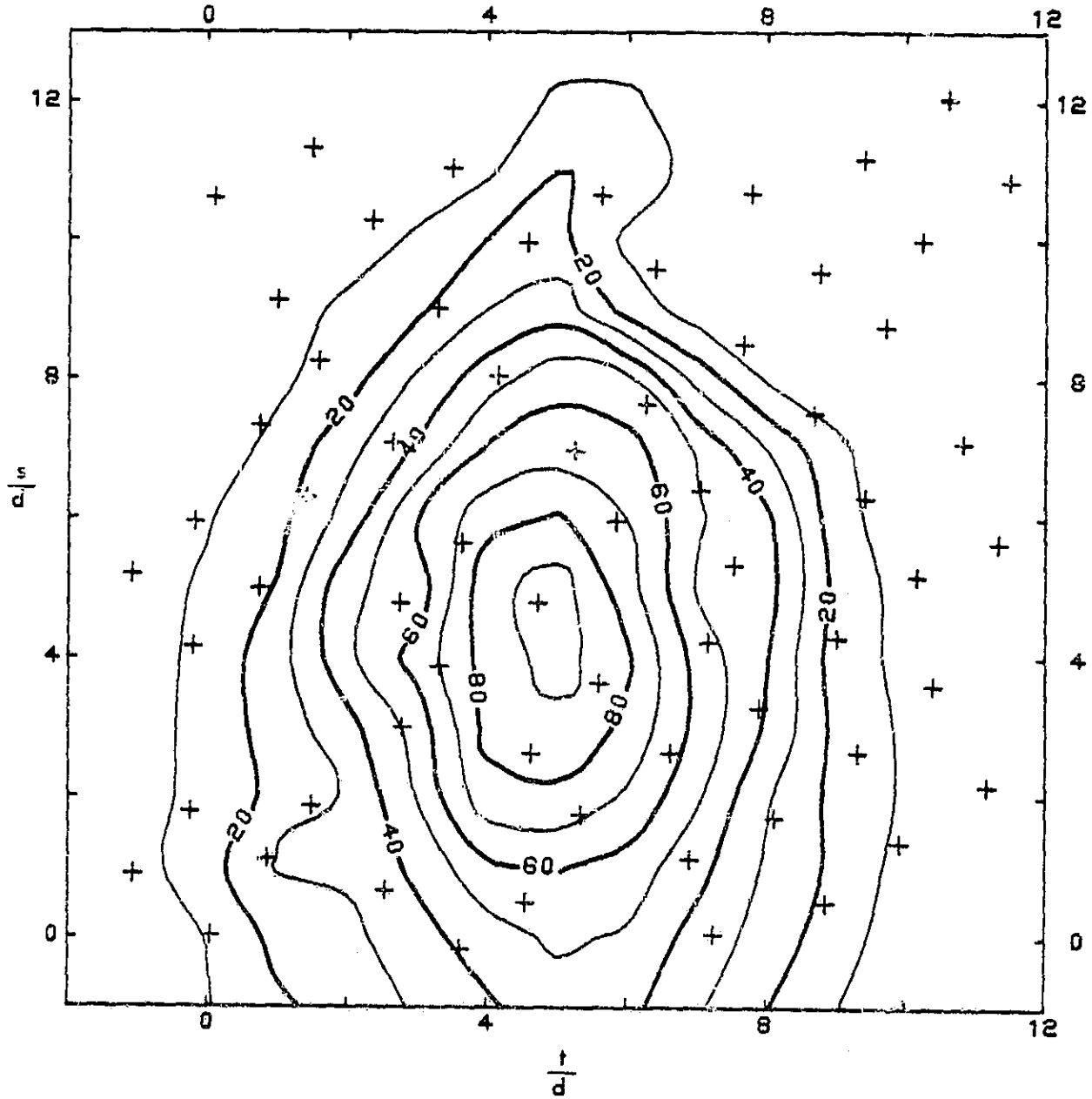

Figure 33. d.c.f. Mean Temperature Isotherms: J = 84, $T_{jet} - T_{\infty}$ = 61.1°C

NOTE: s/d = 16.8(± .7) - z/d, t/d = 4.2(± .5) - y/d

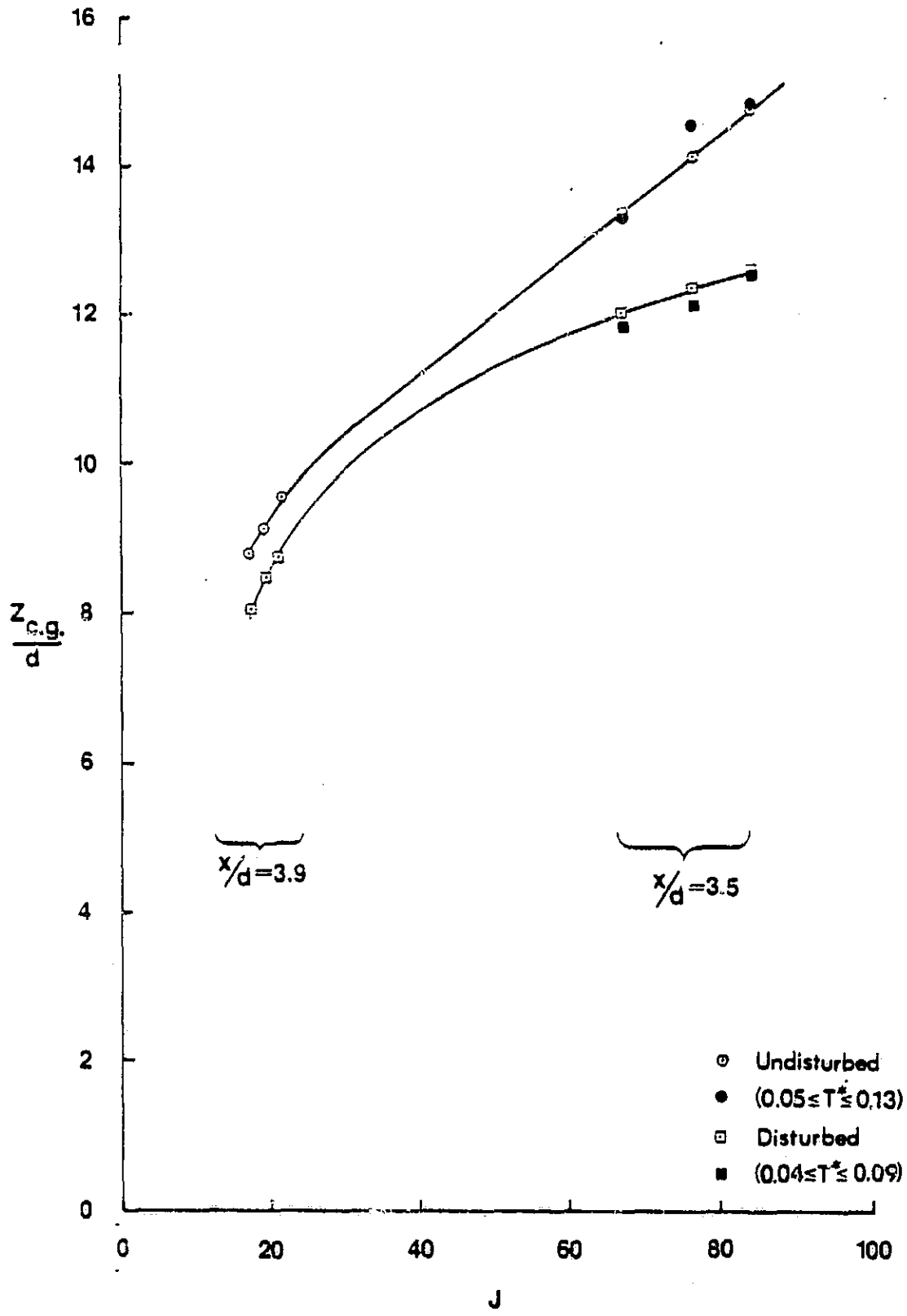

Figure 34 Thermal Centroids as a Function of the Specific Momentum Flux Ratio
Note: Solid Curve added for visual reference only.

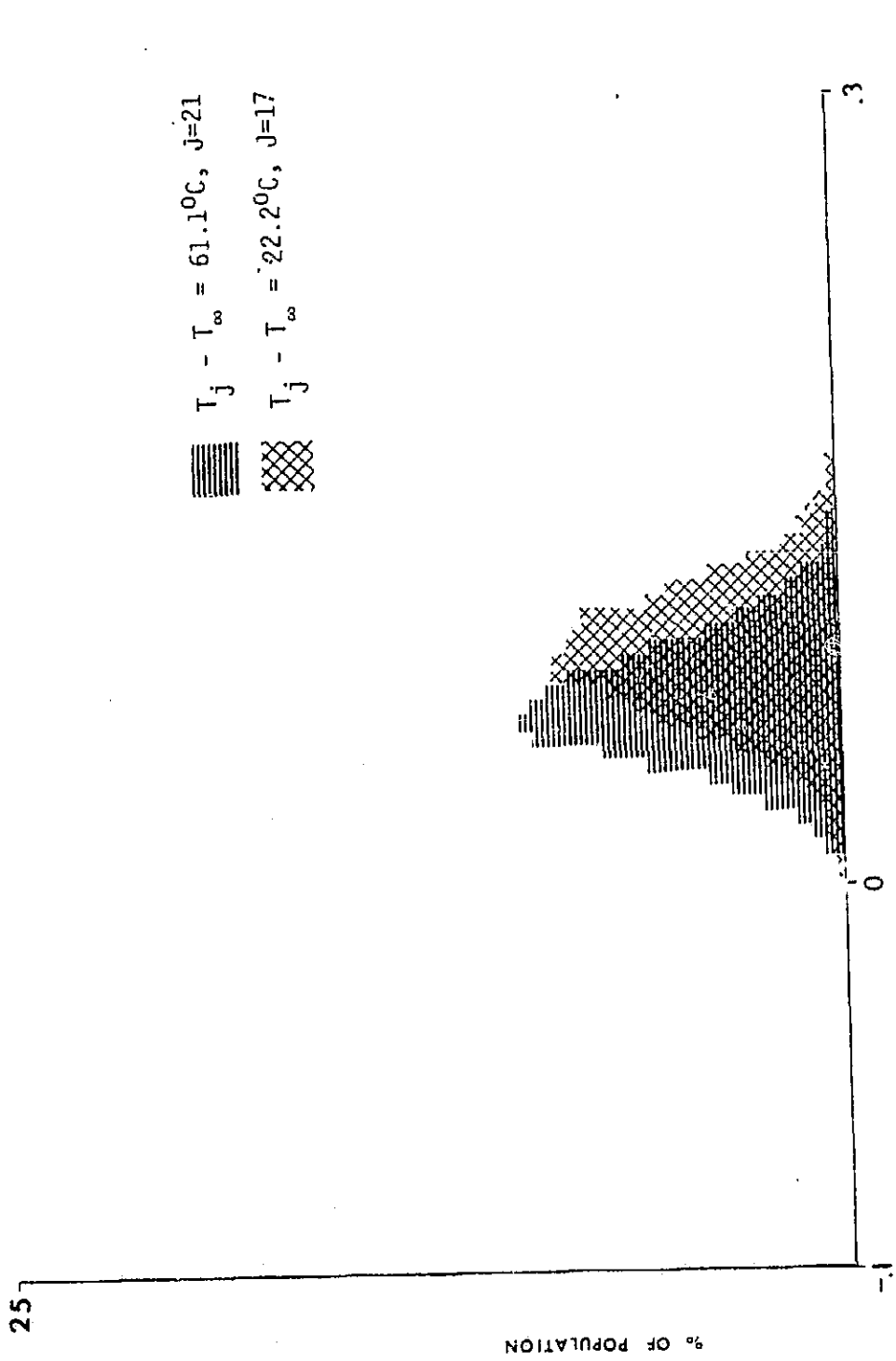

Figure 35. Temperature Histogram for u.c.f.: Thermocouple at s/d = 4.79, t/d = 4.73

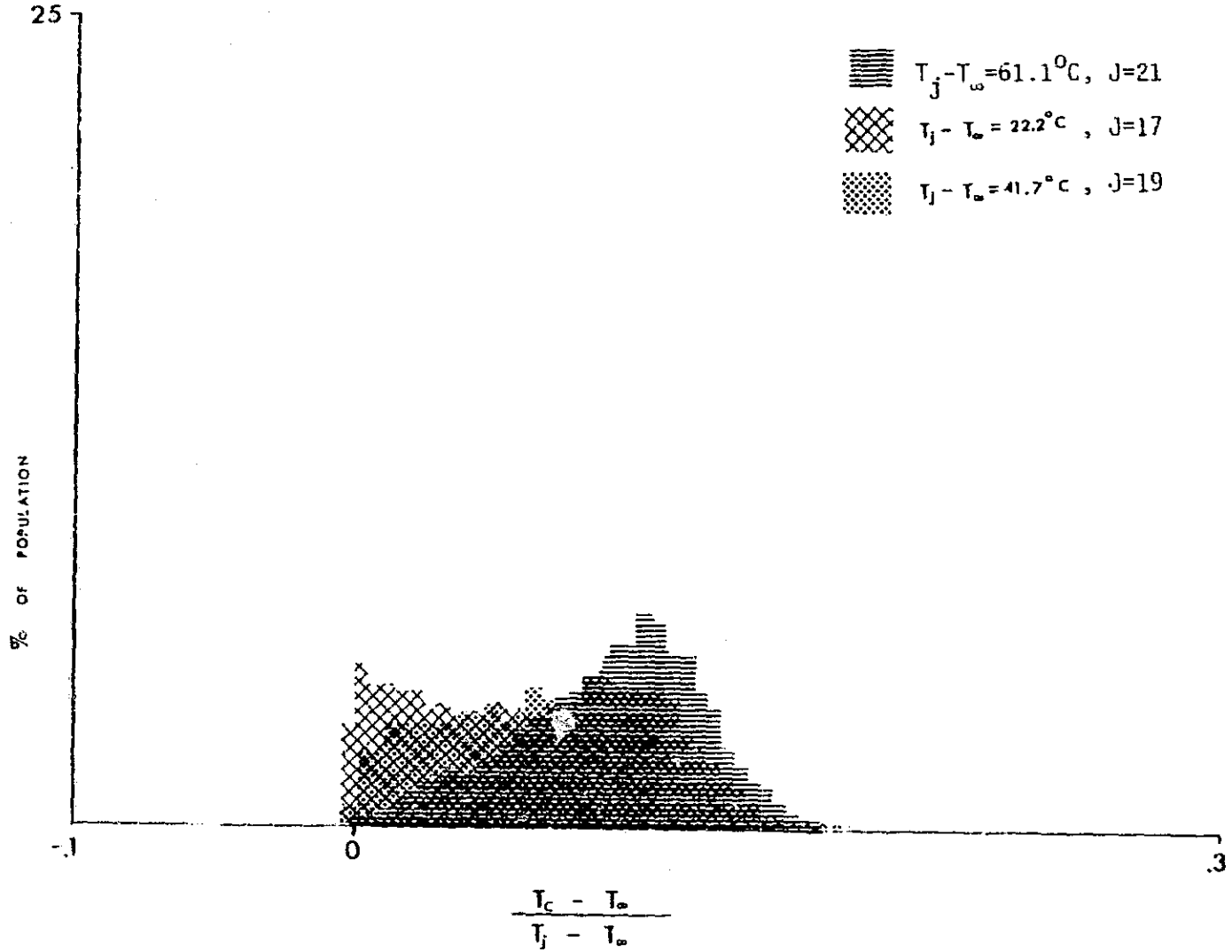

Figure 36. Temperature Histogram for u.c.f.:
Thermocouple at s/d = 2.64, t/d = 4.63

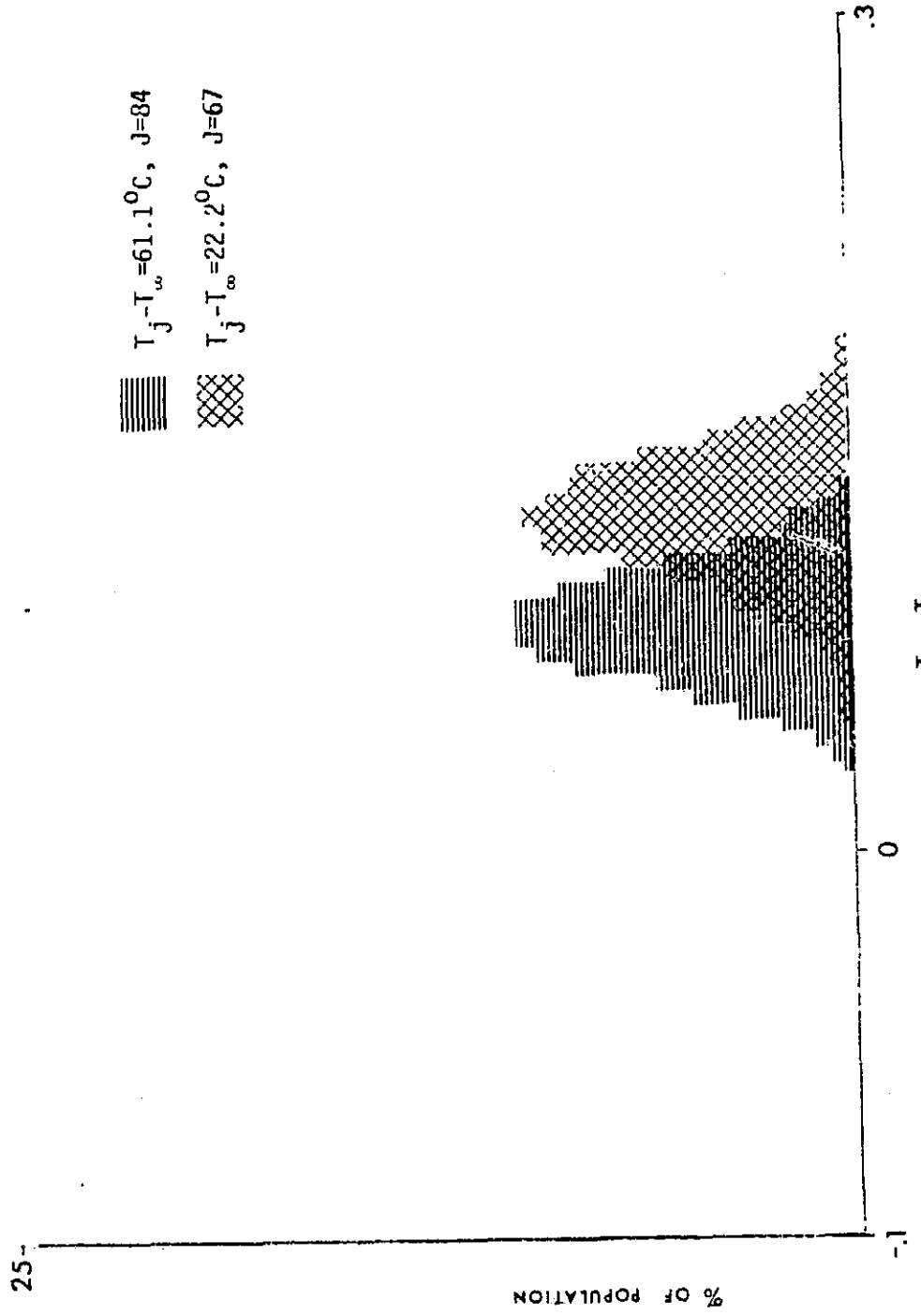

Figure 37. Temperature Histogram for u.c.f.:
Thermocouple at s/d = 4.79, t/d = 4.73

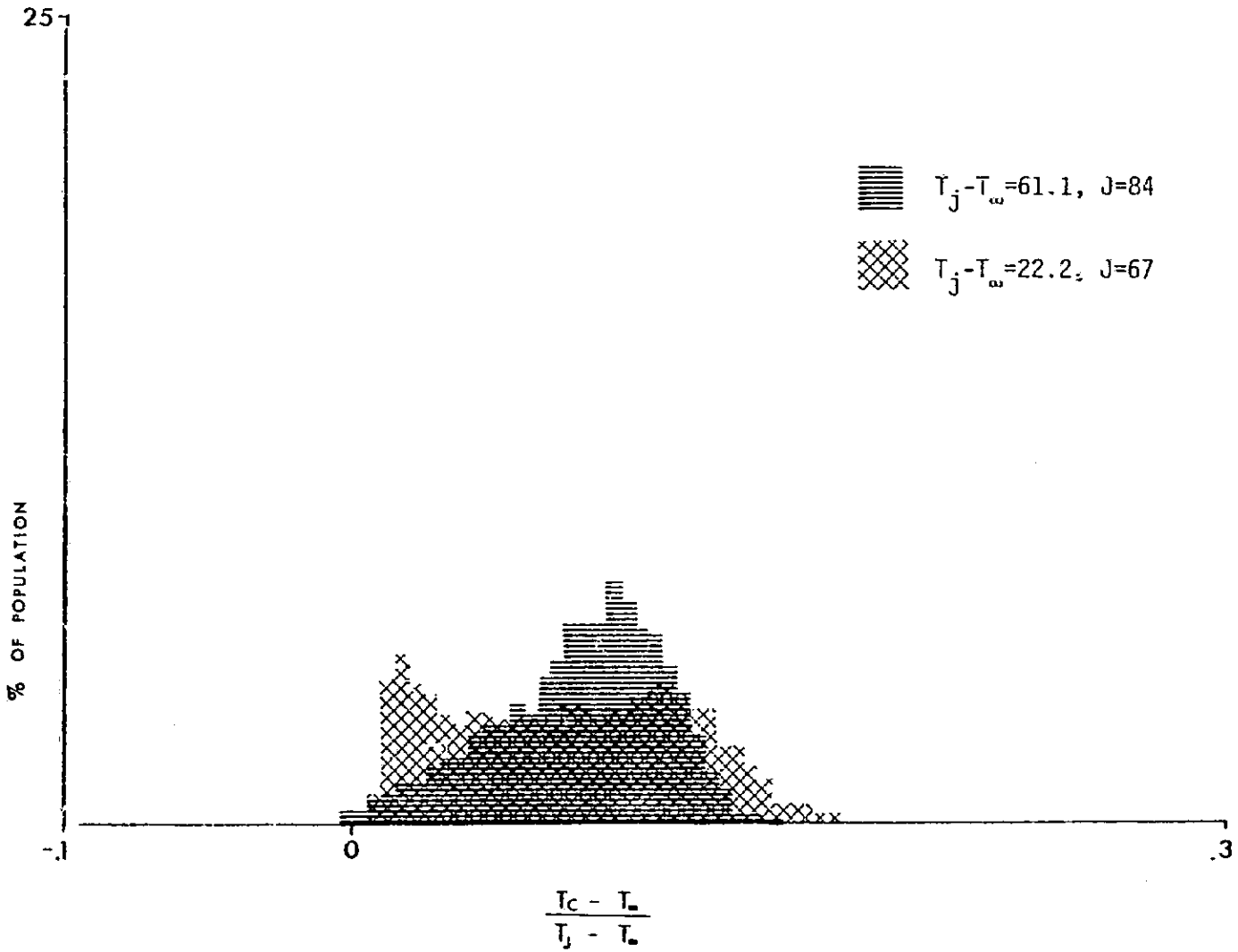

Figure 38. Temperature Histogram for u.c.f.: Thermocouple at s/d = .5, t/d = 4.55

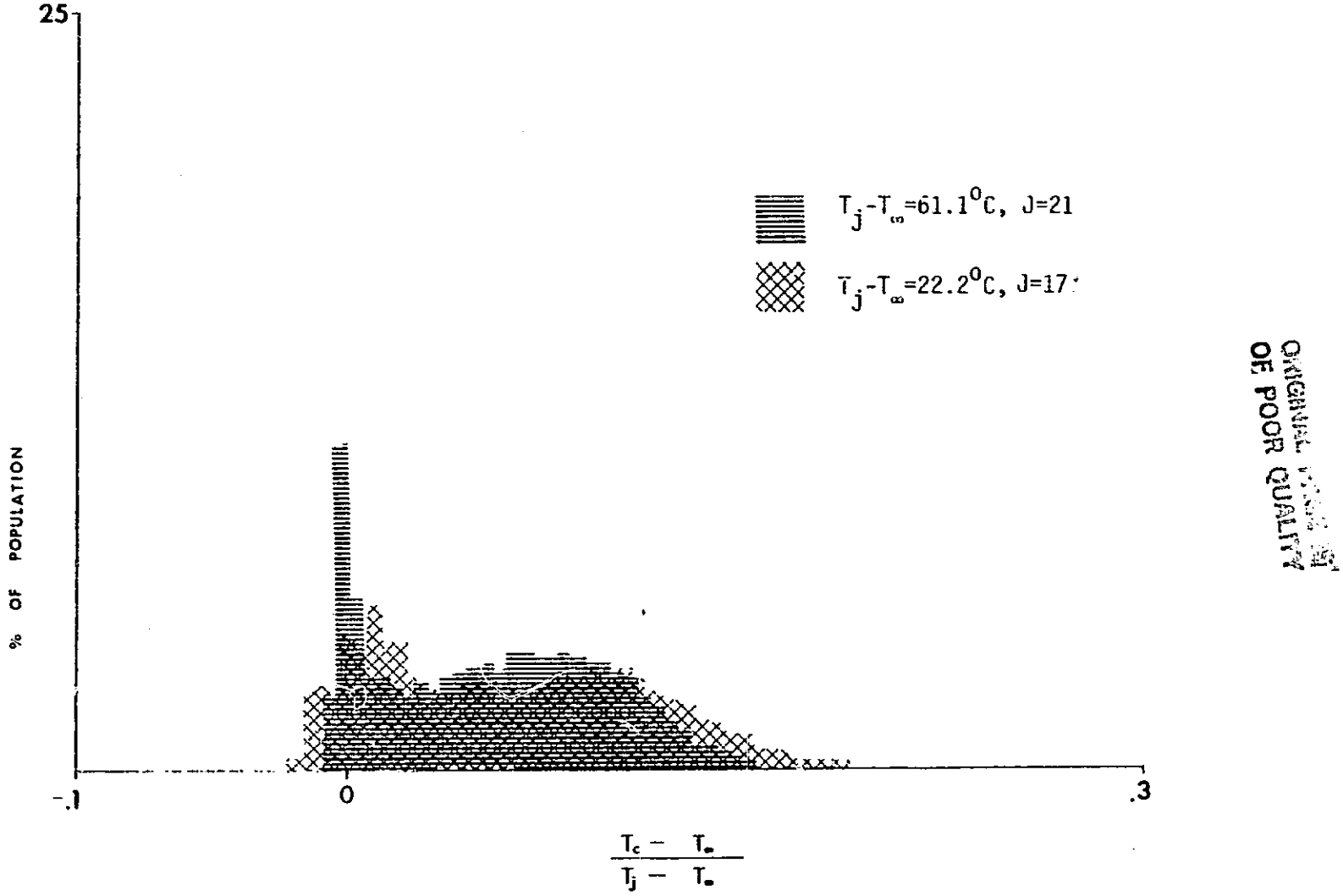

Figure 39. Temperature Histogram for d.c.f.:
Thermocouple at s/d = 5.64, t/d = 3.64

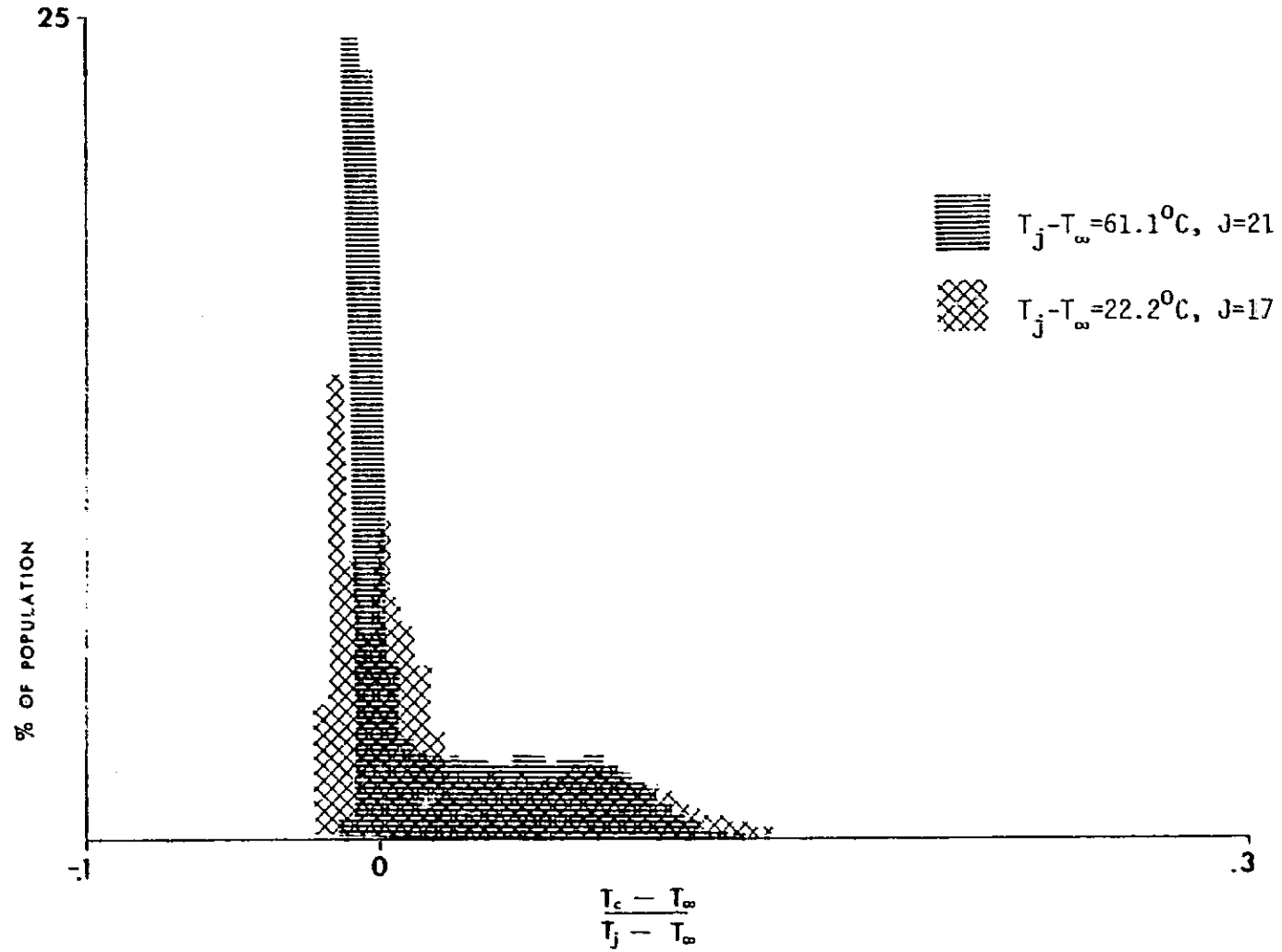

Figure 40. Temperature Histogram for d.c.f.:
Thermocouple at s/d = 2.78, t/d = 3.00

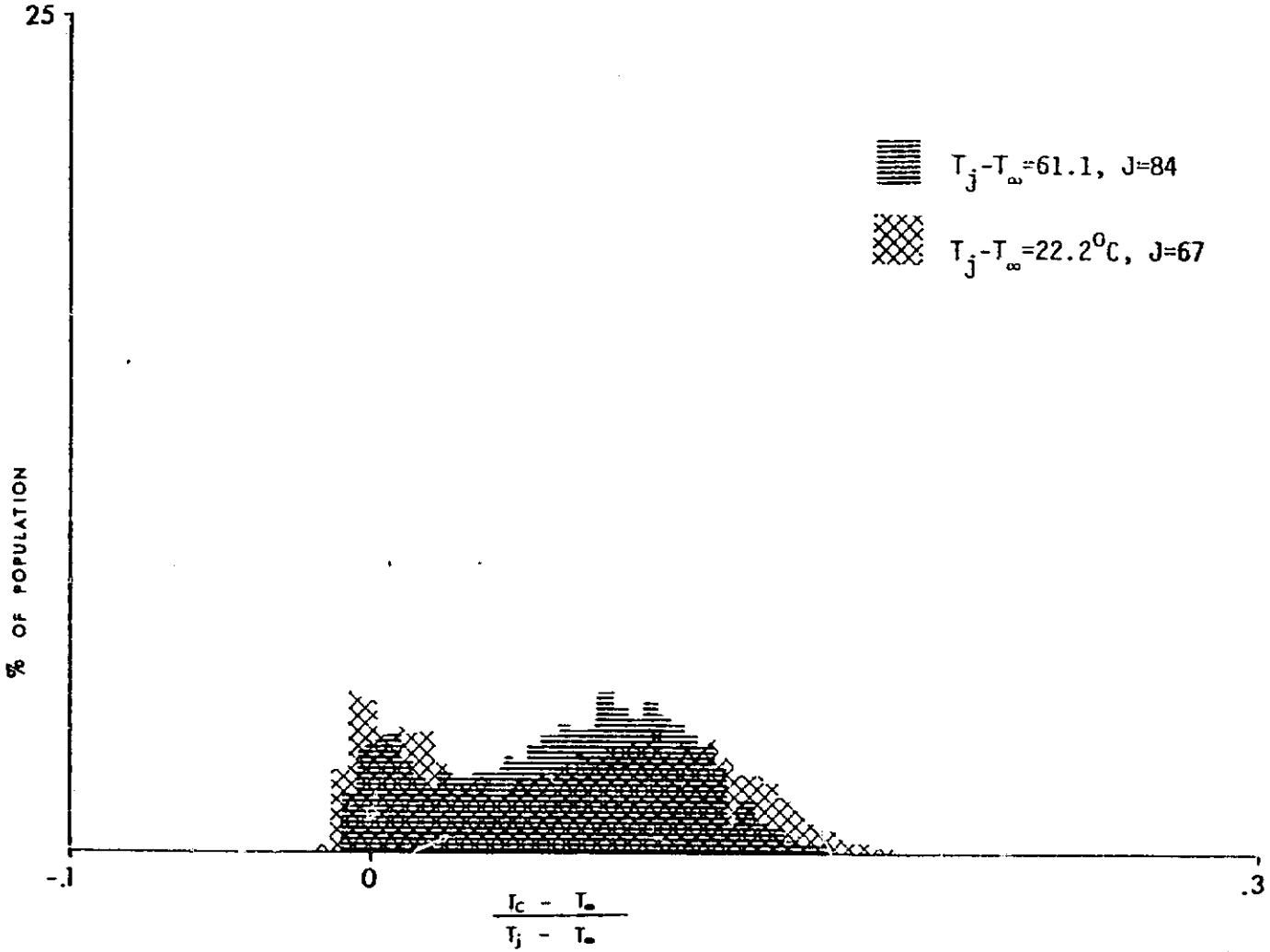

Figure 41. Temperature Histogram for d.c.f.:
Thermocouple at s/d = 3.87, t/d = 3.31

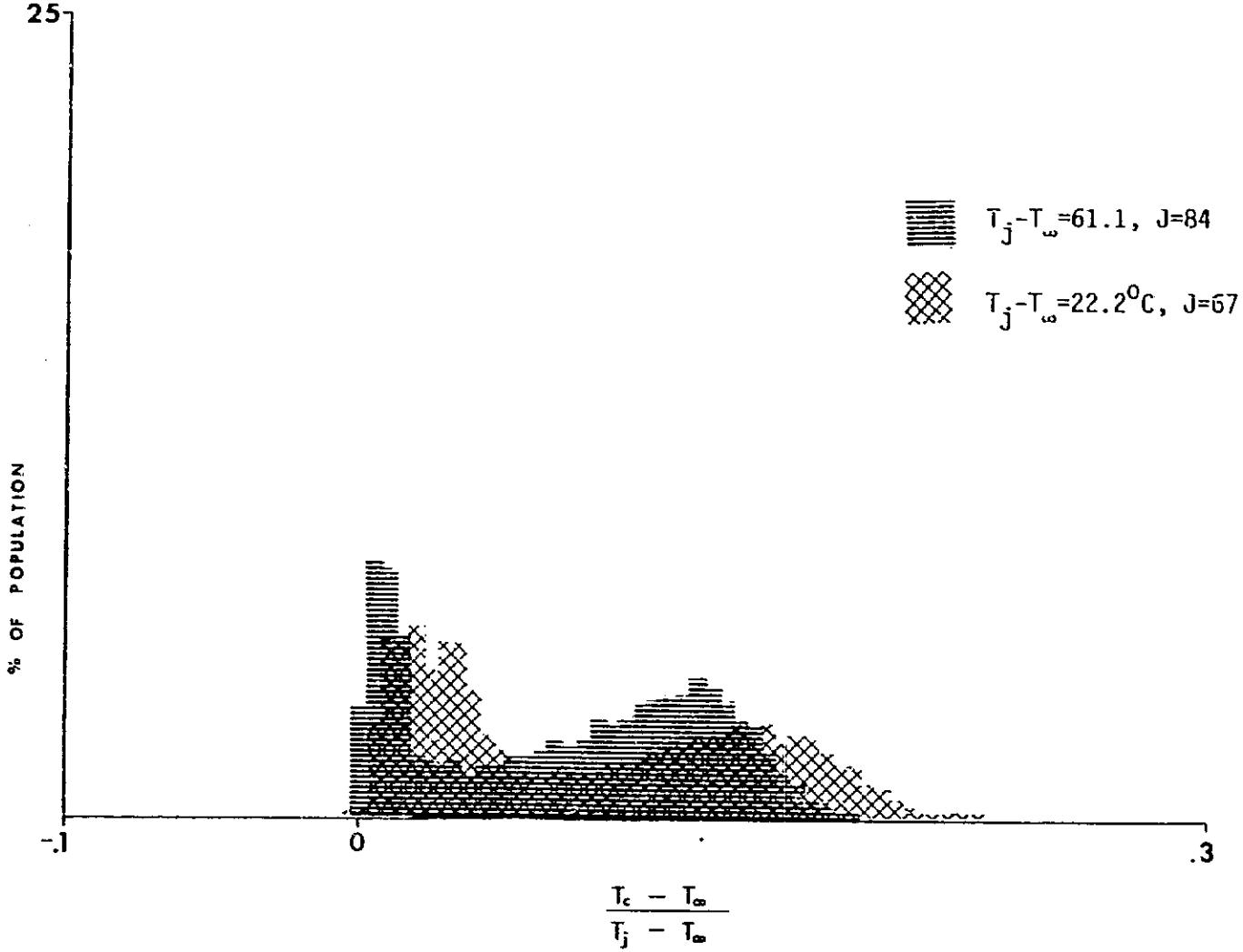

Figure 42. Temperature Histogram for d.c.f.:
Thermocouple at s/d = 1.75, t/d = 5.33

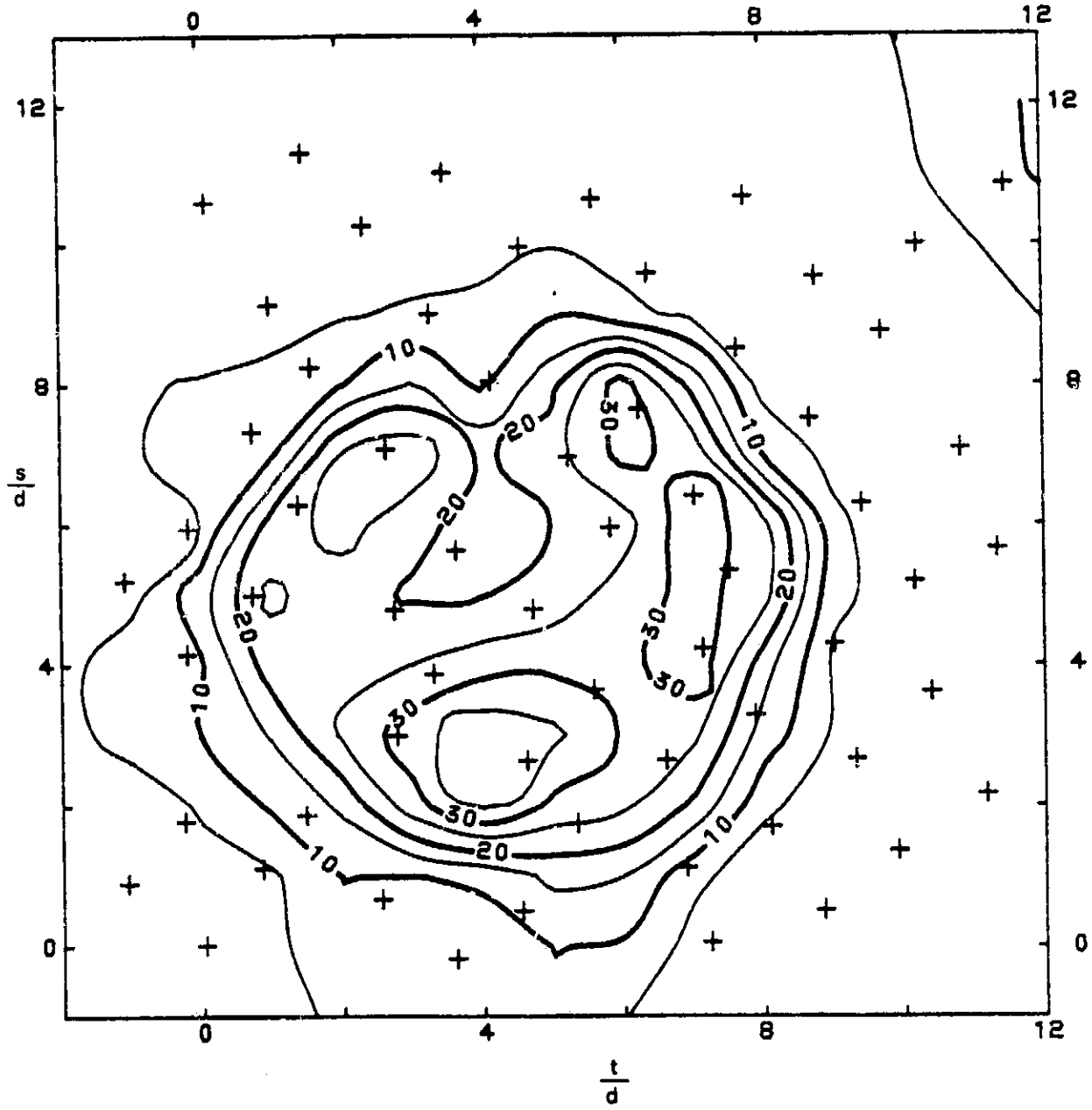

Figure 44. Undisturbed Cross Flow (u.c.f.) Contours of a Temperature Standard Deviation: J=17, $T_{jet} - T_{\infty} = 22.2°C$

NOTE: Values shown are $1000X[T_c(s,t) - T_{\infty}]_{rms}/(T_j - T_{\infty})$
s/d and t/d as defined for the mean temperature isotherms

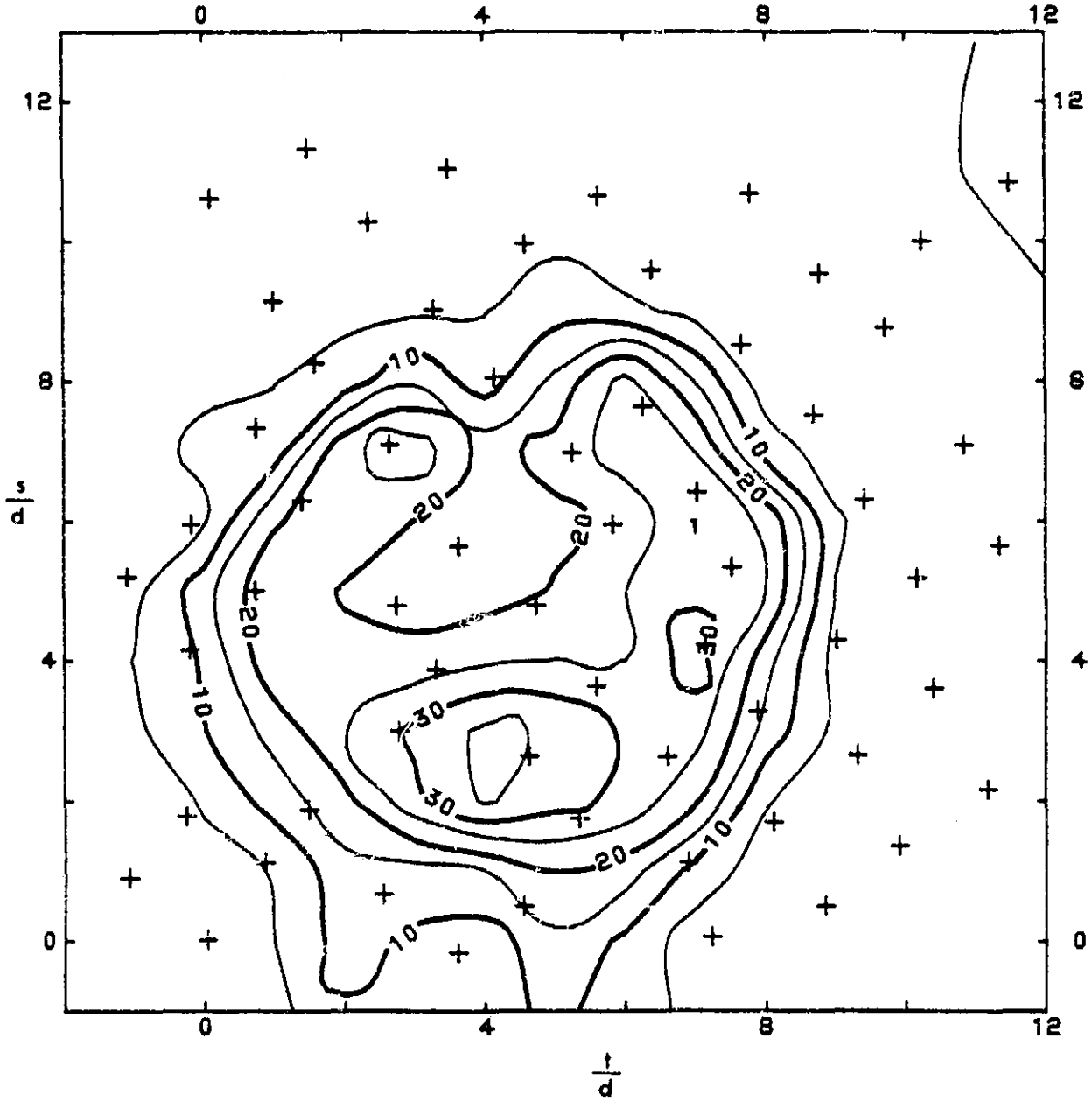

Figure 45. u.c.f. Contours of Constant Temperature Standard Deviation: J=19, $T_{jet} - T_{\infty} = 41.7°C$

NOTE: Values shown are $1000X[T_c(s,t) - T_{\infty}]_{rms}/(T_j - T_{\infty})$
s/d and t/d as defined for the mean temperature isotherms

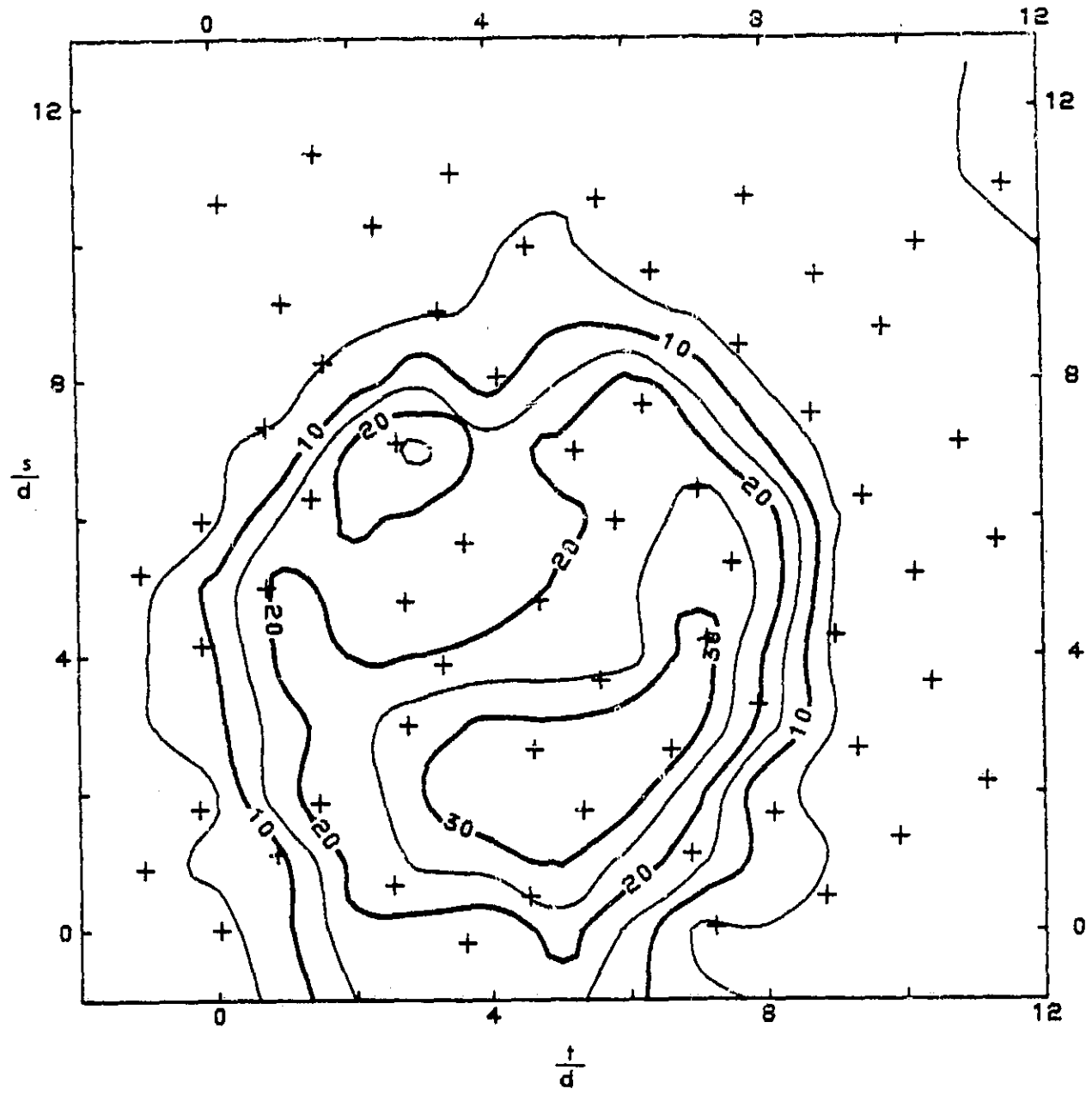

Figure 46. u.c.f. Contours of Constant Temperature Standard Deviation: J=21, $T_{jet} - T_\infty = 61.1°C$

NOTE: Values shown are $1000X[T_c(s,t) - T_\infty]_{rms}/(T_j - T_\infty)$

s/d and t/d as defined for the mean temperature isotherms

C-2

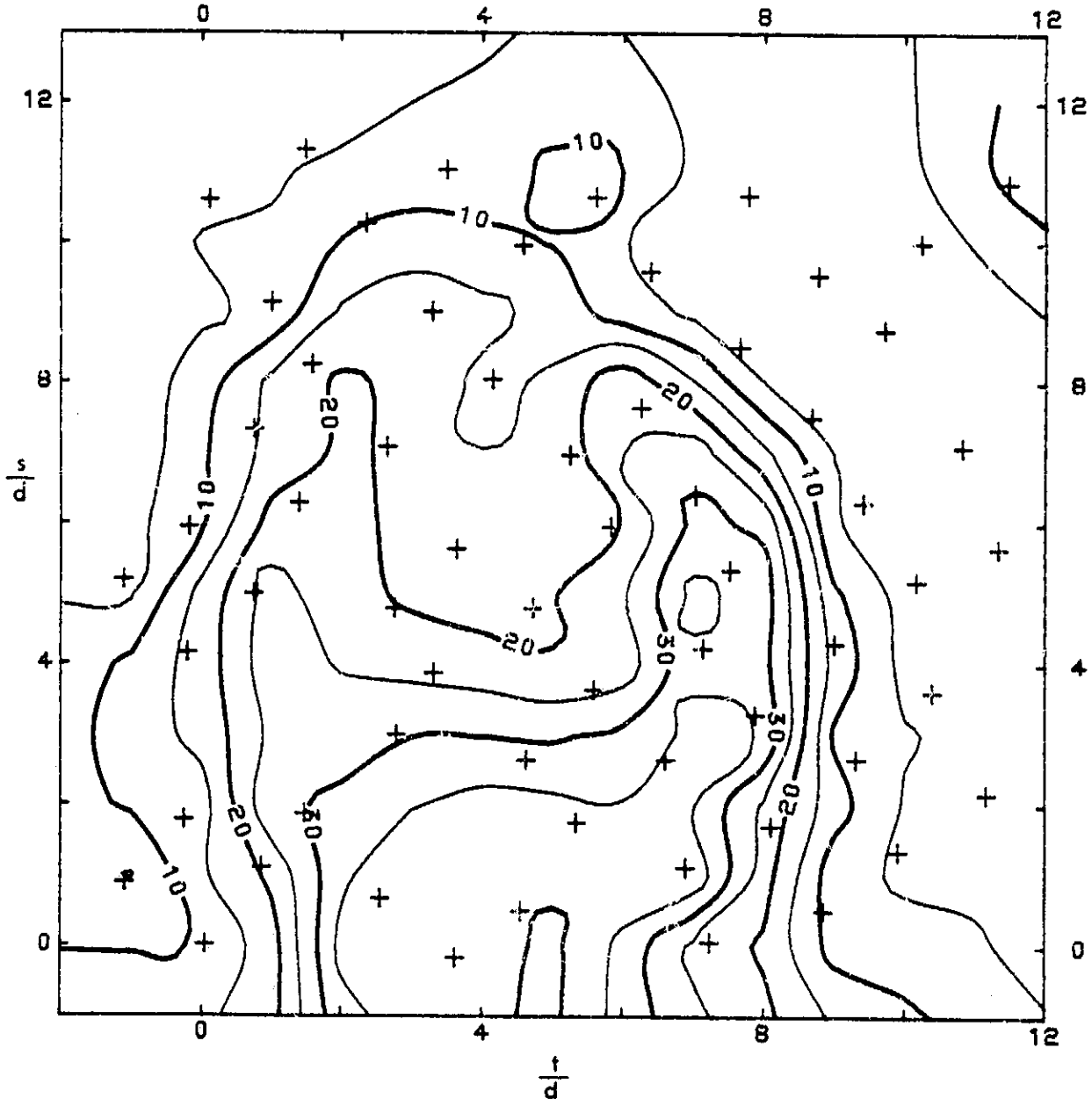

Figure 47. u.c.f. Contours of Constant Temperature Standard Deviation: J=67, $T_{jet} - T_{\infty} = 22.2°C$

NOTE: Values shown are $1000X[T_c(s,t) - T_{\infty}]_{rms}/(T_j - T_{\infty})$
s/d and t/d as defined for the mean temperature isotherms

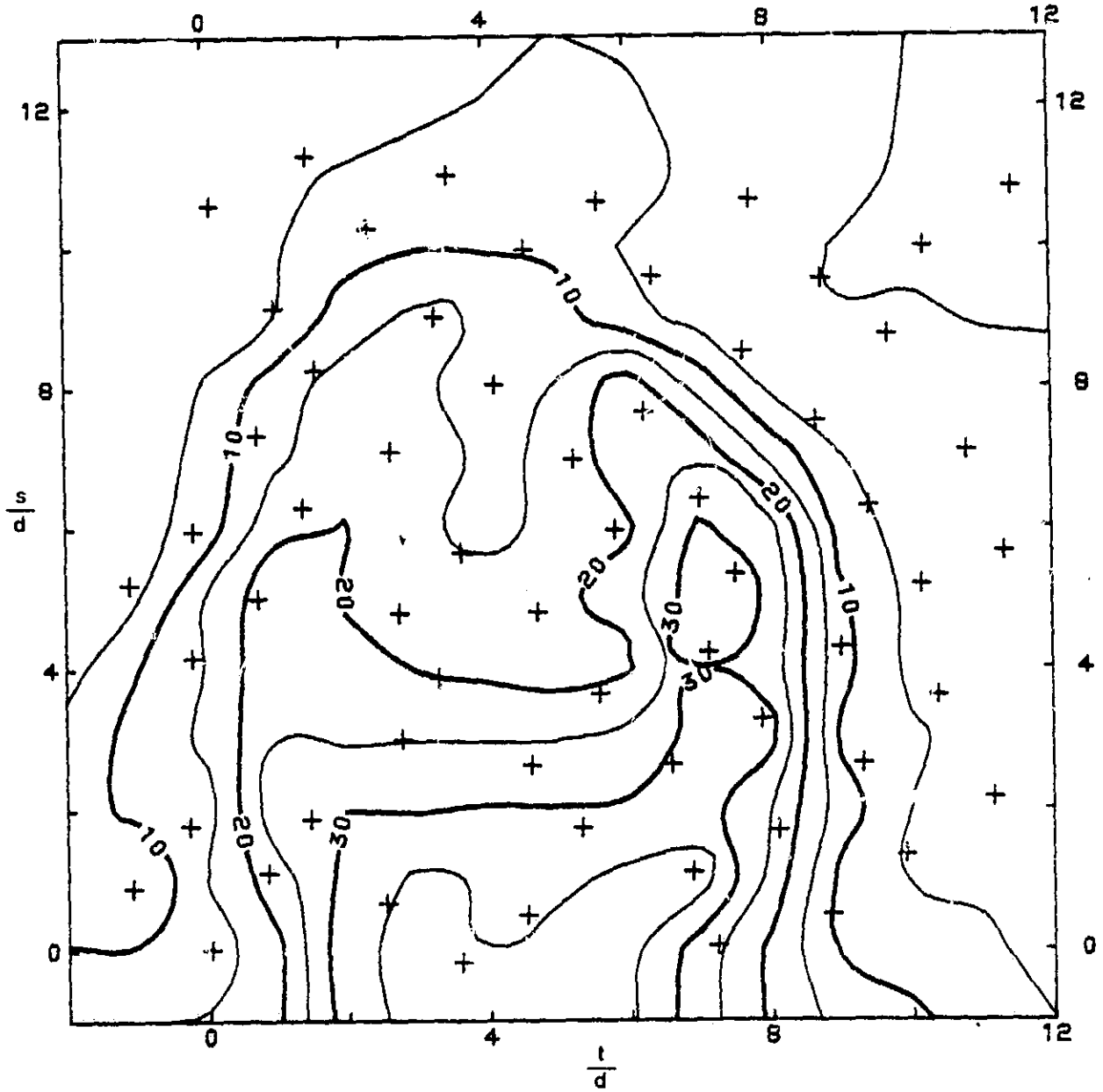

Figure 48. u.c.f. Contours of Constant Temperature Standard Deviation: J=76, $T_{jet} - T_{\infty} = 41.7°C$

NOTE: Values shown are $1000X[T_c(s,t) - T_{\infty}]_{rms}/(T_j - T_{\infty})$

s/d and t/d as defined for the mean temperature isotherms

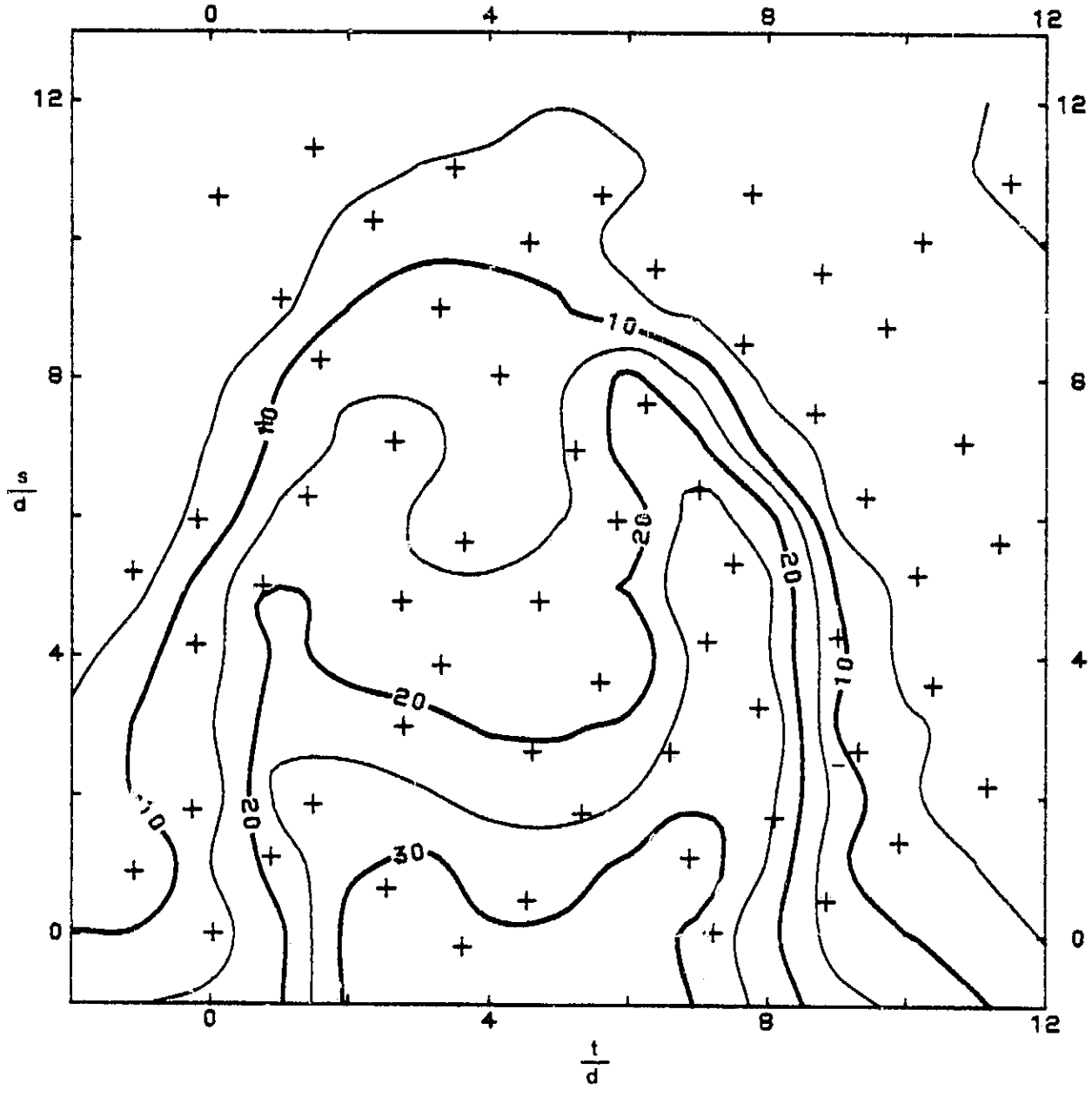

Figure 49. u.c.f. Contours of Constant Temperature Standard Deviation: J = 84, $T_{jet} - T_{\infty} = 61.1°C$

NOTE: Values shown are $1000X[T_c(s,t) - T_{\infty}]_{rms}/(T_j - T_{\infty})$
s/d and t/d as defined for the mean temperature isotherms

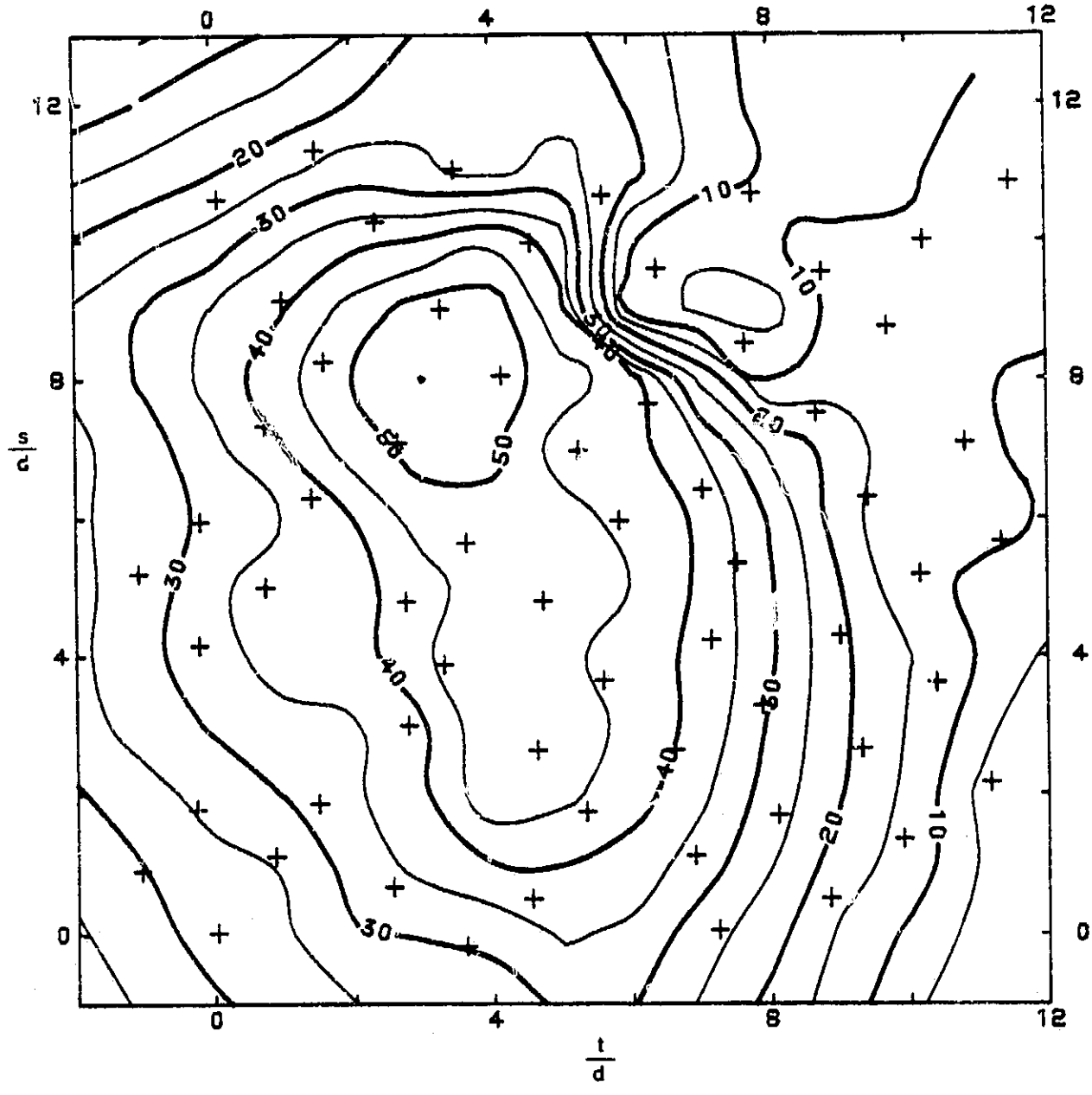

Figure 50. Disturbed Cross Flow (d.c.f.) Contours of Constant Temperature Standard Deviation: $J = 17$, $T_{jet} - T_{\infty} = 22.2°C$

NOTE: Values shown are $1000X[T_c(s,t) - T_{\infty}]_{rms}/(T_j - T_{\infty})$
s/d and t/d as defined for the mean temperature isotherms

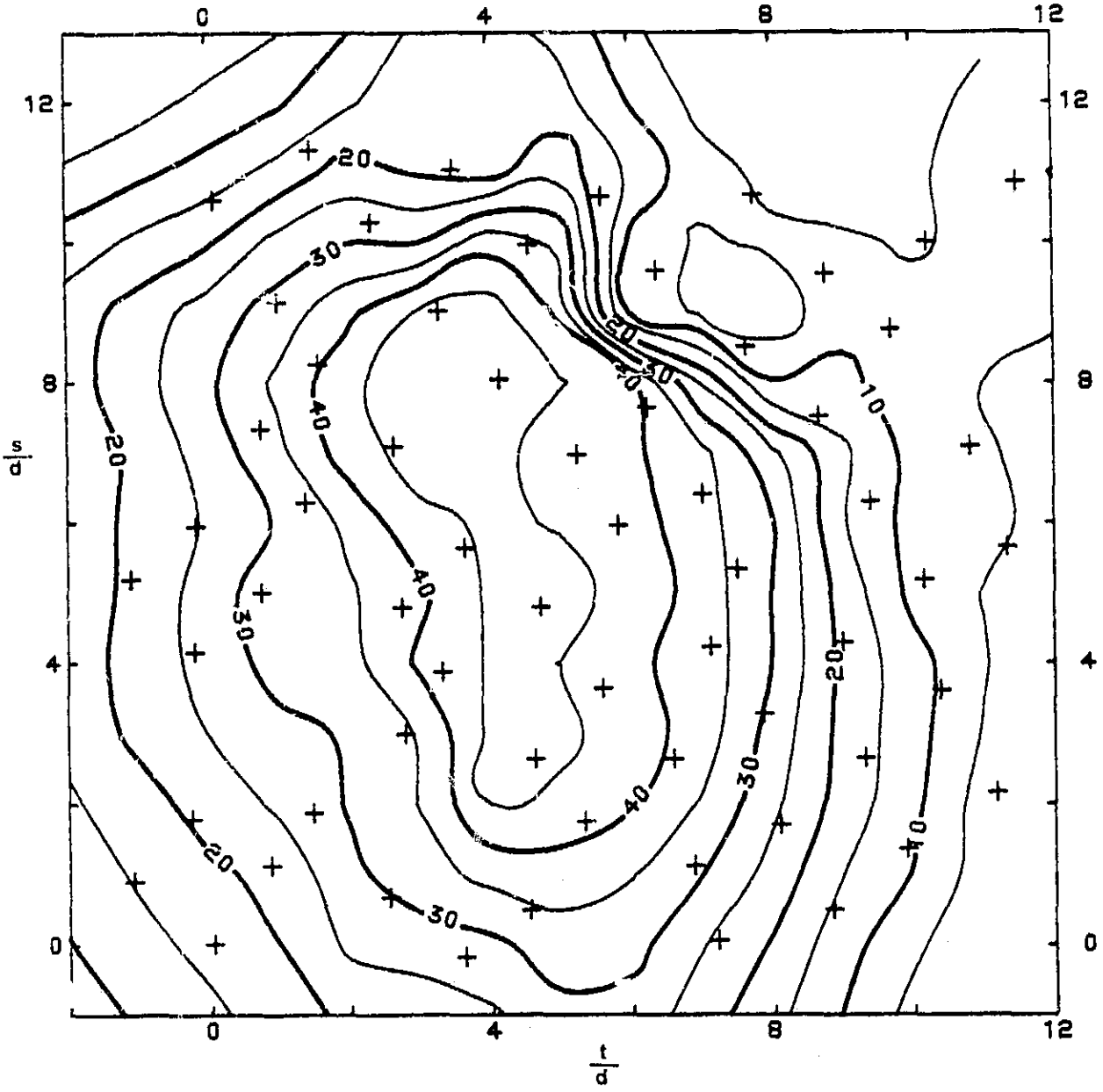

Figure 51. d.c.f. Contours of Constant Temperature Standard Deviation: J = 19, $T_{jet} - T_{\infty} = 41.7°C$

NOTE: Values shown are $1000X[T_c(s,t) - T_{\infty}]_{rms}/T_j - T_{\infty})$
s/d and t/d as defined for the mean temperature isotherms

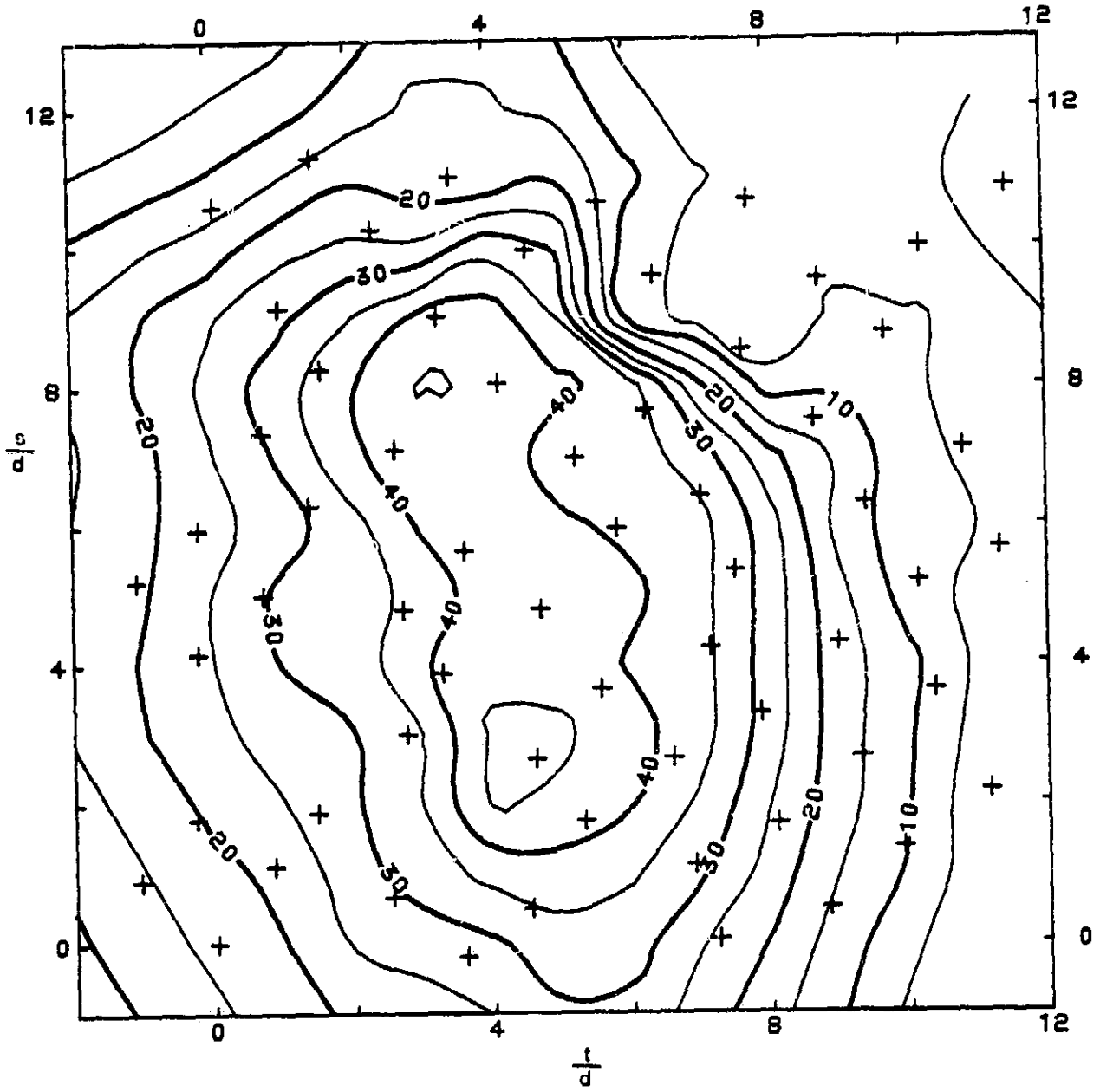

Figure 52. d.c.f. Contours of Constant Temperature Standard Deviation: J = 21, $T_{jet} - T_\infty$ = 61.1°C

NOTE: Values shown are $1000X[T_c(s,t) - T_\infty]_{rms}/T_j - T_\infty)$
s/d and t/d as defined for the mean temperature isotherms

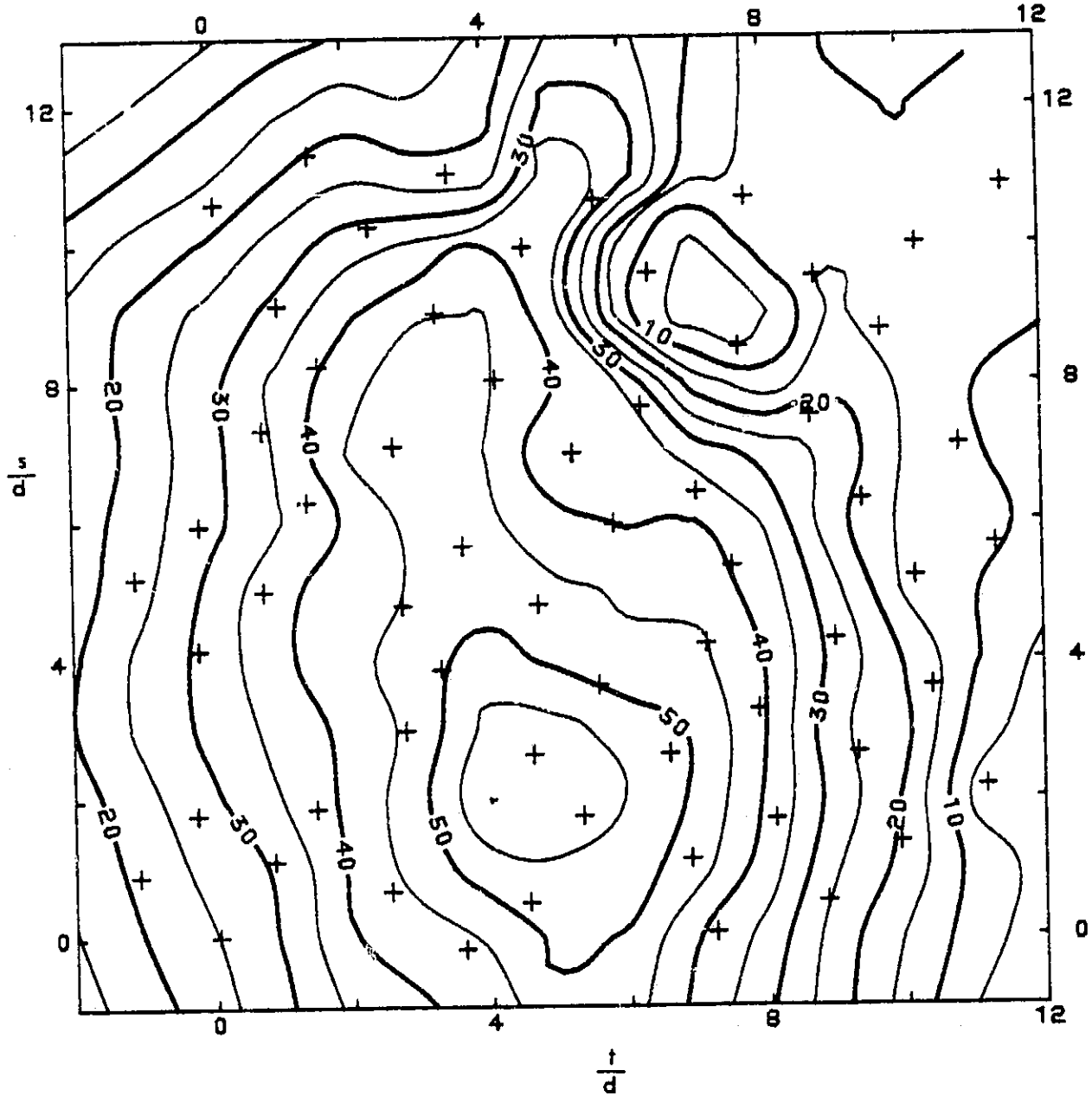

Figure 53. d.c.f. Contour of Constant Temperature Standard Deviation: J = 67, $T_{jet} - T_{\infty} = 22.2°C$

NOTE: Values shown are $1000X[T_c(s,t) - T_{\infty}]_{rms}/T_j - T_{\infty})$
s/d and t/d as defined for the mean temperature isotherms

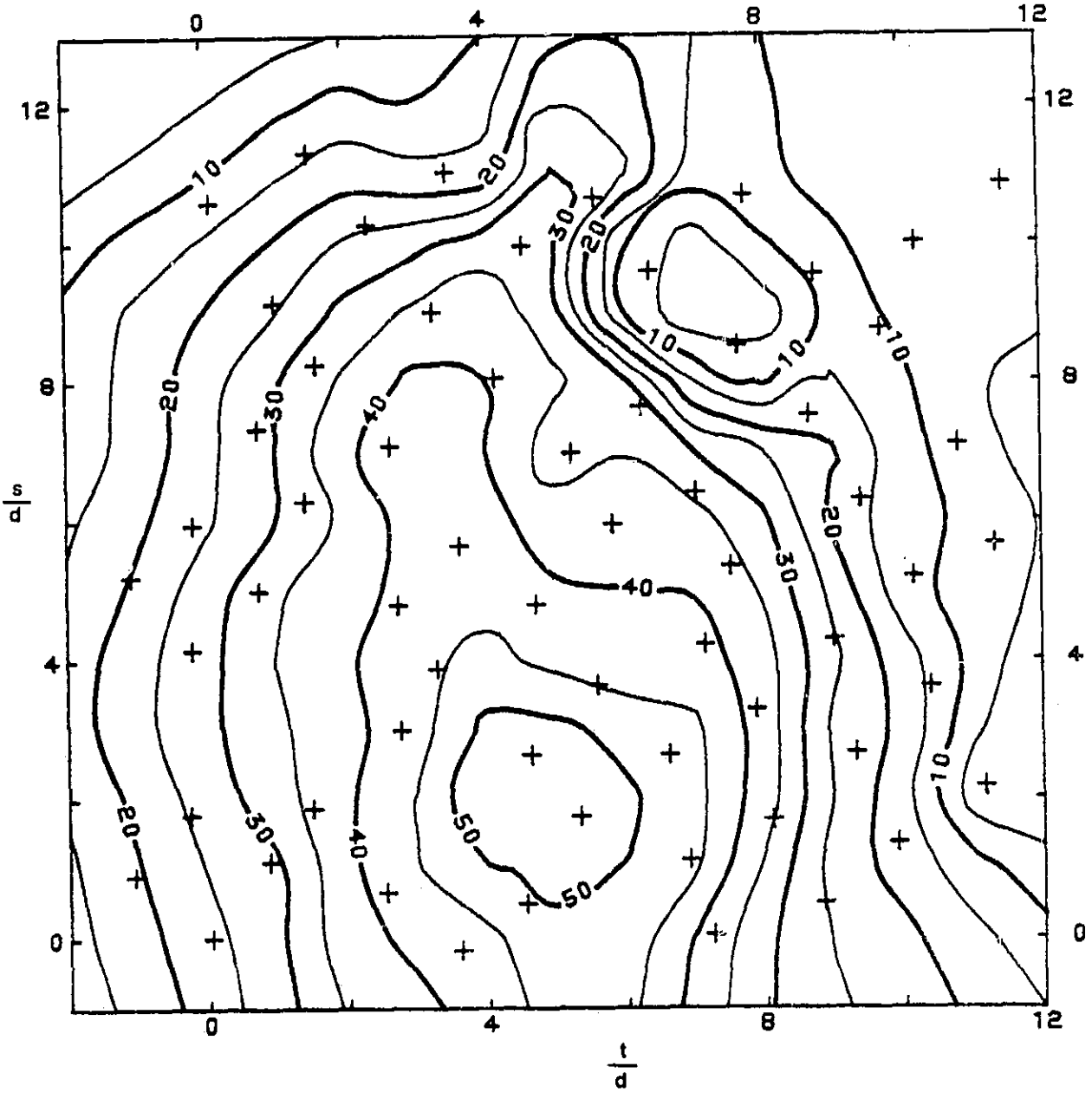

Figure 54. d.c.f. Contour of Constant Temperature Standard Deviation: J = 76, $T_{jet} - T_{\infty} = 41.7°C$

NOTE: Values shown are $1000X[T_c(s,t) - T_{\infty}]_{rms}/T_j - T_{\infty})$
s/d and t/d as defined for the mean temperature isotherms

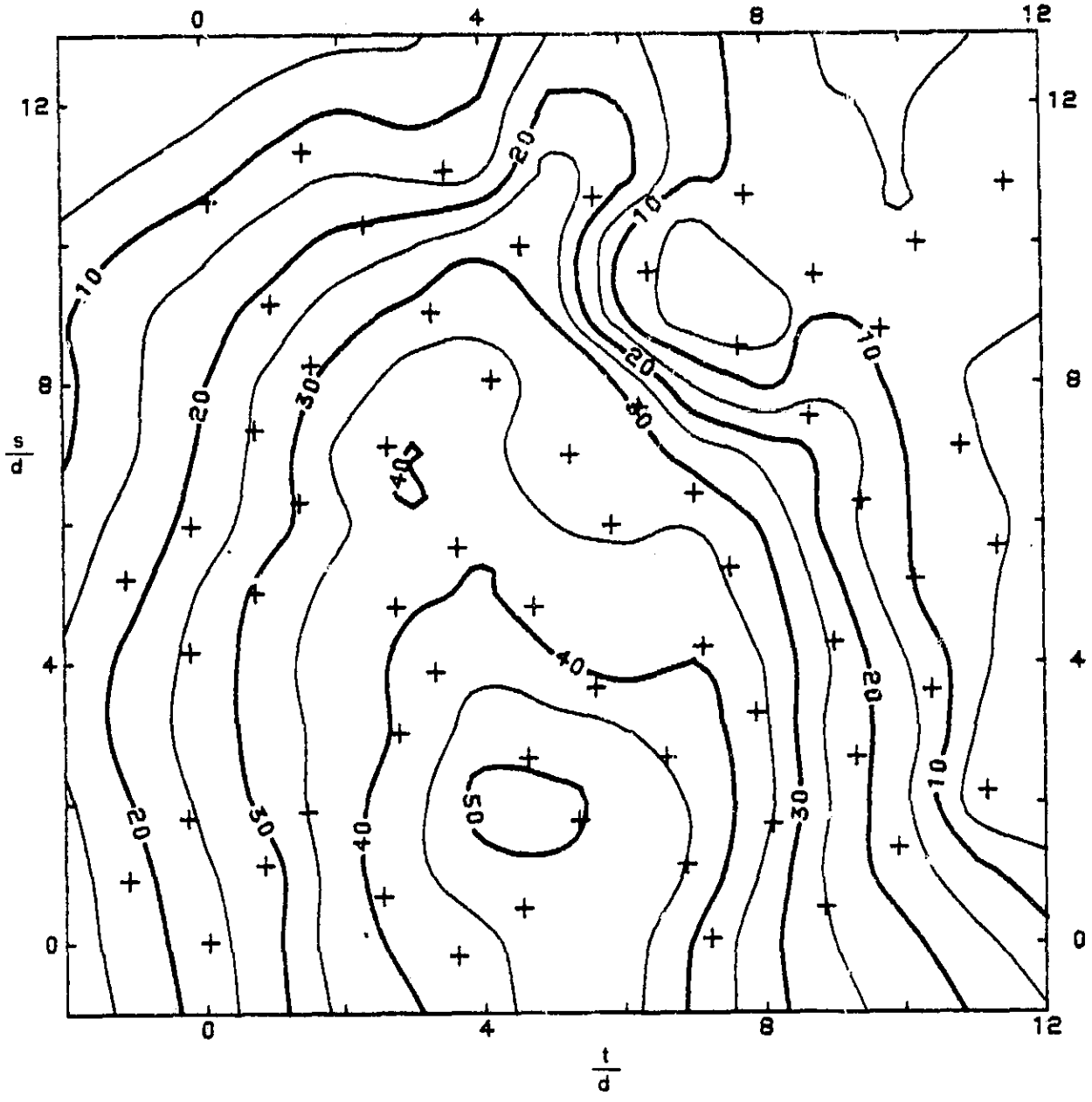

Figure 55. d.c.f. Contour of Constant Temperature Standard Deviation: $J = 84$, $T_{jet} - T_{\infty} = 61.1°C$

NOTE: Values shown are $1000X[T_c(s,t) - T_{\infty}]_{rms}/T_j - T_{\infty})$
s/d and t/d as defined for the mean temperature isotherms

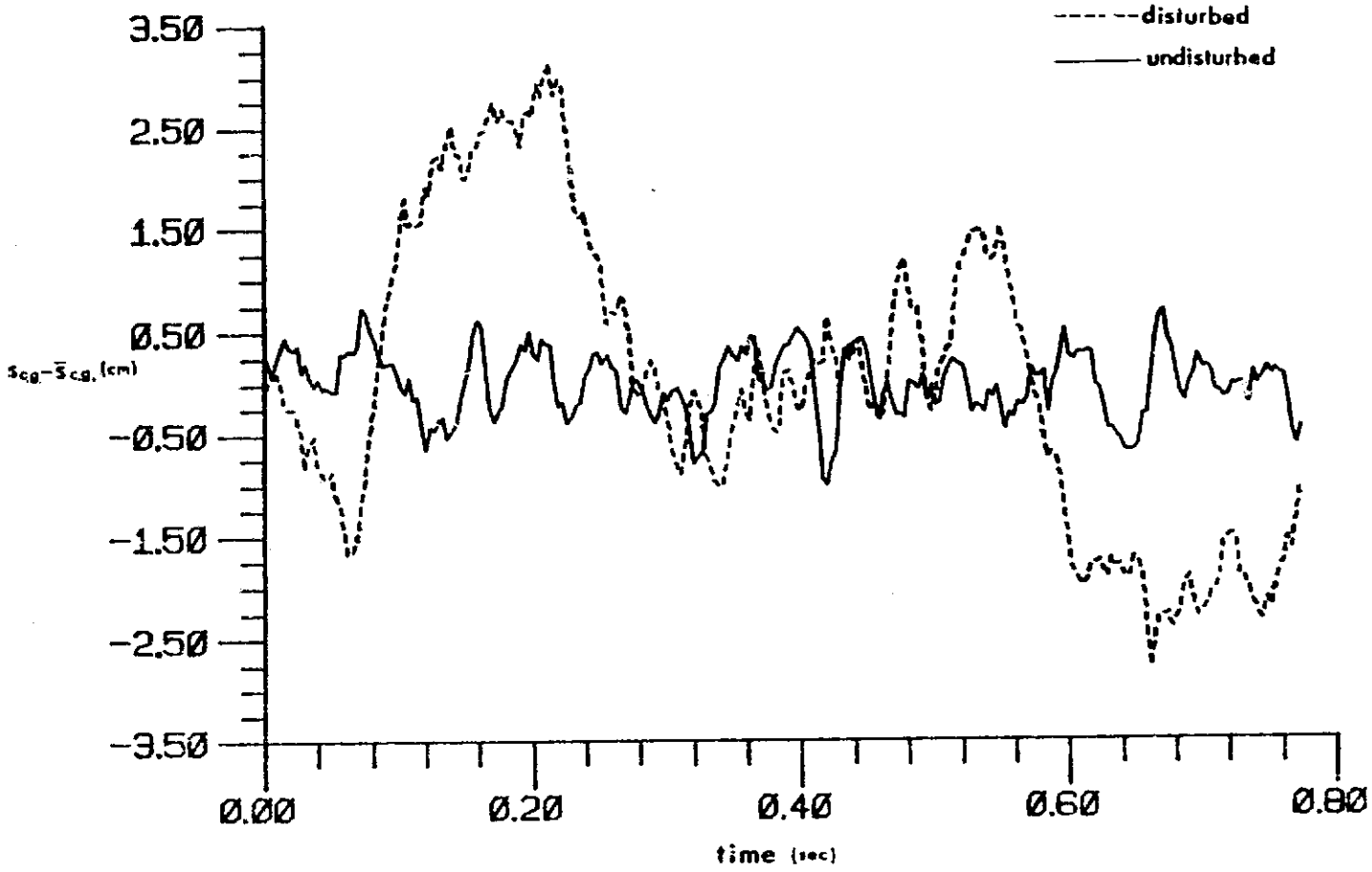

Figure 56. Variation of s Component of Centroid with Time
J = 21, $T_{jet} - T_{\infty} = 61.1°C$

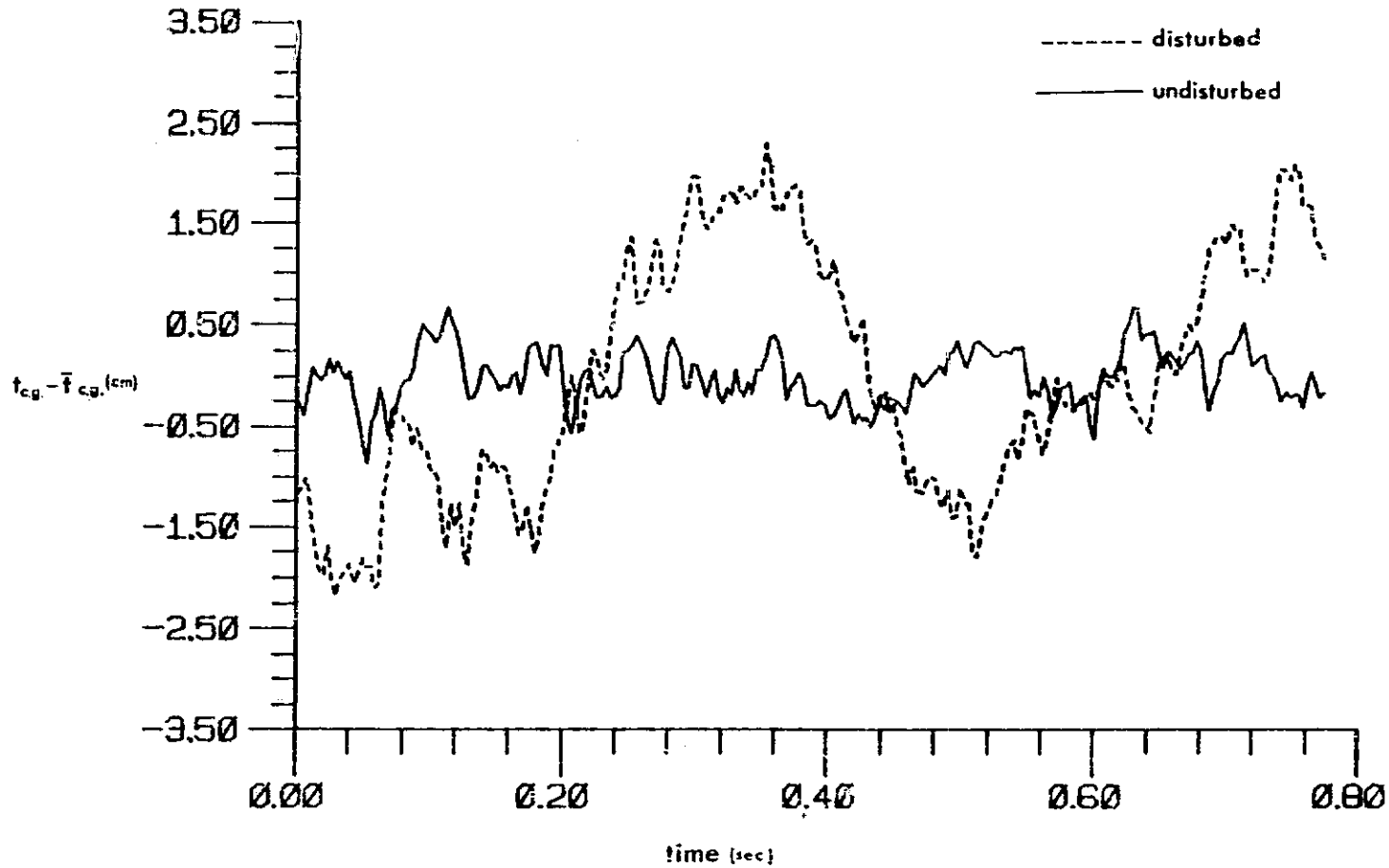

Figure 57. Variation of t Component of Centroid with Time
J = 21, $T_{jet} - T_{\infty} = 61.1°C$

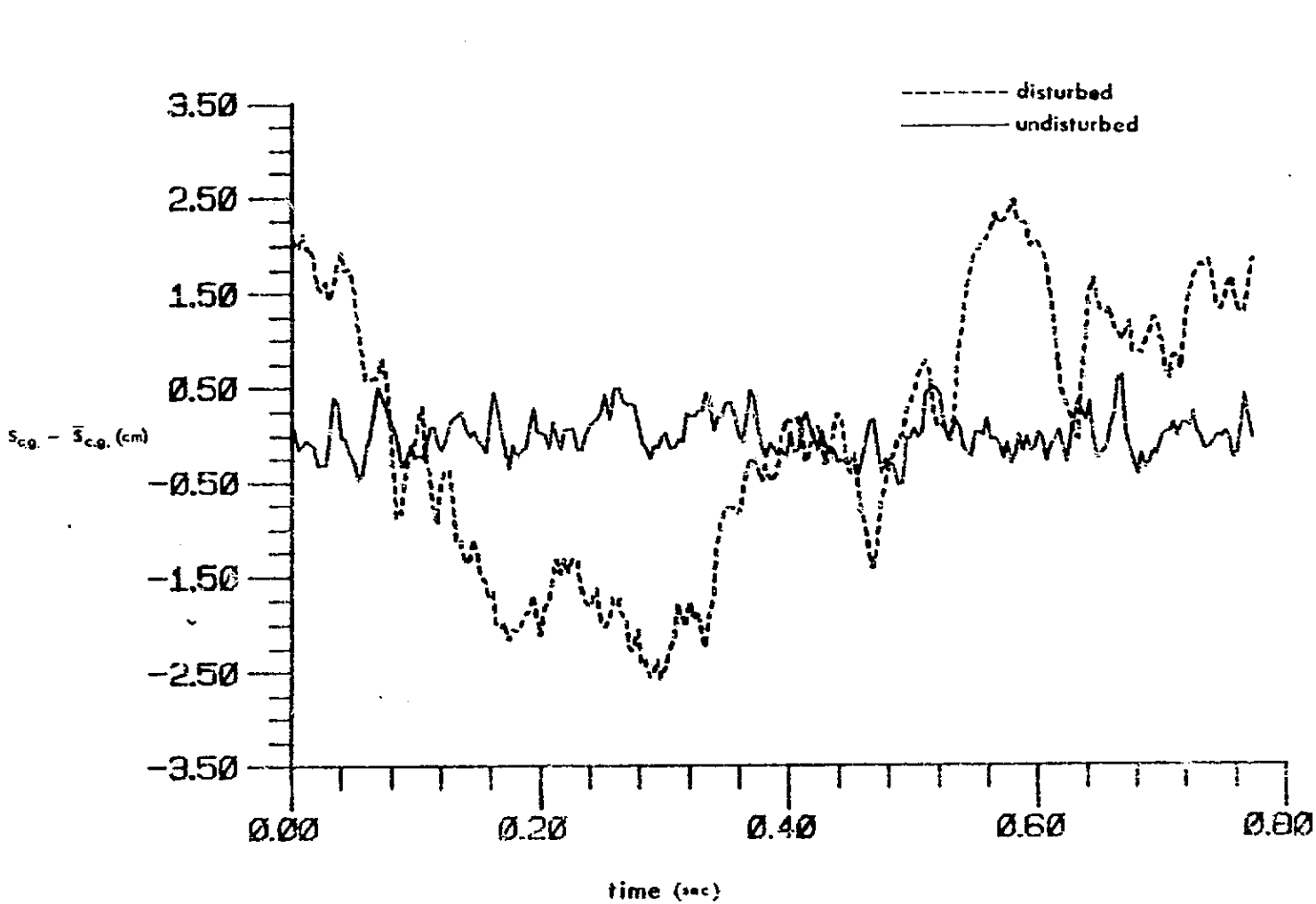

Figure 58. Variation of s Component of Centroid with Time
J = 84, $T_{jet} - T_{\infty} = 61.1°C$

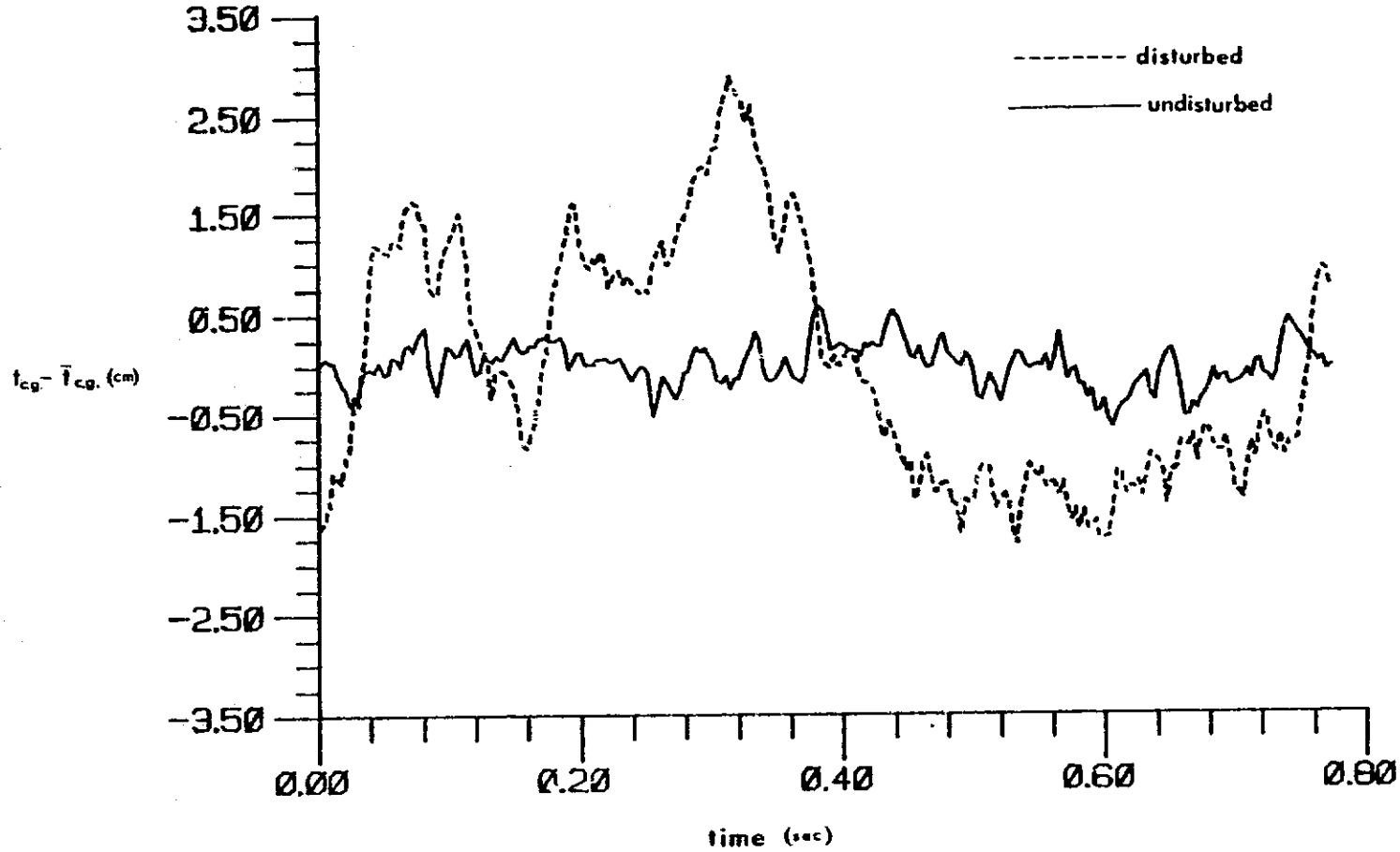

Figure 59. Variation of t Component of Centroid with Time
J = 34, $T_{jet} - T_{\infty}$ = 61.1°C

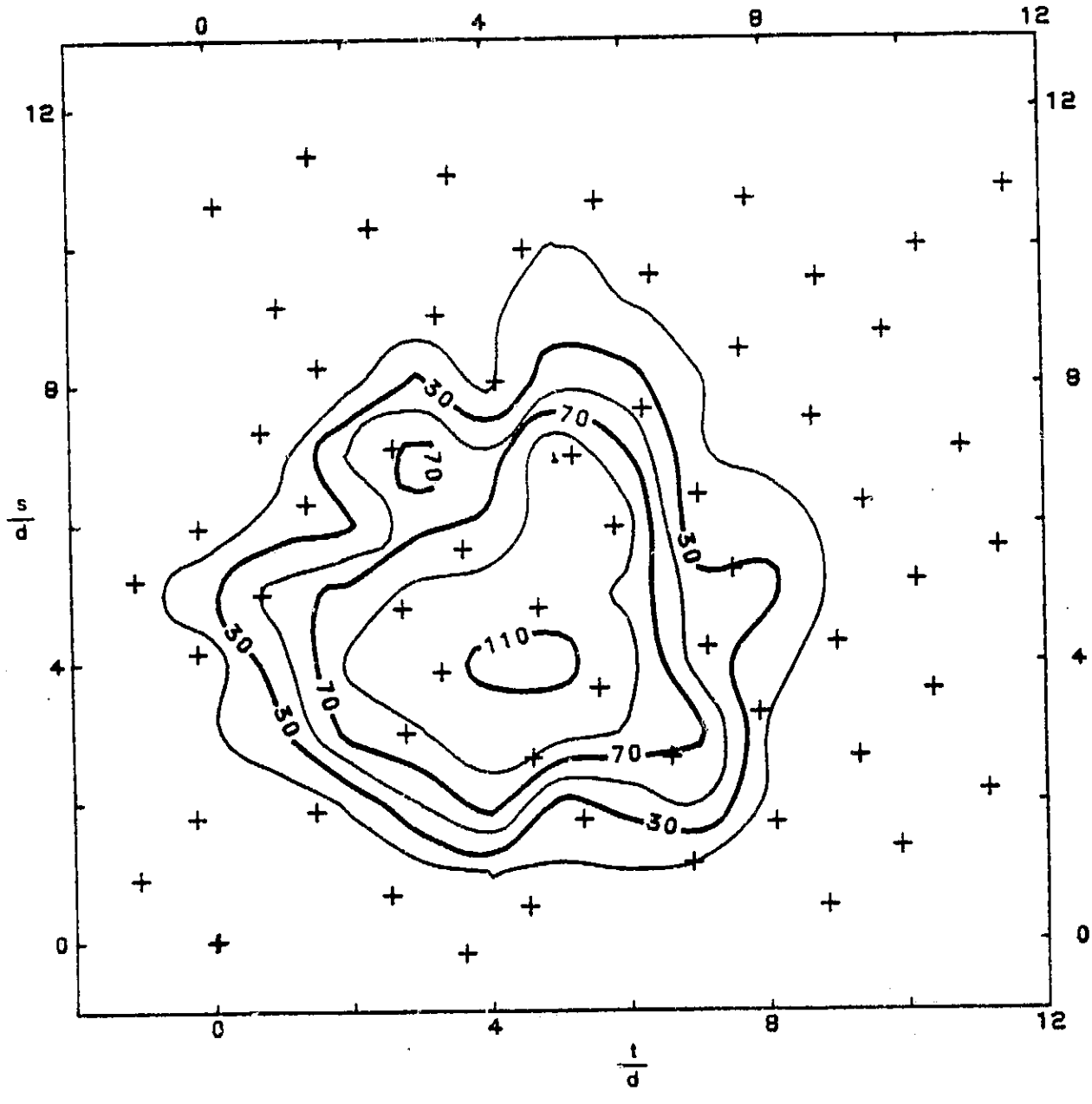

Figure 60. Undisturbed Cross Flow (u.c.f.) Instantaneous Temperature Isotherms, J = 21, $T_{jet} - T_{\infty}$ = 61.1°C, Time = .2 sec

NOTE: Contours shown are $\frac{T_o - T_{\infty}}{T_{jet} - T_{\infty}}$ X 1000, s/d and t/d as defined for the mean temperature isotherms

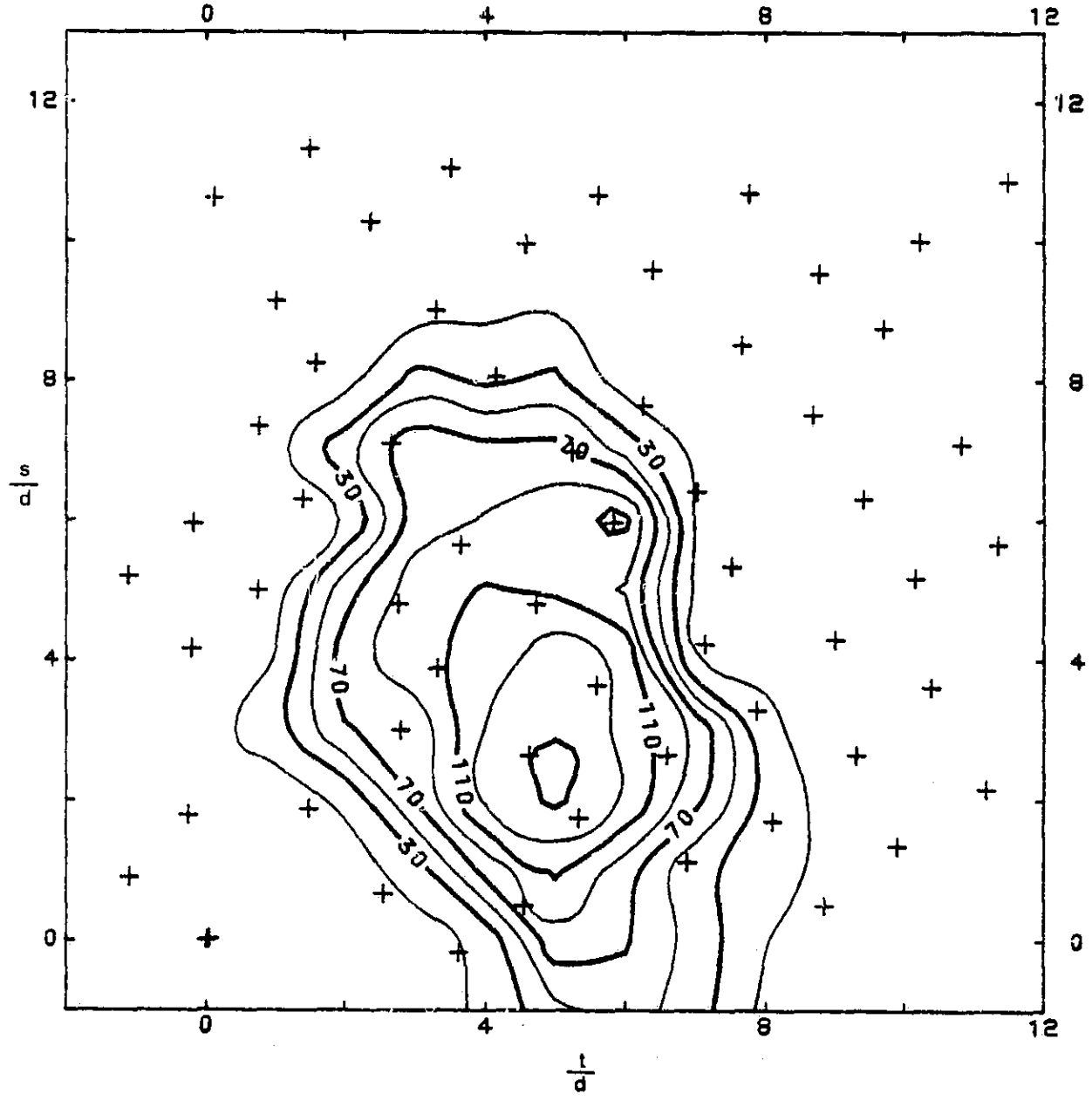

Figure 61. u.c.f. Instantaneous Temperature Isotherms
J = 21, $T_{jet} - T_{\infty}$ = 61.1°C, Time = .65 sec

NOTE: Contours are $\frac{T_o - T_{\infty}}{T_{jet} - T_{\infty}}$ X 1000, s/d and t/d as defined for the mean temperature isotherms

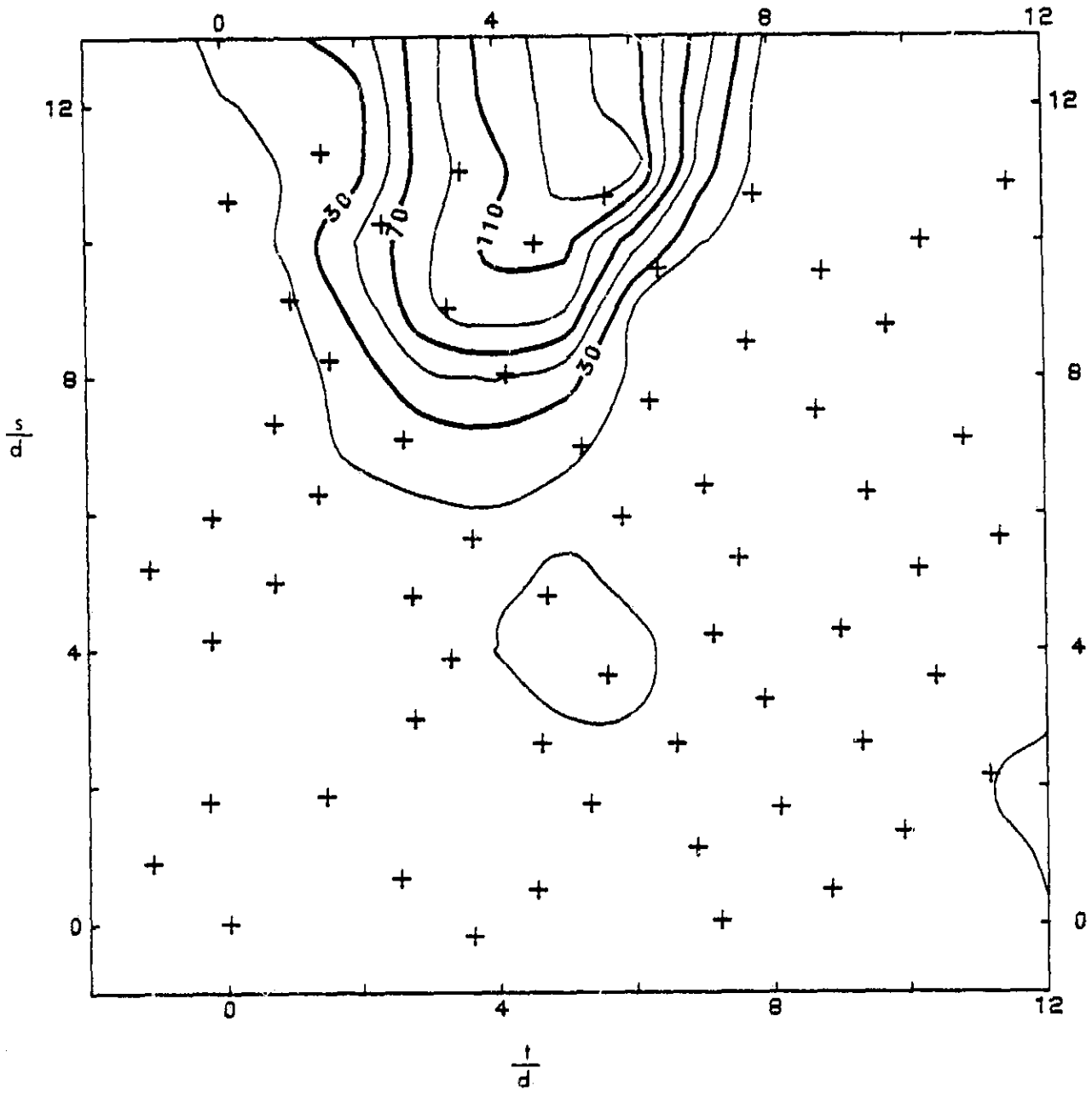

Figure 62. d.c.f. Instantaneous Temperature Isotherms
J = 21, $T_{jet} - T_{\infty}$ = 61.1°C, Time = .2 sec

NOTE: Contours are $\frac{T_o - T_\infty}{T_{jet} - T_\infty}$ X 1000, s/d and t/d as defined for the mean temperature isotherms

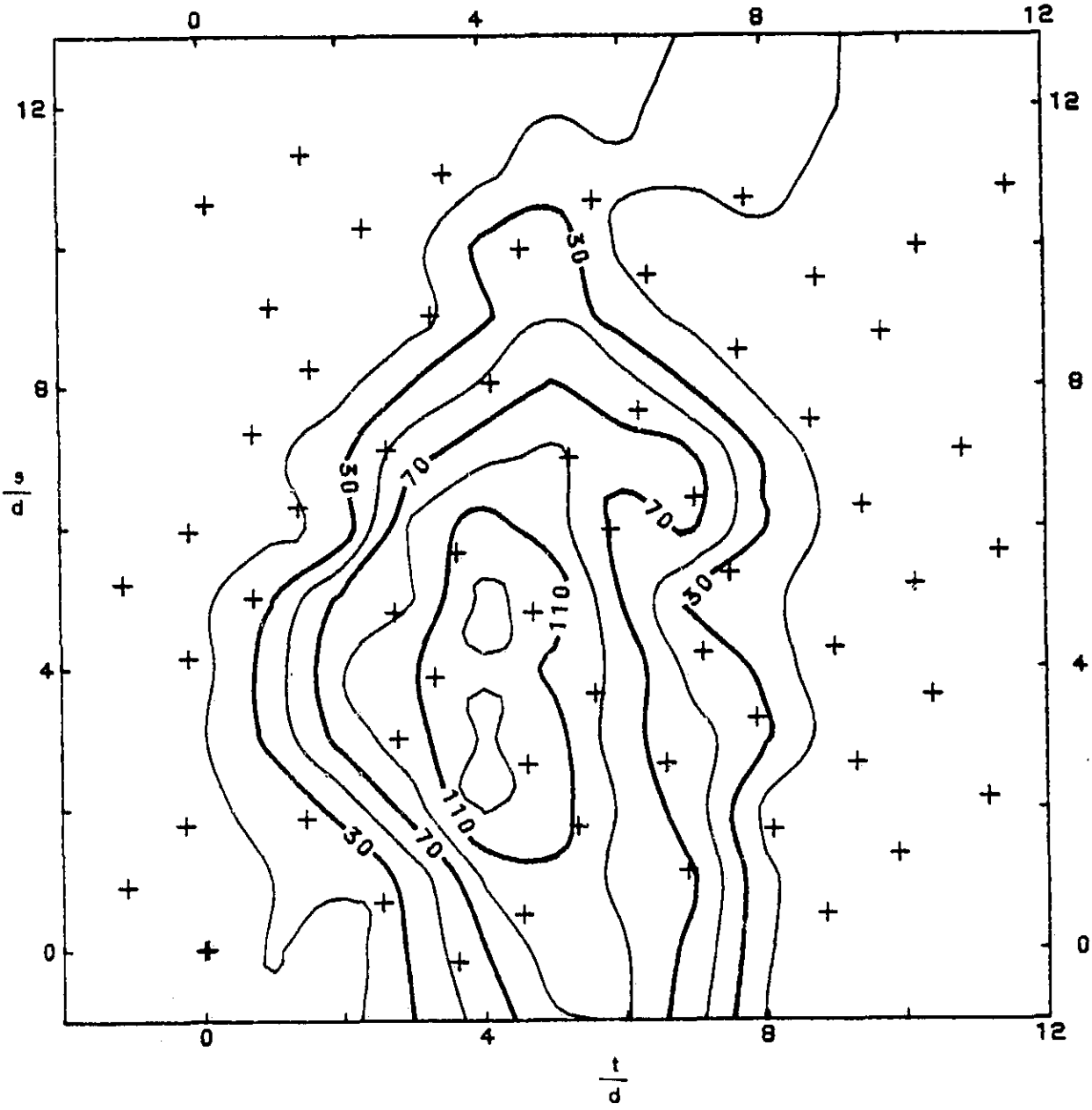

Figure 63. d.c.f. Instantaneous Temperature Isotherms
J = 21, $T_{jet} - T_{\infty}$ = 61.1°C, Time = .65 sec

NOTE: Contours are $\frac{T_0 - T_{\infty}}{T_{jet} - T_{\infty}}$ X 1000, s/d and t/d as defined for the mean temperature isotherms

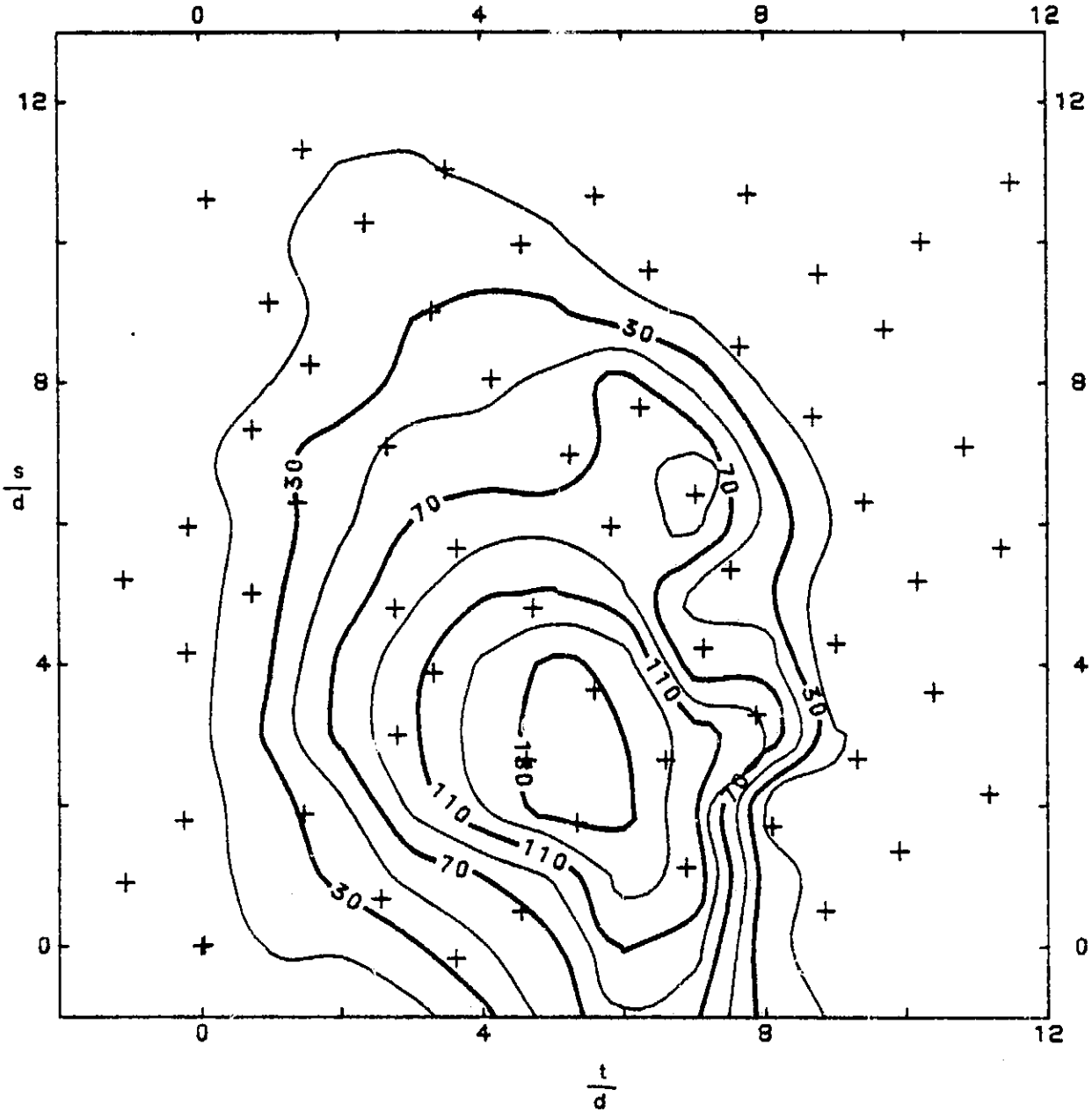

Figure 64. u.c.f. Instantaneous Temperature Isotherms
J = 84, $T_{jet} - T_{\infty}$ = 61.1°C, Time = .3 sec

NOTE: Contours are $\frac{T_0 - T_{\infty}}{T_{jet} - T_{\infty}}$ X 1000, s/d and t/d as defined for the mean temperature isotherms

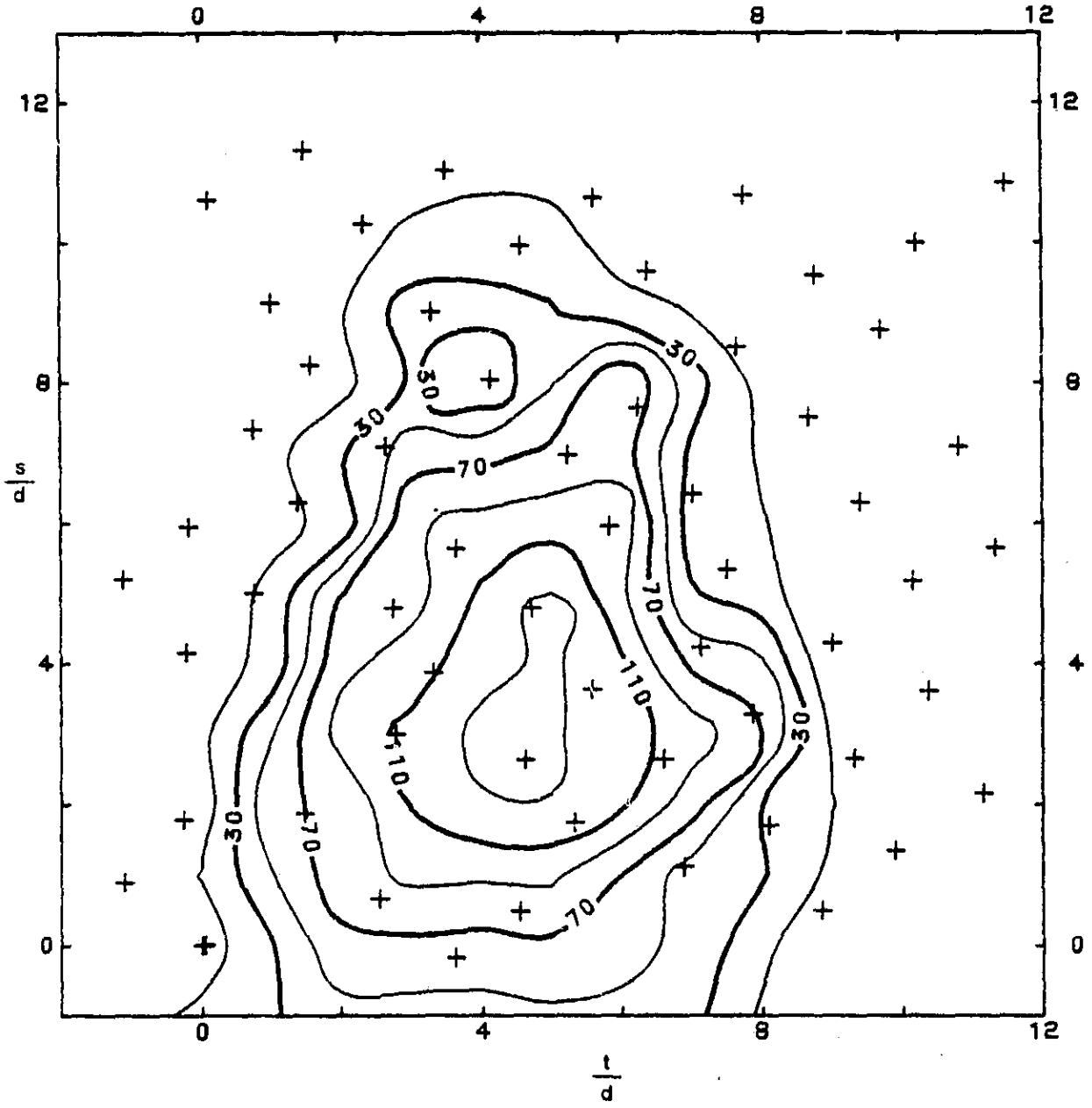

Figure 65. u.c.f. Instantaneous Temperature Isotherms
J = 84, $T_{jet} - T_{\infty}$ = 61.1°C, Time = .58 sec.

NOTE: Contours are $\frac{T_0 - T_{\infty}}{T_{jet} - T_{\infty}}$ X 1000, s/d and t/d as defined for the mean temperature isotherms

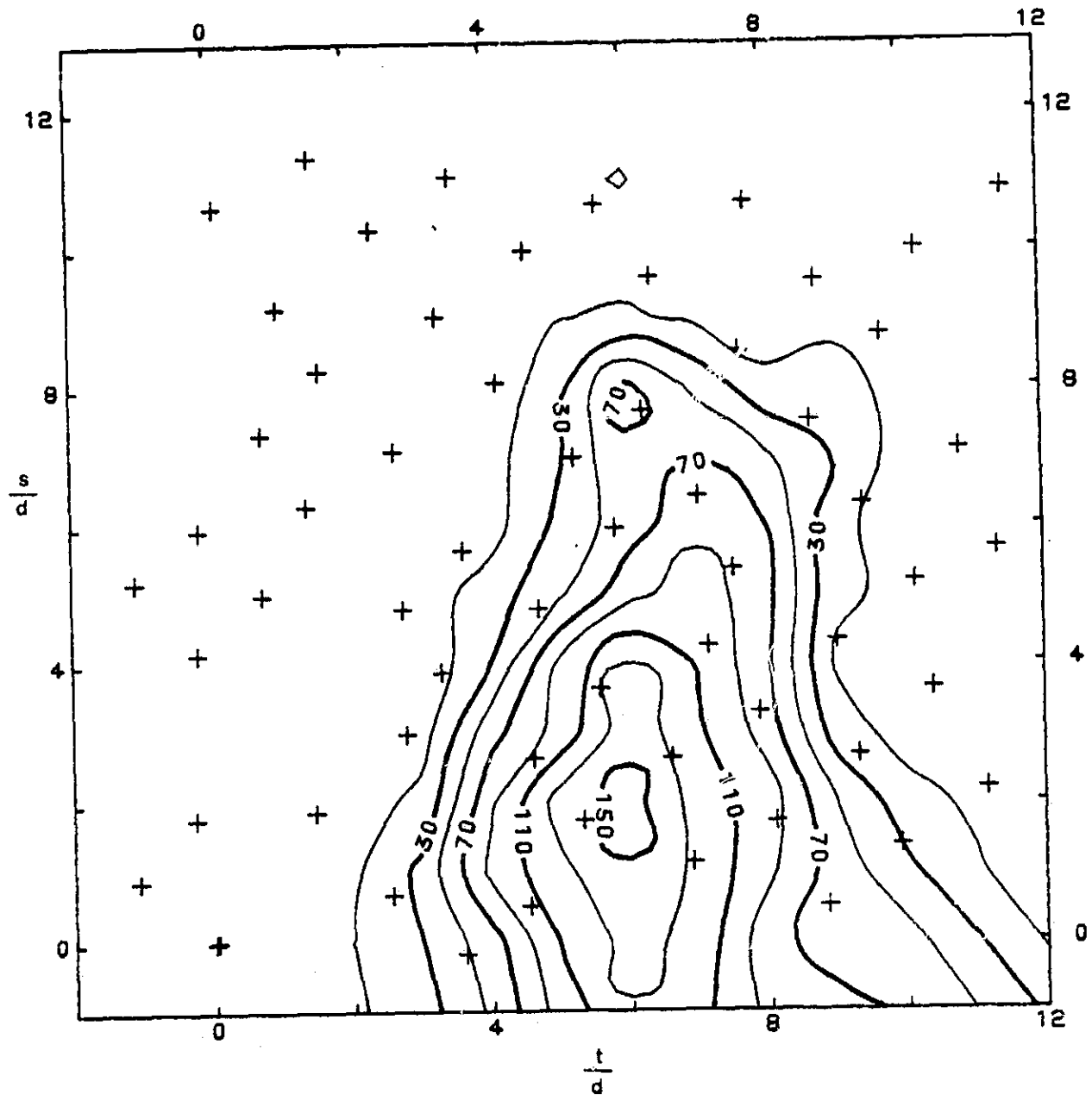

Figure 66. Disturbed Cross Flow (d.c.f.) Instantaneous Temperature Isotherms, J = 84, $T_{jet} - T_{\infty}$ = 61.1°C, Time = .3 sec.

NOTE: Contours are $\frac{T_0 - T_{\infty}}{T_{jet} - T_{\infty}}$ X 1000, s/d and t/d as defined for the mean temperature isotherms

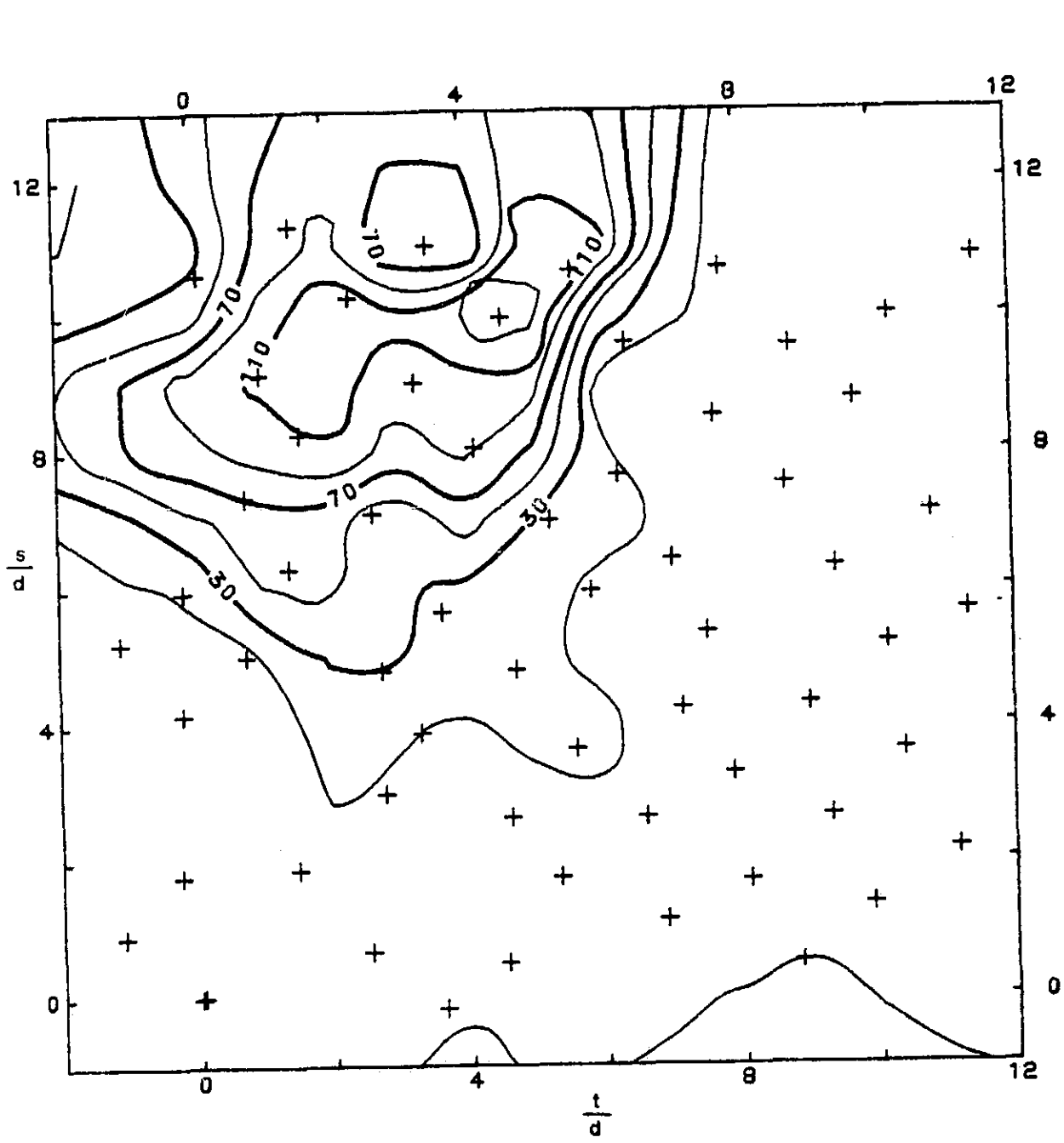

Figure 67. d.c.f. Instantaneous Temperature Isotherms
J = 84, $T_{jet} - T_{\infty}$ = 61.1°C, Time = .58 sec.

NOTE: Contours are $\frac{T_o - T_{\infty}}{T_{jet} - T_{\infty}}$ X 1000, s/d and t/d as defined for the mean temperature isotherms

REFERENCES

1. Peterson, C. W., (1979) "A Survey of the Utilitarian Aspects of Advanced Flowfield Diagnostic Techniques." AIAA J. 17:1252-1360.

2. Doebelin, E. O., (1966) "Measurement System: Application and Design." McGraw-Hill.

3. Bradley, D. and Matthews, K. J., (1968) "Measurements of High Gas Temperatures with Fine Wire Thermocouples." J. Mech. Eng. Sci. 10:299-305.

4. Moffat, R. J., (1958) "Designing Thermocouples for Response Rate." Trans. ASME 80:257-62.

5. Petit, C., Gajan, P., Lecordier, J. C., and Paranthaen, P., (1982) "Frequency Response of Fine Wire Thermocouple." J. Phys. E:Sci. Instrum., Vol. 15:760-764.

6. Shepard, C. E., and Warshawsky, I., (1952) "Electrical Techniques for Time Lag Compensation of Thermocouples Used in Jet Engine Gas Temperature Measurement." NACA TN 2703.

7. Kunugi, M., and Jinno, H., (1959) "Measurements of Fluctuating Temperature." Seventh International Symposium on Combustion, pp. 942.

8. Lockwood, F. C. and Moneib, H. A. (1980) "Fluctuating Temperature Measurements in a Heated Round Free Jet." Combustion Sciences and Technology, 22:63-81.

9. Ballantyne, A. and Moss, J. B. (1977) "Fine Wire Thermocouple Measurements of Fluctuating Temperature." Combustion Science and Technology, 17:63-72.

10. Foss, J. F., (1980) "Interaction Region Phenomena for the Jet in a Cross Flow Problem." Report SFB 80/E/161, University of Karlsruhe.

11. Keffer, J. F., and Baines, W. D., (1963) "The Round Turbulent Jet in a Cross-Wind." Journal of Fluid Mechanics, Vol. 15, 481-497.

12. Fearn, R. L., and Weston, R. P., (1975) "Induced Pressure Distribution of a Jet in a Crossflow." NASA TN D-7916.

13. Ramsey, J. W. and Goldstein, R. J., (1971) "Interaction of a Heated Jet with a Deflecting Stream." Journal of Heat Transfer, Nov. pp. 365-372.

14. Kamotani, Y. and Griber, I., (1971) "Experiments on a Turbulent Jet in a Cross Flow." NASA CR-72893.

15. Andreopoulos, J.,(1983) "Heat Transfer Measurements in a Heated Jet-Pipe Flow Issuing Into a Cold Cross Stream." Phys. Fluids 26(11) pp. 3201-3210.

16. Townsend, A. A., (1976) The Structure of Turbulent Shear Flow, Cambridge University Press, 2nd Ed.

17. Ricou, F. P., and Spalding, D. B., (1956) "Measurements of Entrainment by Axisymmetrical Turbulent Jets." Journal of Fluid Mechanics, Vol. 11, Part 1, p. 21.

18. Holdeman, J. D., and Foss, J. F.,(1975) "The Initiation, Development, and Decay of the Secondary Flow in a Bounded Jet." ASME Trans. Sept. pp. 342-352.

1. Report No.	2. Government Accession No.	3. Recipient's Catalog No.
NASA CR-174896		

4. Title and Subtitle	5. Report Date
Development of a Temperature Measurement System With Application to a Jet in a Cross Flow Experiment	May 1985
	6. Performing Organization Code

7. Author(s)	8. Performing Organization Report No.
Candace Wark and John F. Foss	FSFL-R-85-002
	10. Work Unit No.

9. Performing Organization Name and Address	11. Contract or Grant No.
Michigan State University College of Engineering East Lansing, Michigan 48824	NAG 3-245
	13. Type of Report and Period Covered
12. Sponsoring Agency Name and Address	Contractor Report
National Aeronautics and Space Administration Washington, D.C. 20546	14. Sponsoring Agency Code
	533-04-12

15. Supplementary Notes

Final report. Project Manager, J.D. Holdeman, Internal Fluid Mechanics Division, NASA Lewis Research Center, Cleveland, Ohio 44135.

16. Abstract

A temperature measurement system, which allows the simultaneous sampling (each 0.64 m/s) of up to 80 separate thermocouples, has been developed. The minimum resolution for the system corresponds to ± 0.16 °C per least significant bit of the A/D converter. Electronic and thermal noise give an effective resolution of nominally ± 0.44 °C. The time constant values λ, for each of the 64 thermocouples, were determined experimentally at 7 mps. A "universal" form of the velocity dependence: $\lambda = \lambda(u)$ for $2 \leq u \leq 12$ mps, was analytically inferred and experimentally verified for four thermocouples. Software routines were used to correct the measured temperatures for the effect of λ for each thermocouple. The temperature measurement system has been utilized to study the thermal field of a heated jet discharging perpendicularly into a low ($\tilde{u}/U_\infty$ = 0.6 percent) and a high ($\tilde{u}/U_\infty$ = 34 percent) disturbance level cross stream for a given momentum flux ratio ($J = \rho_j V_j^2/\rho_\infty U_\infty^2$) and for three overheated values ($T_j - T_\infty$ = 22.2, 41.7, 66.2 °C). The peak instantaneous temperatures (X/d = 3 ~ 4) reveal that strong molecular diffusion has been operative: $(T - T_\infty)/(T_j - T_\infty) \leq 0.25$. Various measures of the thermal field, for the disturbed case, suggest that the jet column remains relatively compact while being buffeted by the ambient turbulence field and that its penetration, into the cross wind, is inhibited by the presence of the strong disturbance field.

17. Key Words (Suggested by Author(s))	18. Distribution Statement
Dilution jet mixing Temperature measurement	Unclassified - unlimited STAR Category 07

19. Security Classif. (of this report)	20. Security Classif. (of this page)	21. No. of pages	22. Price*
Unclassified	Unclassified	125	A06

*For sale by the National Technical Information Service, Springfield, Virginia 22161